



Study of the combined roles of the Silica/Oil/UHMWPE formulation and process parameters on morphological and electrical properties of battery Separators

Fabien Toquet

► To cite this version:

Fabien Toquet. Study of the combined roles of the Silica/Oil/UHMWPE formulation and process parameters on morphological and electrical properties of battery Separators. Material chemistry. Université de Lyon, 2017. English. NNT : 2017LYSE1014 . tel-01526682

HAL Id: tel-01526682

<https://theses.hal.science/tel-01526682>

Submitted on 23 May 2017

HAL is a multi-disciplinary open access archive for the deposit and dissemination of scientific research documents, whether they are published or not. The documents may come from teaching and research institutions in France or abroad, or from public or private research centers.

L'archive ouverte pluridisciplinaire **HAL**, est destinée au dépôt et à la diffusion de documents scientifiques de niveau recherche, publiés ou non, émanant des établissements d'enseignement et de recherche français ou étrangers, des laboratoires publics ou privés.

N°d'ordre
NNT :2017LYSE1014



THESE de DOCTORAT DE L'UNIVERSITE DE LYON

opérée au sein de
l'Université Claude Bernard Lyon 1

Ecole Doctorale N° 34
Ecole Doctorale des Matériaux Lyon 1

Spécialité de doctorat : Chimie des matériaux

Soutenue publiquement le 17/02/2017, par :

Fabien TOQUET

Study of the combined roles of the Silica/Oil/UHMWPE formulation and process parameters on morphological and electrical properties of battery Separators

Devant le jury composé de :

Mme. N. El Kissi	Directrice de recherches CNRS	Université Grenoble-Alpes	Rapporteure
M. T. Aubry	Professeur	Université de Bretagne-Occidentale	Rapporteur
Mme. E. Espuche	Professeur	Université Lyon 1	Examinatrice
M. L. Guy	Docteur	Solvay	Examineur
M. P. Cassagnau	Professeur	Université Lyon 1	Co-Directeur de thèse
M. R. Fulchiron	MCF, HDR	Université Lyon 1	Directeur de thèse

UNIVERSITE CLAUDE BERNARD - LYON 1

Président de l'Université

Président du Conseil Académique

Vice-président du Conseil d'Administration

Vice-président du Conseil Formation et Vie Universitaire

Vice-président de la Commission Recherche

Directrice Générale des Services

M. le Professeur Frédéric FLEURY

M. le Professeur Hamda BEN HADID

M. le Professeur Didier REVEL

M. le Professeur Philippe CHEVALIER

M. Fabrice VALLÉE

Mme Dominique MARCHAND

COMPOSANTES SANTE

Faculté de Médecine Lyon Est – Claude Bernard

Directeur : M. le Professeur G.RODE

Faculté de Médecine et de Maïeutique Lyon Sud – Charles Mérieux

Directeur : Mme la Professeure C. BURILLON

Faculté d'Odontologie

Directeur : M. le Professeur D. BOURGEOIS

Institut des Sciences Pharmaceutiques et Biologiques

Directeur : Mme la Professeure C. VINCIGUERRA

Institut des Sciences et Techniques de la Réadaptation

Directeur : M. X. PERROT

Département de formation et Centre de Recherche en Biologie Humaine

Directeur : Mme la Professeure A-M. SCHOTT

COMPOSANTES ET DEPARTEMENTS DE SCIENCES ET TECHNOLOGIE

Faculté des Sciences et Technologies

Directeur : M. F. DE MARCHI

Département Biologie

Directeur : M. le Professeur F. THEVENARD

Département Chimie Biochimie

Directeur : Mme C. FELIX

Département GEP

Directeur : M. Hassan HAMMOURI

Département Informatique

Directeur : M. le Professeur S. AKKOUCHE

Département Mathématiques

Directeur : M. le Professeur G. TOMANOV

Département Mécanique

Directeur : M. le Professeur H. BEN HADID

Département Physique

Directeur : M. le Professeur J-C PLENET

UFR Sciences et Techniques des Activités Physiques et Sportives

Directeur : M. Y.VANPOULLE

Observatoire des Sciences de l'Univers de Lyon

Directeur : M. B. GUIDERDONI

Polytech Lyon

Directeur : M. le Professeur E.PERRIN

Ecole Supérieure de Chimie Physique Electronique

Directeur : M. G. PIGNAULT

Institut Universitaire de Technologie de Lyon 1

Directeur : M. le Professeur C. VITON

Ecole Supérieure du Professorat et de l'Education

Directeur : M. le Professeur A. MOUGNIOTTE

Institut de Science Financière et d'Assurances

Directeur : M. N. LEBOISNE

ABSTRACT

This work is devoted to understand the effect of the formulation and more specifically of the precipitated silica on the resistivity of the PE-separators. The PE-separators are designed for the lead-acid batteries. PE-separators are composed of precipitated silica, ultrahigh molecular weight polyethylene (UHMW-PE) and organic oil. The first part of this work was to elaborate PE-separator models at a laboratory scale. Then, the factors impacting the structural and physico-chemicals properties of PE-separators were investigated. These factors are mainly the amounts of oil, precipitated silica, the grade of the precipitated silica, the temperature conditions of crystallization and the device used to elaborate the membrane. The influence of the amounts of oil and precipitated silica on the crystallization of the polyethylene was thoroughly described showing that the oil helps to increase the final crystallinity of UHMWPE and that the silica plays a role of oil reservoir. Moreover, it was shown that the amount and the grade of precipitated silica have an influence on the wettable part of the porosity of the PE-separators. The coating of the pores by the precipitated silica is responsible of the wettability of the membranes by the electrolyte. Thus, an empirical parameter has been proposed in order to quantify the efficiency of the dispersion and distribution of the precipitated silica in the membrane. The more the membranes are wettable by the electrolyte the more the resistivity of the membranes is decreased. To finish, for a same amount of components and a same method of processing, it is possible to discriminate the efficiency of each grade of precipitated silica for the battery separator application.

RESUME

Ce travail s'est concentré sur la compréhension de l'influence de la formulation et plus spécifiquement de la silice précipitée sur la résistivité électrique de séparateurs en polyéthylène destinés à des batteries au plomb. Les séparateurs de batteries en polyéthylène sont composés de silice précipitée, de polyéthylène ultra haute masse molaire (UHMWPE) et d'huile organique. La première partie de ce travail a été d'élaborer à l'échelle du laboratoire, des membranes modèles en polyéthylène. La seconde a été de comprendre l'influence de certains facteurs sur les propriétés structurales et physicochimiques des membranes. Ces facteurs sont principalement la quantité d'huile, la quantité et le grade de silice précipitée, les conditions de température lors de la cristallisation de la membrane et le mode de mise en œuvre utilisé. Les influences des quantités d'huile et de silice sur la cristallisation du polyéthylène sont méticuleusement étudiées, montrant que l'huile aide à augmenter la cristallinité finale de l'UHMWPE et que la silice joue un rôle de réservoir d'huile. Il a également été mis en évidence que la quantité ainsi que le grade de silice influencent la quantité de porosité de la membrane mouillable par l'électrolyte. La présence de silice en surface des pores est responsable de la mouillabilité de la membrane. Un paramètre empirique a donc été proposé dans le but de pouvoir quantifier l'efficacité de l'état de dispersion/distribution de la silice précipitée dans la membrane. Pour terminer, pour une formulation et un même mode de mise en œuvre, il est possible de discriminer l'efficacité des grades de silice précipitée pour l'application séparateur de batterie.

Remerciements

Voici le moment d'écrire les remerciements...

Je tiens d'abord à remercier mes encadrants de thèse, qui ont tous contribué à leurs manières à enrichir ce travail ainsi que ma vision de la science et du monde du travail. René (Fulchiron), je te remercie pour toutes ces conversations autour de mon sujet qui m'ont données l'envie de faire de la « belle » science. Laurent (Guy), je te remercie pour m'avoir distillé de précieux conseils sur la communication et les relations entre collègues, cela m'a fait grandir humainement et me servira encore après ma thèse. Philippe (Cassagnau), je te remercie pour avoir toujours fait en sorte que cette thèse se déroule dans les meilleures conditions possibles. Brice (Schlegel), je te remercie pour m'avoir apporté ton soutien tout au long de cette thèse. Autant professionnellement qu'humainement, tu m'as fait grandir sur bien des domaines. Plus qu'un directeur de thèse, tu as joué également le rôle de mentor et d'ami pendant ces trois années.

Merci à toute l'équipe technique de l'IMP, sans lesquels le travail de thèse serait beaucoup plus compliqué. Un grand merci également à Lionel Barriquand qui a toujours été de bons conseils et qui a tout fait pour faciliter mon travail.

Merci à la dream team des doctorants et stagiaires pour avoir fait de cette expérience de thèse trois années inoubliables (la dream team : Alice, Anaïs, Antoine, Baptiste, Christophe, Gautier, Guillaume, Imed, Jiji, Julie, Manue, Margarita, Marjorie, Mélanie, Michaël, Nico, Quanji, Quillaja, Sarra, Seb, Sylvain, Thibault, Yann et tous ceux que j'ai pu oublier). J'espère que vous continuerez à supporter mes râleries pendant encore longtemps ! Une petite mention spéciale pour mon comparse Antoine Lucas avec qui j'ai pu faire les quatre cents coups durant cette thèse.

Enfin, je tiens à remercier ma famille et mes amis d'enfances pour m'avoir toujours soutenu jusqu'à maintenant.

I didn't say it would be easy, Neo. I just said it would be the truth.

Morpheus (Matrix 1999)

Table of contents

Abstract	4
Résumé	5
Table of contents	8
Notation and acronyms.....	11
1 General Introduction.....	14
1.1 Lead-acid battery	14
1.1.1 historical of the lead-acid battery [1,2]	14
1.1.2 Overview of the lead-acid battery	14
1.2 Overview of battery separators	16
1.3 Objectives of the study	18
Introduction générale.....	19
2 Elaboration of PE-separators and bibliography associated	20
2.1 Elaboration of the PE-separators.....	20
2.1.1 Dry blend composition and influence on battery separators properties.....	20
2.1.1.1 Formulation of PE-separators prior to extraction	20
2.1.1.2 Influence of the formulation on the PE-separators properties.....	21
2.1.2 Extrusion and Calendering (TIPS process)	24
2.1.2.1 Industrial elaboration of PE-separators	25
2.1.2.2 TIPS Process (Thermally Induced Phase Separation).....	26
2.1.3 Influence of the calendering on the membrane.....	31
2.1.4 Extraction of oil.....	34
2.1.5 Relationships between porosity and resistivity.....	35
2.2 <i>Finishing</i>	36
2.3 Conclusion.....	37
Résumé du chapitre 2.....	38
3 Materials and experimental methods	40
3.1 Materials:	40
3.1.1 Polymer matrix (Polyethylene)	40

3.1.2	Process oil	42
3.1.3	Precipitated silica.....	44
3.2	Techniques used	47
3.2.1	Processing at melting state.....	47
3.2.1.1	Processing in an internal mixer	47
3.2.1.2	Processing by extrusion.....	48
3.2.2	Preparation of membranes	50
3.2.2.1	Protocol of shaping under press.....	50
3.2.2.2	Protocol of process oil extraction.....	50
3.2.2.2.1	Oil extraction by soxhlet	50
3.2.2.2.2	Oil extraction in a bath Oil/solvent.....	51
3.2.3	Structural and physicochemical characterization of materials	52
3.2.3.1	Thickness measurement.....	52
3.2.3.2	Thermal analysis	53
3.2.3.2.1	TGA (Thermogravimetric analysis).....	53
3.2.3.2.2	DSC (Differential Scanning Calorimetry)	53
3.2.3.3	Analysis of dispersion and distribution of the precipitated silica by microscopy.	54
3.2.3.3.1	Optical Microscopy	54
3.2.3.3.2	Scanning Electron Microscopy	55
3.2.3.4	Membranes porosimetry.....	55
3.2.3.4.1	Mercury porosimetry.....	55
3.2.3.4.2	Porosimetry density kit.....	56
3.2.3.5	Electrical resistivity and Tortuosity measurements	58
3.2.3.5.1	Electrical resistivity (Palico system)	59
3.2.3.5.2	Determination of Tortuosity	60
	Résumé du chapitre 3.....	61
	<i>4 Influence of the formulation and cooling rate on the crystallization of membranes</i>	<i>63</i>
4.1	Introduction	63
4.2	Effect of the formulation on the UHMW-PE crystallization.....	63
4.2.1	Effect of the formulation on the composition of the blends after process	63

4.2.2	Effect of the formulation on the UHMW-PE crystallization	65
4.3	Effect of temperature conditions on the crystallization of UHMW-PE sample.	72
4.3.1	Influence of the cooling rate on the membranes crystallization	72
4.3.2	Influence of the temperature on the isothermal crystallization of membranes	75
4.4	Conclusion.....	79
Résumé chapitre 4.....		80
5 Influence of the formulation on the porosity and on the electrical resistivity of membranes		81
5.1	influence of the precipitated silica amount on the membranes porosities	81
5.1.1	Samples preparation.....	81
5.1.2	Influence of the silica amount on the porosity of the membranes.....	82
5.1.3	Influence of the silica amount on the membranes electrical resistivity	89
5.2	Discrimination of silica grades on their efficiency for lead-acid battery separator application.....	92
5.2.1	Samples of the study	92
5.2.2	Dispersion of precipitated silica in membranes	93
5.2.3	Porosity and electrical resistivity of samples.....	96
5.3	Conclusion.....	100
Résumé chapitre 5.....		101
6 General conclusion.....		103
Conclusion générale		106
References.....		109
Appendices		117

NOTATION AND ACRONYMS

ΔH_f°	Heat of fusion of the purely crystalline polyethylene
ε_{total}	Total porosity of the sample
ϕ_{oil}	Volume fraction of oil
OCF	Screw design without reverse element
2CF	Screw design with 2 reverse elements
A	Surface area of the measurement in electrical resistivity measurement
BCI	Battery Council Organization
d	Diameter of the entry of a pore in mercury intrusion
d_i	Diameter of pores i with $d_i > d_{i-1}$
d_{oil}	Density of the oil Edelex 946
d_{PE}	Density of the polyethylene
DSC	Differential Scanning Calorimetry
d_{Si}	Density of the precipitated silica
D_{vm}	Density of the “skeleton” of membranes (polyethylene + silica)
e	Thickness of membranes
f	Correction factor for temperature in electrical resistivity measurement
HDPE	High Density PolyEthylene
HDS	Highly Dispersible precipitated Silica
IPA	Isopropyl Alcohol / propan-2-ol
L	Thickness of the crystalline lamellae
L-LDPE	Linear Low Density PolyEthylene
l_s	Ion path through the separator
m_{bulk}	Mass of the sample
m_{IPA}	Mass of isopropyl alcohol
m_{oil}	Mass of oil
m_{PE}	Mass of polyethylene
m_{Si}	Mass of precipitated silica
N_m	MacMullin number
Oil _{wt%}	Oil weight percentage

$PE_{wt\%}$	Polyethylene weight percentage
R	Resistance of samples
SEM	Scanning Electron Microscopy
$Silica_{wt\%}$	Precipitated silica weight percentage
T_c	Crystallization temperature
TGA	Thermogravimetric analysis
TIPS	Thermally Induced Phase separation
T_m	Melting temperature
$T_{m,Eq}$	Equilibrium melting temperature of the polymer
UHMW-PE	Ultra High Molecular Weight PolyEthylene
V_{bulk}	Volume of the samples
V_d	Molar volume of the diluent
V_i	Porous volume of the pores with at least a diameter d_i
V_{iHg}	Volume of the penetrometer
v_m	Volume of material in the sample
V_{pHg}	Volume of mercury having penetrated the samples
v_{pores}	Volume of pores in the sample
V_{totHg}	Total volume of mercury inside the penetrometer
V_u	Molar volume of the repeat unit
w_1	Dry weight of the samples
w_{ipa2}	Weight of the sample in isopropyl alcohol
w_{ipa3}	Weight of the sample in air wetted by IPA
w_{w2}	Weight of the sample in water
w_{w3}	Weight of the sample in air wetted by water
α	Parameter of the coating of the pores by the precipitated silica
ΔHm_{Blend}	Melting enthalpy of the blend
ΔHm_{PE}	Melting enthalpy of the polyethylene in the blend
ΔH_u	Heat of fusion of the repeat unit
$-\Delta V_i$	Incremental pore volume
$\Delta \epsilon_i$	Incremental porosity
$\Delta \epsilon_i (\%)$	Incremental porosity in percentage
$\Delta \epsilon_{Si} (\%)$	Percentage of porosity attributed to the pic of precipitated silica

ε	Porosity
ε_{Hg}	Porosity of the membranes obtained by mercury intrusion
ε_i	Contribution on porosity of the pores with a diameter $d \geq d_i$
ε_{IPA}	Porosity of the membranes obtained with a density kit and IPA
ε_{nw}	Porosity non wettable by water
ε_{ww}	Porosity wettable by water
ρ	Resistivity
ρ_e	Resistivity of the electrolyte
σ	Conductivity of the porous membrane
σ_e	Conductivity of the electrolyte
τ	Tortuosity
Φ_{Si}	Volume fraction of precipitated silica
χ	Interaction parameter
χ_c	Crystallinity
ϕ_d	Volume fraction of the diluent
ϕ_p	Volume fraction of the polymer
ρ_c	Crystal density
σ	Specific surface energy

1 GENERAL INTRODUCTION

This chapter presents the context of the thesis work. The lead-acid battery market trends are discussed and generalities about the lead-acid battery are presented. Then, in the section 1.2, the lead-acid battery separators requirements and PE-separators are introduced.

1.1 LEAD-ACID BATTERY

1.1.1 *HISTORICAL OF THE LEAD-ACID BATTERY [1,2]*

G. Planté, a French scientist, was the first to construct technical cells made from pure lead immersed in sulfuric acid in 1859. Then in 1880, the invention of the Dynamo combined to the accumulator with lead oxide grid permit to this technology to growth. Since 1859, the lead acid battery is studied. Nowadays each components of the battery is being studied and improved in order to enhance the lead-acid battery properties. The components of the lead acid battery will be presented in the following section.

1.1.2 *OVERVIEW OF THE LEAD-ACID BATTERY*

The Lead acid battery exists since more than 160 years and is still the preferred technology in many applications which need accumulators as it shown in Figure 1. From this figure, it can be seen that lead-acid batteries represent more than 90 % of the market. Moreover, the trend is clearly for growth for the coming years.

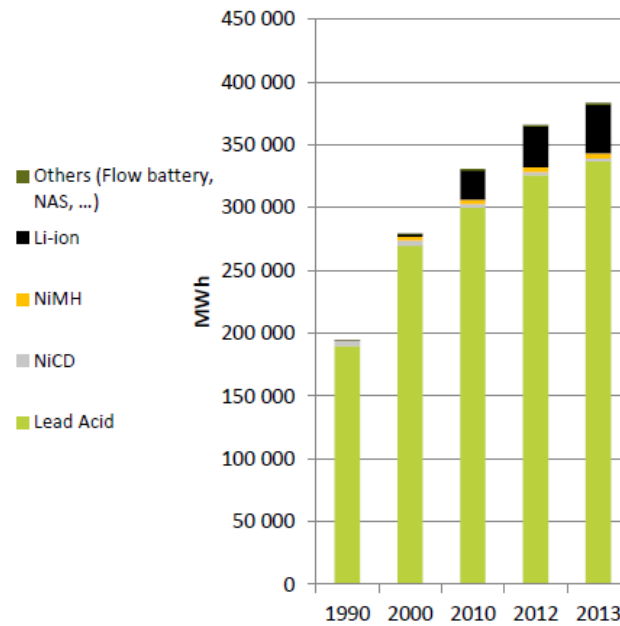


Figure 1: Evolution of the battery market between 1990 and 2013 (Graphic extract from the presentation of Avicenne Energy at the batteries congress of 2014 [3])

The enthusiasm around the lead-acid battery can be explained by several key advantages: a low cost to produce, reliable safety conditions and its recycling rate of around 99 % [4,5]. Nowadays, lead-acid batteries are mostly used for SLI (Starting Lighting Ignition) application. SLI batteries are used in automotive and an example of SLI battery is presented in Figure 2.

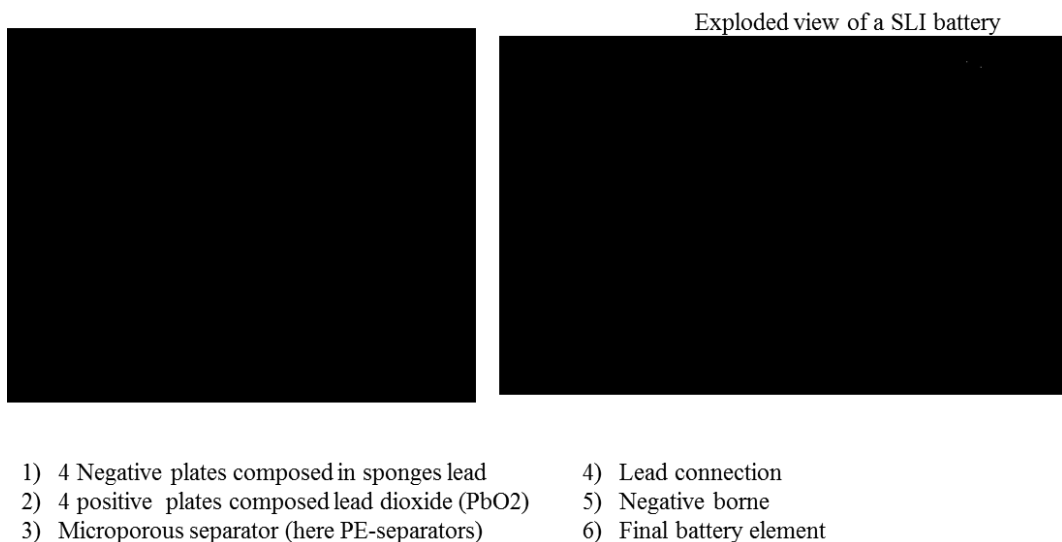


Figure 2: Exploded view of SLI battery with focus on an element [6]

As it can be seen in Figure 2, a SLI battery is composed of several accumulator elements immersed in sulfuric acid [2,6]. An element is composed of positive and negative grids separated with a battery separator. These battery separators must provide an electric insulation ability in between positive and negative plates to prevent electric shortcut and also permit a ionic conduction with a minimum resistance to the ionic flow [7–10]. An overview of lead-acid battery separators is discussed in the following section.

1.2 OVERVIEW OF BATTERY SEPARATORS

There are different types of lead-acid battery separators, but nowadays, PE-separators account for more than 90 % of the total worldwide lead-acid battery separator market [8,11]. These separators are the most common because of their capability to be used as an “envelope” around the negative/positive plates [7,12].

The two most crucial battery separators properties are the electrical resistance and the electric insulation [10,13]. The battery separators must provide the lowest resistance to the ionic flow and also provide a total electrical insulation to avoid shortcut between positive and negative plates. The secondary properties of battery separators are the mechanical and dimensional stability, the chemical resistance and the wettability to the electrolyte. Separators must have a high puncture resistance and to prevent the growth of lead dendrite when in cycling processes to prevent a short cut by connecting positive and negative plates [14].

A non-exhaustive list of lead-acid battery separators and their relative properties are presented in Table 1.

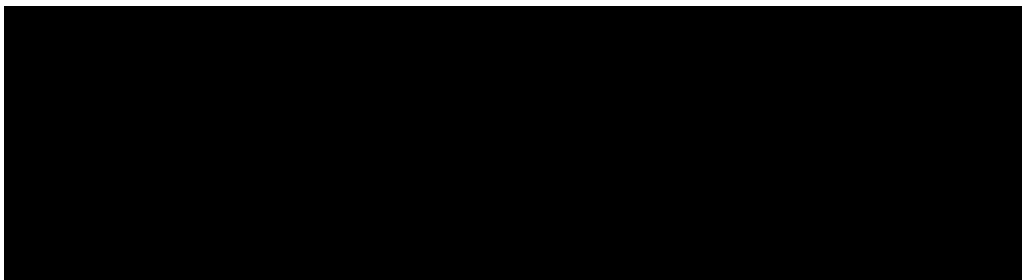


Table 1: Comparison of properties of different separators used in lead-acid batteries (extract from the review on battery separators of P.Arora and Z.Zhang [7])

One of the ways to enhance PE-battery separators performance is to adjust the design of the envelope. On the surface of PE-separator, small ribs are printed to protect the separator backweb and to maintain a distance between positive and

negative plates without increasing the electrical resistivity of the PE-separator [9]. These ribs can also prevent or limit the acid stratification process which can occur in the battery when in cycling process[15]. An example of PE-separator is presented in Figure 3. A PE-separator is composed of a backweb (200 μm) and ribs (800 μm) in surface. In this work, the influence of the thin backweb is only investigated.



Figure 3: PE-Pocket separator (extract from the Handbook of Battery Materials [16])

The PE-pocket separators (or PE-separator) are composed of precipitated silica (≈ 60 wt%), UHMW-PE (≈ 20 Wt%) and mineral oil (≈ 15 wt%) and some other minor components such as carbon black or stearate de calcium [7,9]. Basically, a PE-separator is a porous membrane made of a blend of a polyethylene network and precipitated silica. The porosity usually expressed in volume is around 60 % with a pore size below 1 μm [12], as it can be seen in Figure 4.

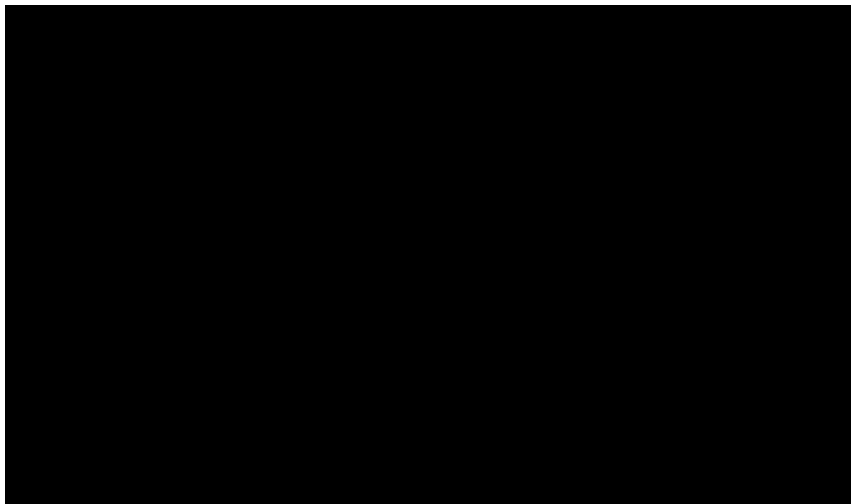


Figure 4: SEM analysis of a PE-separator realized by the manufacturer ENTEK [17]

The materials used in the PE-separators elaboration will be presented in the section 3.1 of this work.

1.3 OBJECTIVES OF THE STUDY

The PE-separator is a complex porous composite which is mostly composed of precipitated silica, UHMW-PE and organic oil. The aim of this thesis work was to answer these questions:

- How the formulation of a PE-separator influences the final properties of the porous membranes?
- How does precipitated silica participate to reduce the resistivity of PE-separators?
- Is it possible to discriminate and predict the efficiency of various precipitated silica grades on the electrical resistivity of PE-separators?

In order to answer to these questions, the manuscript is organized as follows:

The chapter 2 introduces the process of elaboration of a PE-separator and the bibliography associated to each step of the process.

The chapter 3 describes the used materials, the membrane elaboration and characterizations of the PE-separators used during this thesis work.

The chapter 4 proposes to study the influence of the formulation and the cooling rate during the Thermally Induced Phase Separation (TIPS) on the crystallization of UHMW-PE in PE-separators.

The chapter 5 highlights the comprehension of the role of precipitated silica on the electrical resistivity of PE-separators. The effect of the precipitated silica grade is also discussed in this chapter.

INTRODUCTION GENERALE

Ce premier chapitre a pour but de présenter le contexte et les objectifs de ce travail de thèse. Dans un premier temps, un court rappel historique de la batterie est présenté. Puis dans un second, la fonction des séparateurs dans la batterie y est discutée. Pour rappel, les deux fonctions principales d'un séparateur sont d'assurer une conduction ionique maximale tout en jouant le rôle d'isolant électrique entre la cathode et l'anode. Une rapide comparaison des types de séparateur pour batterie au plomb existant sur le marché est réalisée. Une attention particulière est portée sur les PE-séparateurs qui sont utilisés et étudiés dans ce travail de thèse. Un PE-séparateur est un type de séparateur composé de silice précipitée, de polyéthylène d'ultra haute masse molaire et d'huile organique avec une porosité d'environ 60 % et des tailles de pore inférieur à 1 μm .

Les PE-séparateurs sont des membranes poreuses composites complexes qui sont composées majoritairement de silice précipitée. Le but de cette thèse était de répondre aux questions suivantes :

- Comment la formulation d'un PE-séparateur influence les propriétés finales de la membrane poreuse.
- Comment la silice précipitée participe à diminuer la résistivité des séparateurs en polyéthylène.
- Est-il possible de discriminer et/ou prédire l'efficacité de différent grade de silice précipitée pour l'application séparateur de batterie au plomb.

Dans le but de répondre à ces questions, le manuscrit de thèse est organisé de la façon suivante :

Le chapitre 2 introduit le procédé d'élaboration des séparateurs en polyéthylène et la bibliographie associée à chacune des étapes d'élaboration.

Le chapitre 3 décrit les matériaux utilisés, le protocole d'élaboration des membranes ainsi que les techniques de caractérisation utilisées dans le cadre de ce travail de thèse.

Le chapitre 4 présente une étude de l'influence de la formulation et des conditions de température sur la cristallisation de polyéthylène de ultra haute masse molaire au sein du séparateur.

Le chapitre 5 met en évidence la compréhension du rôle de la silice précipitée ainsi que l'importance du grade de silice utilisée sur la résistivité des séparateurs en polyéthylène.

2 ELABORATION OF PE-SEPARATORS AND BIBLIOGRAPHY ASSOCIATED

As evoked before, PE-separators are porous media composed of precipitated silica, UHMW-PE and process oil. Before obtaining the porous membrane, several steps of process are required. These different steps will be presented in this chapter. Moreover the roles of each step on the final properties of the membranes will also be also discussed.

2.1 ELABORATION OF THE PE-SEPARATORS

The process of elaboration of PE-separators is widely described in the scientific literature as well as in patents [16,18–22] or even provided by manufacturer themselves [23]. The process for manufacturing PE separators was first developed in 1967 by W. R. Grace company and there is basically five steps [24]:

1. Dry Blend Preparation
2. Extrusion
3. Calendering
4. Extraction and drying
5. Finishing (Slitting and Winding)

Several steps of the elaboration are crucial to control the final properties of the membranes. In this section, information reported in the literature on each step will be presented.

2.1.1 DRY BLEND COMPOSITION AND INFLUENCE ON BATTERY SEPARATORS PROPERTIES

The formulation of PE-separators obviously influences the final properties of the membrane. In this section, examples of formulation reported in the literature will be presented as well as the influence of the formulation on the final properties of the membrane.

2.1.1.1 Formulation of PE-separators prior to extraction

The dry blend preparation consists in mixing UHMW-PE powder, Silica, plasticizer (also called process oil or just oil) and various minor components together. At the end of this step, a dry blend is obtained with the appearance of “corn starch”. Then,

the dry blend is used to feed a twin screw extruder. An additional quantity of oil is added during the extrusion with a pump. This additional quantity of oil is reported in several patents but the ratio between the oil inside the dry blend and the oil added during extrusion is never clearly described [10,19,25]. With the information given by some patents it is possible to calculate that about 60 wt% of the total amount of oil comes from the dry blend and the other 40 wt% is added thanks to a pump during the extrusion to obtain 63 wt% of oil in the membrane [25].

Inside the extruder, the final composition is well described in the literature [10,19,25–28]. A formulation of 50 - 60 wt% oil, 30 -40 wt% of silica and 10-20 wt% UHMW-PE and some minor components was reported by *Whang et al.* [26]. Formulation of around 30 wt% of filler (precipitated silica and minor ingredients), 10 wt% of UHMW-PE and 60 wt% of oil has been reported by *Whear et al.* [28]. A more precise composition is given in the examples section of the patent, 9.6 wt% UHMWPE, 25 wt% of filler (Precipitated silica and minor ingredients) and 64 wt% of oil [19]. For the last formulation, the weight ratio between precipitated silica and UHMW-PE is $Si/PE = 2.6$ and the weight ratio between oil and UHMW-PE is $Oil/PE = 6.7$. Typically, in the patent literature, Si/PE varies between 1.8 to 3 and Oil/PE varies between 6 to 8.5.

This step is crucial to guarantee a controlled feeding of the extruder. Thus, the dry blend must preserve a minimum of flowability. If too much oil is added to the dry blend, the “powder” will exudate some oil and it will turn into non-homogeneous agglomerates. Therefore, the quantity of the total oil inserted in the dry blend should be adjusted to this requirement.

2.1.1.2 Influence of the formulation on the PE-separators properties

The amount of each component of the formulation could have a strong impact on the properties of the separator. In this section, only the influence of the ratio Si/PE and the presence of minor ingredients will be discussed. The Influence of the oil content in the formulation will be discussed in the section 2.1.2 and the influence of the residual content of oil in the membrane after extraction will be discussed in section 2.1.4.

The influence of the Si/PE ratio on the properties of PE-membranes is very well described by Böhnstedt in the publication “Aspect of optimizing polyethylene separators” [9]. Thus, this section of the manuscript will be mostly based on this work.

The ratio Si/PE could influence critical properties of the PE-separators such as the puncture strength. The puncture strength is one of the prior properties of PE-

separators to avoid short cut in the battery. The SI/PE ratio has a strong impact on the puncture strength of PE-separators as it can be seen in Figure 5.

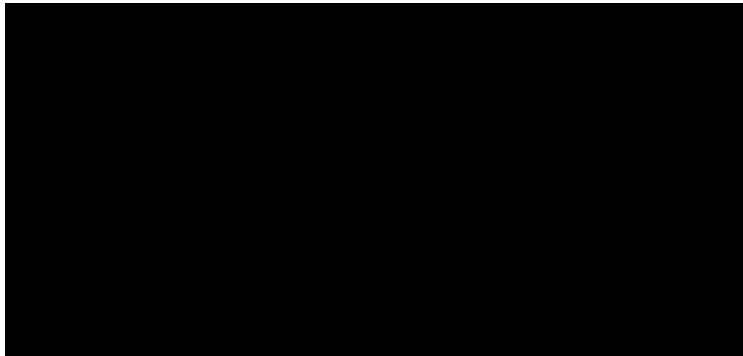


Figure 5: Puncture strength as a function of Si/PE ratio [9]

In this study a membrane with a thickness of 0.2 mm was used. In Figure 5, it can be seen that the puncture strength varies from 4 to 12 N when the Si/PE varies from 4.7 to 2.3. Thus the amount of UHMW-PE should not be too low in the membrane in order to preserve a minimum value of puncture strength. Typically, a PE-separator for SLI battery has a puncture strength between 7 and 10 with a backweb thickness between 0.15 and 0.25 mm [23].

Moreover, growth of lead dendrite on negative plate can occur [14,29]. In these cases, the unique mechanical properties of the UHMW-PE, as the abrasive wear resistance are useful to prevent a perforation of the membranes and shortcut of the battery. Indeed, the UHMWPE, because of its very long chains and compared to the classical HDPE, has a high wear resistance, puncture strength resistance, impact resistance and chemical resistance [30–32].

Therefore, the molecular weight of the UHMW-PE has also an influence on the mechanical properties of the membrane. Thus, as it can be seen in Figure 6, the higher is the molar mass of the UHMW-PE, the higher is the puncture resistance of the membrane.



Figure 6: Puncture resistance as a function of polyethylene molar mass
(adapted from [33])

The Si/PE ratio can also influence the durability of PE-Separators. A PE-separator will be immersed in the sulfuric acid of the battery. Thus, the separator should resist to the chemical oxidation. A standardized test, called “PEROX 80 test”, exists in the lead-acid battery separators industry to examine this property. This test procedure is intended to simulate resistance of separators to oxidative degradation in lead-acid batteries at an accelerated rate. In this test, elongation at break of PE-separators is measured after a prior exposition to a blend of sulfuric acid and hydrogen peroxide at 80 °C. Then, the Elongation at break is normalized by the elongation at break prior to the exposition at the sulfuric acid. An Elongation loss is finally obtained and used to quantify the oxidation resistance of PE-Separator. the higher the elongation loss, the more the PE-separator is considered resistant to the chemical oxidation. Böhnstedt reported an elongation loss 2 times smaller for a Si/PE ratio of 2.3 compared to a Si/PE ratio of 4.7 [9]. Therefore, the higher the Si/PE ratio the worst the membranes are resistant to the chemical oxidation.

The Si/PE ratio has also a strong influence on the electrical resistivity, property which impacts directly the lead acid battery performance. The amount of silica is often described as responsible for the low electrical resistivity of PE-separators [7,22,23]. The higher the silica content in PE-separator, the lower is the electrical resistivity. As it can be seen in Figure 7, the resistivity of a PE-separator is strongly impacted by the Si/PE ratio. The electrical resistance varies from 50 to 100 mΩ.cm² when the Si/PE ratio varies from 4.7 to 2.3 without the usage of a wetting agent. This effect of the precipitated silica on resistivity is sometimes attributed to the porosity of the precipitated silica [7,9]. Because the electrical resistance is dependent on the porosity of the membrane, the intrinsic porosity included in the precipitated silica may enhance the total porosity of the membrane and therefore reduces its

resistivity. However, this hypothesis is claimed without any proof available in the literature to our knowledge.

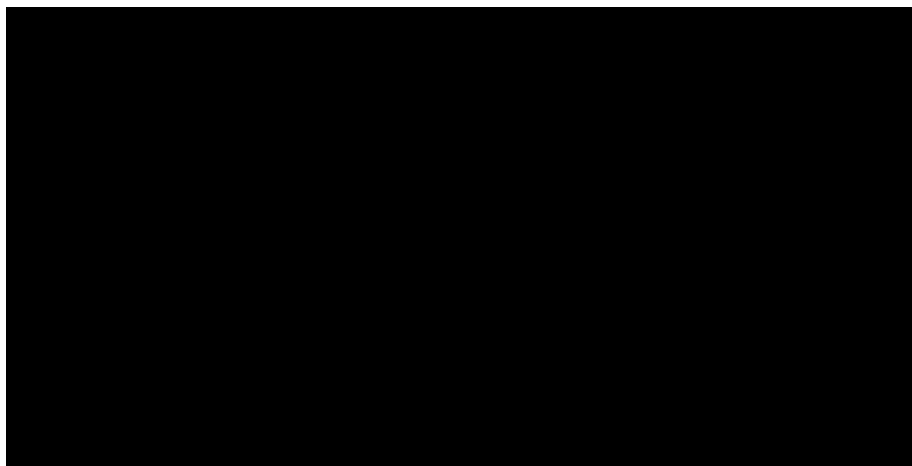


Figure 7: Electrical resistance as a function of Si/PE ratio [9]

As shown in Figure 7, minor components can have also a strong impact on battery separators properties. Here, a wetting agent is used to decrease the electrical resistivity of the membrane. The wettability of the separator by the electrolyte is enhanced by the use of a wetting agent. This can optimize the electrical resistance the separator. This effect of the surfactant is widely described in the patent literature [10,19,28,34]. In Figure 7, it can be seen that the use of a wetting agent decreases the electrical resistance of 40 % for a Si/PE ratio of 2.3. The electrical resistance is less impacted at high Si/PE ratio, the difference of resistivity with or without wetting agent is only of 5 mΩ.cm² for a Si/PE ratio of 4.7.

Sodium dihexylsulfosuccinate between 2 wt% and 3 wt% could be used in commercial PE-separator in order to enhance its wettability [34]. In this work, the authors claimed an electrical resistance reduction of 25 % with the use of 3 wt% of sodium dihexylsulfosuccinate. Other surfactants are cited in the literature, such as ammonium lauryl sulfate, sodium lauryl sulfate, Sodium stearate etc. but their influence on the electrical resistance is not clearly described [10,28,34]. Other minor ingredients used in PE-separators are carbon blacks and antioxidants like the calcium stearate compounds.

2.1.2 EXTRUSION AND CALENDERING (TIPS PROCESS)

In this section of the manuscript, the industrial elaboration of PE-separators by extrusion will be presented as well as the bibliography associated to this process.

2.1.2.1 Industrial elaboration of PE-separators

The key part of the elaboration is the extrusion step, each property of the battery separators is impacted by this step [26]. To manufacture PE-separators, the dry blend is used to feed a twin screw extruder with an additional quantity of oil. Generally, co-rotating extruder technology is preferred to design a PE-separator [35]. The dry blend and the extra oil added during the extrusion are mixed at high temperature, higher than the melting temperature of the UHMW-PE. Then the resultant melt is passed through a sheet die in order to be calendered as it can be seen in Figure 8. The calender gap is used to control the thickness of the membrane. Commercial PE-separators have a thickness in a range between 0.15 mm to 0.6 mm as a function of the battery application. For SLI-battery commercial separators have a thickness around 0.2 mm [7,10,23,28].

The temperature of process is relatively high compared to the melting temperature of the UHMW-PE. Pekala *et al.* proposed a temperature of extrusion around 215 °C to obtain a good miscibility of the UHMW-PE and the oil [10]. Wayne and Leroy proposed a temperature of 175 °C during the extrusion process [24]. Whear *et al.* have proposed a temperature of extrusion around 180 °C.

At the melting state, the process oil and the UHMW-PE are expected to form a homogeneous blend. In this process, the UHMW-PE is dissolved in a process oil in other words a plasticizer and then extruded to form a gel sheet. Whear *et al.* reported that the oil used has mostly no solvating effect on the UHMW-PE at 60 °C, has little solvating effect around 100 °C and has a significant effect at elevated temperatures on the order of 200 °C [19].

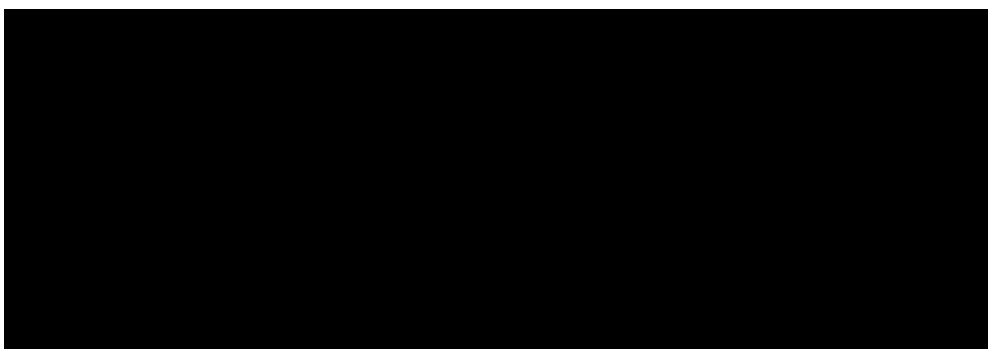


Figure 8: Extrusion process of PE-separator [22]

Because of its really high viscosity at the melting state, the UHMW-PE is not possible to process by extrusion without lubricant. If the plasticizer and the UHMW-PE are miscible at the melting state, this extrusion technic could be characterized as a

process named as a Thermally Induced Phase Separation (TIPS) process. In the TIPS process, a polymer (UHMW-PE) and a diluent (process oil) are blended at a sufficiently high temperature to obtain a homogeneous phase, then after cooling, the process oil is no longer a diluent for the polymer. By removing the oil, the porosity required for the battery separators application is obtained. The next section will present the TIPS process literature.

2.1.2.2 TIPS Process (Thermally Induced Phase Separation)

The Thermally Induced Phase Separation is well studied in scientific literature [36–41]. D. R. LLOYD *et al.* provide a lot of publications about TIPS process. The definition of the TIPS process given by LLOYD is really closed to the steps of PE-separators elaboration [36]:

1. A homogeneous solution is formed by melt-blending the polymer with a high boiling, low molecular weight liquid or solid referred to as the diluent.
2. The solution is then cast into the desired shape.
3. The cast solution is cooled to induce phase separation and solidification of the polymer.
4. The diluent is removed (typically by solvent extraction) to produce a microporous sheet.

In the PE-separator industry, the elaboration process is not called a TIPS process but it is obviously the case. The main advantage of the TIPS process is the ability to prepare porous membranes from semi-crystalline polymers [36,42].

The TIPS process could be influenced by a lot of parameters such as the cooling rate, the dilution concentration or the interaction between the polymer and the diluent. These influences of elaboration parameters on the TIPS will be presented below.

The dual system polymer/diluent has been widely studied. However the influence of filler in the blend is not well described in the literature. First of all, in polymer / diluent system, the crystallization temperatures (T_c) as well as the melting temperature (T_m) are function of the dilution of the polymer. LLOYD reported for different polymer/diluent systems an increase of the crystallization temperature with the increase of the weight fraction of polymer between 0.2 and 1 [36]. For a cooling rate of 10 °C/min, the crystallization temperature varies from 90 °C to 115 °C for a PP/mineral oil blends; For HDPE/mineral oil blends the crystallization temperature varies from 115 °C to around 139 °C. Moreover, the HDPE used was a HDPE with a molar mass of 225 000 g/mol. Thus, we can expect result in this range for a PE/oil blend even if the polyethylene is a UHMW-PE. Moreover, some authors reported

similar results with blends of UHMW-PE/Liquid paraffin [41,43]. They observed a decrease of around 10 °C of T_c for blends of 60 wt% to 10 wt% of UHMW-PE.

In TIPS, if the polymeric component of the binary polymer/diluent system is capable of crystallizing, the melting point of the polymer can be expressed as follows [36,44]:

$$\frac{1}{T_{m,Eq}} - \frac{1}{T_{m,Eq}^0} = \frac{RV_u}{\Delta h_u V_d} (\phi_d - \chi \phi_d^2) \quad \text{Equation 1}$$

Equation 1 is based on the Flory-Huggins theory where $T_{m,Eq}$ and $T_{m,Eq}^0$ are the equilibrium melting temperatures of respectively the polymer in solution and the bulk polymer ($T_{m,Eq}^0 = 414.6 \text{ K}$ for polyethylene) and V_d is the molar volume of the diluent, V_u is the molar volume of the repeat unit, ΔH_u is the heat of fusion of the repeat unit (4110 J.mol^{-1} for polyethylene if the considered repeat unit is $(-\text{CH}_2-)$ [45]), ϕ_d is the volume fraction of the diluent in the blend (here the process oil) and χ is the Flory-Huggins interaction parameter. An interaction parameter value lower than 0.5 indicates a total miscibility while the miscibility is only partial for χ greater than 0.5 [44]. From this equation, it is easy to obtain a relation between the melting temperature and the volume fraction of polymer ($\phi_p = 1 - \phi_d$) in the blend as it is represented in Figure 9.



Figure 9: Melting temperature as a function of the volume fraction of polymer in a blend for a polymer/diluent blend in which the polymer is semi-crystalline. Note the effect of strength of interaction for the hypothetical case of all other variables in Equation 1 being fixed [36].

The melting temperature decreases if the amount of polymer decreases in the polymer/diluent blend. Moreover, this figure allows us to understand the effect of the interaction parameter of the polymer/diluent system. If χ is equal to 0 the relationship between the melting temperature and the volume fraction of polymer is

linear. An interaction parameter value lower than 0.5 indicates a total miscibility while the miscibility is only partial for χ greater than 0.5 [44]. Thus, the interaction parameter for polymer/diluent system should be lower than 0.5 in the TIPS process. Chen *et al.* have found an interaction parameter of approximately 0.06 for Polyethylene/paraffin blends [46].

During the TIPS the amount of polymer in the blend has also an influence on the final porosity after the extraction of the diluent. This influence for HDPE/liquid paraffin blends was investigated by Akbari and Yegani [47]. For a melted polymer sheet quenched at 0 °C, they found that the porosity varies from 82 % to 75 % when the concentration of polymer varies from 15 wt% to 25 wt% (respectively Oil/PE = 5.6 and Oil/PE= 3). Moreover, liu *et al.* reported a porosity around 60 % for a UHMW-PE / liquid paraffin system with 25 wt% of UHMW-PE [41]. Ding *et al.* studied UHMW-PE/Diphenyl ether (DPE) systems where the amount of UHMW-PE varies from 10 wt% to 50 wt%. They obtained a nonlinear loss of porosity from 60 % to 23 % with a big drop of 25 % between 40 wt% and 50 wt% of UHMW-PE [37]. The porosity in industrial PE-separators (with precipitated silica) ranges between 55 % and 65 % with a residual quantity of oil around 15 wt% in the backweb [7,23]. These 15 wt% of oil represent around 10 vol% of the bulk volume [48], thus we can expect a porosity of PE-separator without oil around 70 % [47]. The effect of the precipitated silica on the porosity of the membrane is not really disclosed in the literature. To our knowledge, only C.Zhang *et al* have studied the effect of silica addition on a PE/DOP system. In this study, four blends were made with 0 to 3 wt% of nanosilica. The electrolyte uptake, which is the amount of electrolyte that the membrane can absorb, varies from 30 to 65 wt% of the dry blend of the membrane [40]. Nevertheless, the electrolyte uptake is not necessary connected to the porosity of membranes. Two hypotheses are proposed by the authors. On the one hand, the total porosity of the membrane is enhanced, on the other hand, the wettability of the membrane is enhanced by the presence of silica inside the blend.

The amount of polymer in the polymer / diluent systems could have also an influence on the porosity profile of the membrane. By using the TIPS process, several types of microporous structures can be achieved. Lloyd listed these structures as tie fibrils, leafy and leafy spherulitic [36]. HDPE/liquid paraffin system or UHMW-PE/liquid Paraffin system gives leafy structure as it can be seen in Figure 10. This type of structure is also obtained with HDPE/diluent (diluent other than paraffin) system [36,40,47,49]. Nevertheless, the microstructure obtained with the addition of precipitated silica is more a fibrous structure as it is shown in Figure 4. The addition of precipitated silica seems to reduce the size of the pores and also implicates a transition from a leafy structure to a fibrous structure. Some authors resume the effect of silica on the microstructure as “The gel (UHMW-PE/oil melt blend) smears over the silica particles in a weblike structure without flowing into the silica pores

and clogging them. Once the calendered separator is extracted and cooled, the web structure hardens and links the silica particles while only minimally reducing the porosity of the silica particles. A lower molecular weight polyethylene would melt and create more a continuous film that would cover the silica and block the pores.” [26]. Unfortunately, no data or SEM-analysis are provided with this hypothesis.

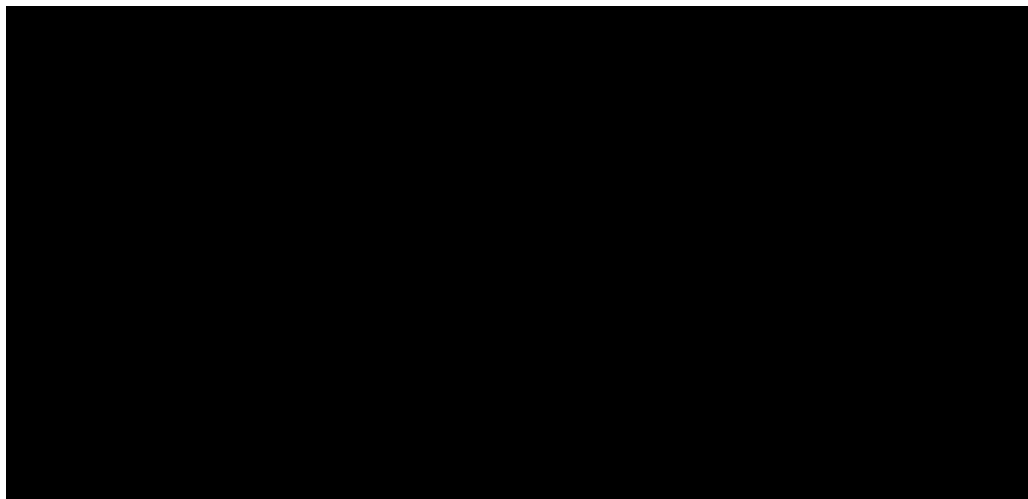


Figure 10: The surface (up) and cross section (bottom) of UHMW-PE microporous membrane with 25 wt% of UHMW-PE in a UHMW-PE/liquid paraffin system quenched at different temperature a)116 °C, b) 115 °C, c) 113 °C and d) 111°C [41]

Moreover, the cooling rate appears to be a key parameter in several studies. There are two possibilities in the TIPS process. The first is to begin the phase separation and the crystallization at an isothermal equilibrium by annealing the melt blend just below the temperature of melting of the UHMW-PE. The second is to apply a cooling at high cooling rate in order to crystallize the UHMW-PE under non-isothermal condition.

In Figure 10, the authors have preferred the first option, a phase separation and crystallization under isothermal condition [41]. First of all, even if the sample crystallizes under isothermal condition, there is a difference of structure between the surface and the bulk. The surface pores size is smaller than the pores size in the bulk. According to the authors, this difference of morphology is due to different cooling rate near the surface and in the bulk. Moreover, the porosity of the membrane can also be increased by the temperature of the TIPS. Hence, the porosity is about 50 % for sample *a* and 35 % for sample *d*.

As shown in Figure 11 [42], it is well known that for a non-isothermal crystallization process, the crystallization temperature decreases for increasing cooling rates. In other words, when the cooling rate is increased, the crystallization occurs for higher

supercooling (difference between the equilibrium melting and the actual temperature of crystallization). Moreover when the diluent volume fraction increases, the equilibrium melting temperature decreases leading to a lower crystallization temperature for a given cooling rate.

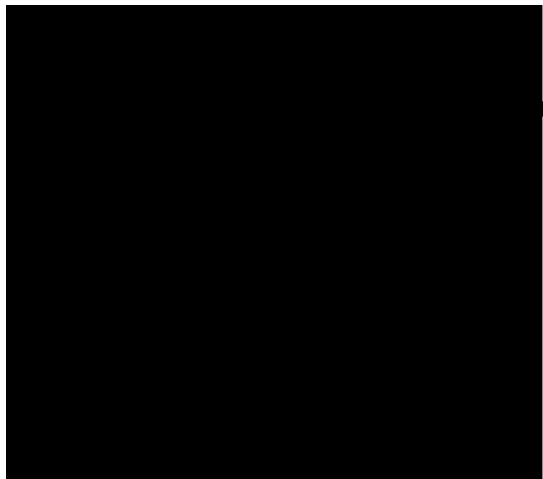


Figure 11: Idealized solid-liquid TIPS phase diagram that incorporates the effect of cooling rate on crystallization [42]

S.Liu *et al.* have observed the effect of the cooling rate on the non-isothermal crystallization of UHMW-PE/liquid paraffin blend with 25 wt% of UHMW-PE. They observed a diminution of the crystallization temperature from 109 °C to 105 °C with an increase of the cooling rate from 1 °C/min to 10 °C/min [41]. At these cooling rates, they also found that the phase separation and the crystallization occurs almost simultaneously in PE/liquid paraffin blends. C. Zhang *et al.* also observed a diminution of the crystallization temperature in UHMW-PE/liquid paraffin blends with an increase of the cooling rates from 2 to 30 °C/min. For UHMW-PE/liquid paraffin blends with 20 wt% of UHMW-PE the crystallization decreased from 107 °C to 104 °C and they obtained almost the same results ± 1 °C for blends with 10 wt% of UHMW-PE [43].

The effect of the cooling rate on the porosity formed by TIPS process has been also studied. Akbari and Yegani have studied the effect of the quenching temperature on the porosity formation during TIPS process for HDPE/liquid paraffin blend [47]. They used three temperatures for the quenching bath, 0 °C, 30 °C and 60 °C. For a blend with 15 wt% of polyethylene, the obtained porosity varies almost linearly from 74 % (0 °C) to 82 % (60 °C). They obtained similar results for membranes with 20 wt% and 25 wt% of UHMW-PE. For other systems such as UHMW-PE/DPE, the relationship between cooling rate and porosity is not obvious. For this kind of systems, a difference of about 5 % of porosity is obtained between a cooling in water and a cooling in air. This difference of porosity could be positive or negative as a function of the amount of UHMW-PE [37]. However, in this kind of systems, the phase

separation does not appear at the same temperature than the crystallization temperature [37,50]. Moreover the authors reported mixing problem between the DPE and the UHMW-PE, thus the control of the porosity could be affected at the end by the TIPS process. However, for a UHMW-PE/diluent system, with an interaction parameter smaller than 0.5, the cooling rate has an influence on the porosity amount in the membrane. Thus the cooling step should be ideally always the same for each sample in order to be able to compare the porosity of membranes.

2.1.3 INFLUENCE OF THE CALENDERING ON THE MEMBRANE

In order to obtain a membrane, the melting blend is calendered between two heated rolls as it can be seen in Figure 8 [7,16,23]. The transfer from one roll to the next is accomplished by some combination of differentials in rolls speed, temperature, and surface finish [51]. Here, only the influence of the speed which is leading to different draw ratio will be considered. A draw ratio is defined by the ratio between the deformed length and underformed length of a polymer sheet. During this step the gel is stretched at a controlled temperature.

The influence of stretching in TIPS process has been studied by several teams and especially for porous fiber material [49,52,53]. Matsuyama *et al.* studied two systems HDPE/liquid paraffin blend and HDPE/diisodecyl phthalate (DIDP) blend. For both of these systems, they produced fibers taken up by winder at different speeds, from 0.15 m/s to 0.3 m/s. In both of these systems, they did not highlight any influence of the take up speed on the average size of pores [49]. However, in this work the blend was stretch in a cooling bath. Thus, according to the authors, the crystallization and phase separation occurs before the stretching. Li and Xiao produced fiber membranes by TIPS process with a blend of UHMW-PE/mineral oil/Silica with Si/PE = 0.2 and Oil/PE = 19. They applied a draw ratio between 0 and 6 at 100 °C. They observed a porosity increase from 40 % to 80 % with an increase of the draw ratio [52]. Moreover, they observed the same tendency when the sample is directly stretched in the air just after the mixing chamber with an increase of porosity from 50 % to 70 % when the draw ratio varies from 0 to 6. Simultaneously, they also observed an increase of the average pores diameter from 0.1 to 0.4 μm . Thus, under specific conditions of temperature, an increase of the draw ratio could increase the porosity in membranes.

The polyethylene chains can crystallize in three different phases: orthorhombic, monoclinic or hexagonal. The orthorhombic phase is the most common and appears under classical condition of pressure and temperature [54–57]. The monoclinic phase is a metastable state and appears when the polyethylene is highly stretched at low

temperature [58–60]. The monoclinic phase will evolve into an orthorhombic phase if the polymer is heated above 70 °C [59,60]. The hexagonal phase is really rare for polyethylene. The polyethylene will only crystallize in hexagonal phase if the pressure during the crystallization is higher than 500 MPa [61,62]. During the elaboration of PE-separator, the polyethylene will obviously crystallize in the orthorhombic phase (which is presented in Figure 12). In Figure 12, a , b and c are the lattice parameter of the unit cell, respectively equal to 7.41, 4.95 and 2.55 Å [55].

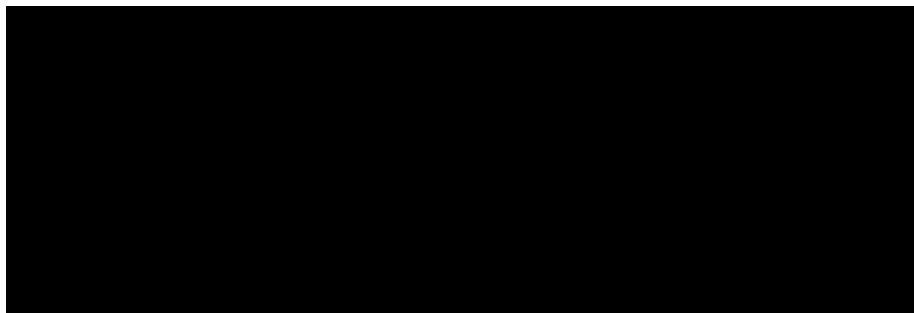


Figure 12: Representation of the polyethylene orthorhombic phase unit cell [63]

Beyond the crystalline form wherein the polyethylene chains are organized according to the crystallization conditions, the solid phase of a polymer is also characterized by its superstructure resulting from the arrangement of the crystalline lamellae.

Crystalline lamellae are really thin for polymers. This thickness is of the order of tens nanometers and can be measured by X-ray scattering, Raman spectroscopy or Transmission Electron Microscopy (TEM) [64]. The thickness of lamellae depends on the crystallization temperature [65]. Thus, each macromolecule, measuring several hundreds or several thousands nanometers in the case of UHMWPE, can be part of several crystalline lamellae or fall back several times in the same lamellae [66]. In the crystalline lamellae, the chain axis (c axis in Figure 12) is oriented perpendicularly to the lateral dimension of the crystal. The polymer chains can be also shared between two or more lamellae thus creating a tie (also called bridge) between lamellae as is presented in Figure 13. These bridges are responsible of some mechanical properties in polyethylene membranes, such as the elongation at break [63,67,68].

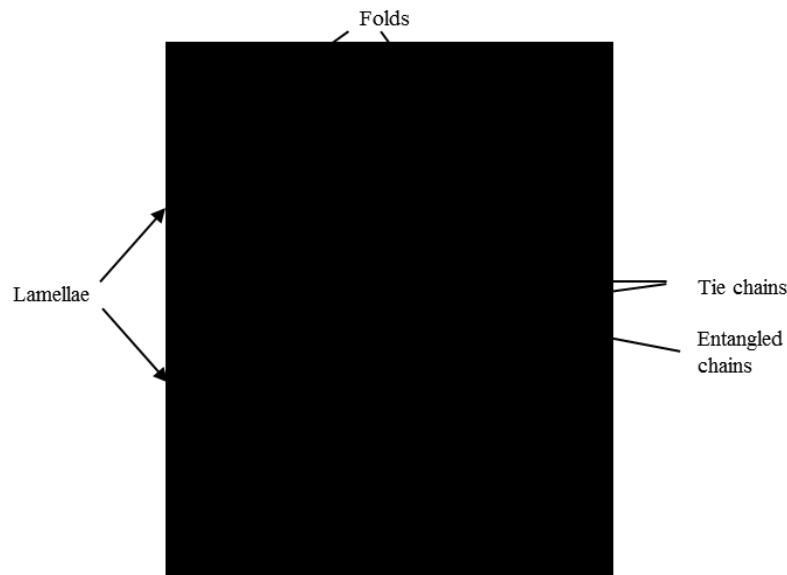


Figure 13: Schematic view of two polyethylene lamellae [63]

The polyethylene lamellae can be reorganized into at least three superstructures: loosely connected lamellae, spherulite or shish kebabs [63].

In the patent literature or in the presentation given by PE-separators manufacturer, the presence of shish-kebab structure in PE-separator are evoked [69–71]. It is reported that the presence of shish-kebab improve the puncture resistance and the oxidation resistance of PE-separator [69].

From a dilute solution with more than 2 wt% of polyethylene, a structure of lamellae loosely connected to their neighbors by tie chains can be obtained. For example, a UHMW-PE/xylene blend with 2 wt% of UHMW-PE leads by evaporation of the xylene, to a thin film composed of these loosely connected lamellae [63]. If a high shear is applied during the crystallization at a temperature just above the crystallization temperature, some fibrils of polyethylene precipitate. These precipitated fibrils can act as nuclei for lamellar crystallization. Thus the shish-kebab structure is obtained [63,72–74]. The shish-kebab structure and a SEM analysis of a PE-separator with shish kebab structure are presented in Figure 14.



Figure 14: PE-separator without Shish-kebab structure at left. PE-separator with shish-kebab structures and its model representation on the right [69].

In Figure 14, two separators from Daramic Company are presented, one without Shish-kebab and one with. It is obvious that the PE-separator presented at right has been more stretched than the separator presented at left.

If the blend is not stretched during crystallization of the polyethylene, the crystallization can lead to spherulite superstructures. Without stretching, the lamellae will grow in all directions from a nucleus as represented in Figure 15.

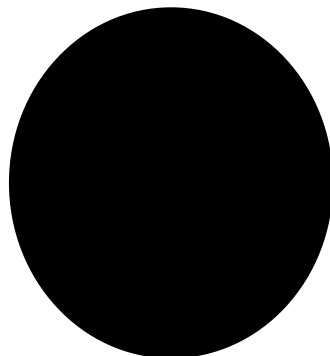


Figure 15: Schematic representation of a spherulite [75]

However, to our knowledge, none spherulitic superstructure are evoked in the literature of TIPS process with polyethylene. Thus it is more likely to obtain loosely connected lamellae structure in the PE-separator elaboration without shear during the crystallization.

2.1.4 EXTRACTION OF OIL

The porosity of the membrane is full of oil after the calendering step. In order to liberate this porosity it is necessary to totally or partially extract the oil of the

membrane. After calendering, the continuous membrane goes in a solvent bath in order to remove the oil. Example of solvent are presented in the literature such as: hexane, 1,1,2-trichloroethylene, perchloroethylene, 1,2-dichloroethane, methylene chloride, chloroform, isopropyl alcohol, diethyl ether and acetone [19,34]. Preferably, the solvent has a boiling point that makes it practical to separate the solvent from the plasticizer in order to reuse it directly in an industrial process. Just after extraction, separators are dried and the solvent is removed from separators. After the step of oil extraction, classical industrial membranes contain around 15 wt% of oil. Moreover, the membranes porosity is around 60 % and shows a pore size distribution below 1 μ m [12]. The residual content of oil has a strong influence on the membranes properties. The oxidation resistance performance is really sensitive to the residual oil content and a lower residual oil content than 15 wt% leads to a faster degradation of the membrane by chemical oxidation [13].

2.1.5 RELATIONSHIPS BETWEEN POROSITY AND RESISTIVITY

The shape of the porosity obtained after the extraction of oil has obviously an effect on the resistivity of the separator. First of all, the porosity must percolate throughout the separator in order to enable the electrolyte to go from one edge to the other. The ratio of length of a path for an ion and the thickness of a separator is called the tortuosity. Pores with same tortuosity but different shape are presented in Figure 16.

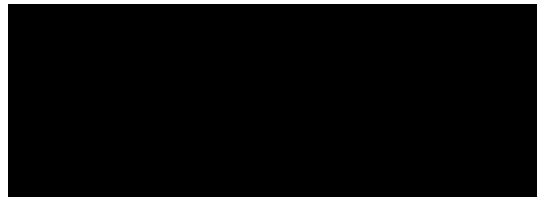


Figure 16: Pores of identical tortuosity [76]

A lot of empirical model have been proposed to link porosity, resistivity and tortuosity [77]. The last one and the most use nowadays is the model of Pirson presented in the following equation [7,17,76–84]:

$$\rho = \frac{\tau^2}{\varepsilon} \times \rho_e \quad \text{Equation 2}$$

Where: ρ is the resistivity of the membrane wetted by the electrolyte; τ is the tortuosity of the membrane; ε is the porosity of the membrane and ρ_e is the resistivity of the electrolyte.

Obviously from this equation, the closer to one is the tortuosity the better is the membrane.

In the same year as Pirson, Tye proposed a theoretical relation between the tortuosity of pores and the resistivity in membranes leading to the same model as Pirson [76]. Moreover, Tye obtained an analogous equation for diffusion. Garrouch *et al.* studied the tortuosity of various membranes by resistivity and by diffusion. They reported some tortuosity obtained by electrical measurements equal to the tortuosity obtained by diffusion measurements [77].

In the literature, the model of Pirson is more often expressed by MacMullin number [7,82,83,85] as described in Equation 3.

$$N_m = \frac{\sigma_e}{\sigma} = \frac{\tau^2}{\varepsilon} \quad \text{Equation 3}$$

Where σ_e is the conductivity of the electrolyte and σ is the conductivity of the porous membrane wetted by the electrolyte.

Using the MacMullin number, several authors determined the tortuosity of separators for lithium-ion (Li-Ion) batteries or lead-acid batteries. D.Djian *et al.* determined tortuosities between 3.3 and 1.9 for separator designed for Li-ion battery [85]. Pekala *et al.* determined tortuosities between 1.8 and 1.3 for battery separator designed for lead-acid battery [17]. Different authors [78,80,82,83] reported some measurement of the tortuosity of the commercial Celgard membranes designed for Li-Ion battery application. They obtained similar result of tortuosity varying from 2.1 to 4.5.

Tortuosity of membranes designed for lead-acid battery separator application appears to be a little lower than the tortuosity of membranes designed for Li-Ion separator application. Thus, in this PhD thesis work, a tortuosity around 1.5 is expected for the membranes elaborated in the lab.

2.2 FINISHING

The finishing step consists in slitting and winding up the membrane. This step of the process does not influence the final properties of the membrane apart the fact that the mechanical properties of the membrane make this step possible [22]. Thus, during this work, this step is not reproduced in the laboratory protocol of elaboration of PE-separators.

2.3 CONCLUSION

A lot of parameters influence the elaboration of PE-separators and their properties. During this PhD work, the influence of each parameter must be taken into account. As it can be seen before, more than one parameter can influence a single property. Thus, when a parameter will vary in our study, it will be crucial to avoid synergy of influence in order to fully understand the influence of a unique parameter on the membranes properties. It is necessary to prevent or identify the variation of one parameter with another.

The first part of this bibliography has shown that the formulation could have a strong influence on the electrical resistivity of PE-separators. Moreover, the formulation can also have an influence on the TIPS process. The crystallization and the porosity induced by the TIPS process are strongly influenced by the amount of each component in a binary or ternary system. One of the aims of this work is to understand the effect of the precipitated silica on the porosity development of the membranes. To achieve this aim, the influence of the cooling rate on the porosity must be also understood or at least be always the same during the cooling of membranes.

Finally, the influences of the formulation and of the process on PE-separator on HDPE/oil system are widely studied in the literature. According to our knowledge, no study deals with the influence of the amount of precipitated silica on the crystallization of UHMW-PE. Thus, the results discussed in chapter 4 about the effect of the formulation on the crystallization of UHMW-PE appear to be a new contribution to the state of the art. Moreover, none of these studies have reported the mechanism of influence of precipitated silica on the porosity and electrical resistivity of membranes. This will be the topic of chapter 5.

RÉSUMÉ DU CHAPITRE 2

Ce chapitre introduit le procédé d'élaboration des séparateurs en polyéthylène et la bibliographie associée à chacune des étapes d'élaboration.

Le procédé d'élaboration d'un séparateur en polyéthylène se déroule en 5 étapes :

1. La préparation d'un prémix (formulation)
2. L'extrusion
3. Le calandrage
4. L'extraction d'huile et le séchage de la membrane
5. Le découpage et l'enroulage des membranes

Seules les quatre premières étapes influencent les propriétés finales du séparateur.

Au cours de ce chapitre, il a été montré que la formulation avait une forte influence sur la résistivité électrique des membranes. De plus, la cristallisation et la création de porosité des membranes, qui se déroulent lors de la séparation de phase induite par la température, sont contrôlées majoritairement par la quantité de chaque composé dans le système ternaire silice précipitée / UHMW-PE / huile organique. L'un des objectifs de ce travail de thèse est de comprendre le rôle de la silice précipitée sur la porosité des séparateurs. Les conditions de température lors de la cristallisation et le procédé de mise en œuvre utilisés influencent également la création de porosité au sein de la membrane. La quantité totale de porosité, la taille des pores ainsi que leur morphologie sont donc impactés par de nombreux facteurs au cours de l'élaboration des membranes.

Au cours de ce travail de thèse, les quatre premières étapes d'élaboration des séparateurs en polyéthylène seront donc adaptées à l'échelle laboratoire. Pour finir, l'impact de chaque paramètre de chacune des étapes d'élaboration sur la cristallisation et la création de porosité des membranes sera étudié. Le prochain chapitre décrit les techniques d'élaboration et de caractérisation utilisées au cours de ce travail de thèse.

3 MATERIALS AND EXPERIMENTAL METHODS

In this section, the materials used for the elaboration of studied membranes will be presented.

3.1 MATERIALS:

3.1.1 POLYMER MATRIX (POLYETHYLENE)

In this thesis work, three kinds of polyethylene were used: A High-Density Polyethylene (HDPE), an Ultra-High Molecular Weight PolyEthylene (UHMW-PE) and a Linear Low Density PolyEthylene (L-LDPE). The repeat unit of the polyethylene is $-(CH_2-CH_2)-$. Moreover, a L-LDPE is basically a linear polyethylene with significant numbers of short ethylene branches.

The ultra-high molecular weight polyethylene (UHMW-PE) is the polymer used for elaborating PE-separators. The UHMW-PE and the HDPE are linear polyethylenes. An UHMW-PE is linear polyethylene with a molar mass of at least $1 \times 10^6 \text{ g.mol}^{-1}$ [31].

In the present work, the HDPE and the L-LDPE are used in order to understand the influence of the long chains of UHMW-PE. The HDPE is a grade HDT10 provided by Haldia Petrochemicals Limited. The L-LDPE is a grade TM50-U provided by Snetor. The HDPE and L-LDPE have been used as received from the suppliers. This work has benefited from the facilities and expertise of the Liquid Chromatography Platform (Institut de Chimie de Lyon) for the characterization of polymers. The molar mass of the HDPE obtained by SEC (Size Exclusion Chromatography) is $\bar{M}_w = 10^5 \text{ g.mol}^{-1}$ and with a polydispersity index $\mathcal{D}_M = 3.2$ and that of the LDPE is $\bar{M}_w = 8 \times 10^4 \text{ g.mol}^{-1}$ with a $\mathcal{D}_M = 2.5$. Moreover, a Carbon-13 nuclear magnetic resonance (^{13}C RMN) has been performed. The ^{13}C NMR spectra were recorded at $T = 393 \text{ K}$ on a Bruker Avance-II spectrometer equipped with a 10 mm ^{13}C selective probe operating at 100.6 MHz. The PE was analyzed in a mixture of TCB/DCB- d^2 (80:20 v/v, Tri-Chloro-Benzene/Di-Chloro-Benzene) with a concentration of 70 mg/mL. This ^{13}C RMN analysis confirms that the TM50-U is a L-LDPE with statistically one ethyl branches every 50 carbons of the linear chain.

The UHWMW-PE is mostly synthetized by Ziegler-Natta polymerization since the 50's [30,31,86]. In a smaller proportion, some processes are also based on metallocene catalyst system with limited capacities [86]. The Ziegler-Natta polymerization leads to the formation of PE powder called nascent powder. This nascent powder has a mean diameter around 100 μm and have a crystallinity around 65 % [87]. Moreover,

the native structure is lost during the first melting. The crystallinity and the entanglement of UHMW-PE chains are affected by the first melting [87–91]. After a first melting of the UHMW-PE, an increase of the entanglements will lead to a decrease of the crystallinity. Typically, this decrease of crystallinity is dependent on the molar mass of the polyethylene. Deplancke *et. al.* have reported a decrease of crystallinity from 68 % to 62 % for an UHMW-PE with a molar mass of $0.6 \times 10^6 \text{ mol.g}^{-1}$ and a decrease from 59 % to 41 % for an UHMWPE with a molar mass of $6.8 \times 10^6 \text{ mol.g}^{-1}$ [87]. Rudnik and Dubkowski have also reported a similar dependency between the molar mass and the decrease of crystallinity after recrystallization [91].

Due to the entanglement of its very long chains and ultra high molecular weight of the UHMW-PE chains, it is not possible to measure the zero-shear viscosity by parallel plates or capillary rheometry. Thus, only a dilute solution viscosimetric method can be used to measure the average size of the polymer chains (\bar{M}_v) [92]. Measurement of molar mass by solution viscosimetry is only relevant for virgin UHMW-PE powder that has not already melted.

Gur®4150 is a UHMW-PE grade and is used in this study for elaborating the microporous membranes studied in the thesis work. The Gur®4150 was produced and kindly provided by Celanese Ticona. The Gur®4150 is presented by Ticona as a grade of UHMW-PE used in compression molding, ram extrusion and battery separators elaboration [32]. Some of the characteristics of the Gur®4150 given by Ticona are presented in Table 2.

Chemical resistance ^(*) to Sulfuric acid/distilled water (70/30)	\bar{M}_v (g/mol)	density (g/cm ³)	melting point (°C)	Volume resistivity (Ω.m)
Yes	9.2×10^6	0.93	135	42

(*): Plastic test pieces were laid in the solution for 60 days. If the weight loss is inferior to 0.5 % and if there is no variation on elongation at break, the polymer is considered as chemically resistant to the solution.

Table 2: Properties of the GUR4150® provided by Celanese Ticona.

From Table 2, it is easy to understand why Gur® 4150 could be a relevant candidate for battery separator application. A battery separator must be resistant to a chemical bath of 50/50 sulfuric acid/ water in volume ($d= 1.28 \text{ g.cm}^{-3}$), provided an electric insulation between the negative and positive plate and also conserve a mechanical integrity up to 75 °C [7,93].

The UHMW-PE is generally processes by compression molding in order to keep the nascent crystallinity [31,90]. But in some cases, as the elaboration of PE-separators, the TIPS process by the extrusion with a diluent is preferred [26].

Characterization of the GUR®4150

The GUR®4150 has been characterized in our laboratory in order to be sure of its processability by TIPS extrusion. The melting temperature has been determined by DSC.

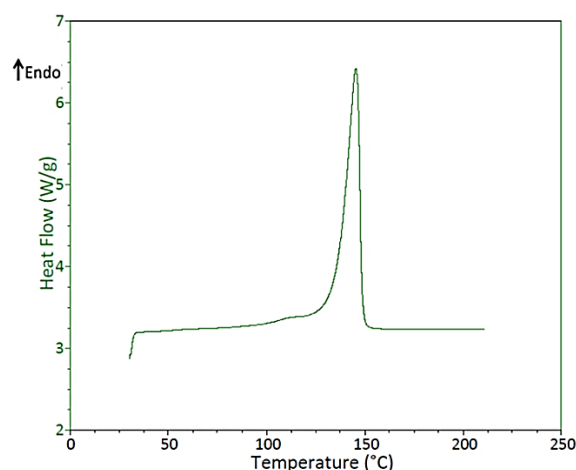


Figure 17: Heating DSC curve for nascent power of UHMW-PE

From Figure 17, it easy to see that the first melting of the UHMW-PE powder has a maximum at 149 °C. The melting temperature of the nascent powder must be exceeded during the processing. Thus, the processing temperature should be at least 160 °C in order to ensure a total melting of the UHMW-PE.

3.1.2 PROCESS OIL

Because of the use of the TIPS process, the process oil must be a diluent of the UHMW-PE at its melting state. From the work of Coran and Anagnostopoulos Alkanes, Alkenes, Naphthenes or limonene are diluent for linear polyethylene at the melting state [9,94]. In the literature, liquid paraffin oils are the diluent the most used for TIPS with polyethylene. Weston *et al.* used paraffin oil as a diluent in order to extrude an UHMW-PE/carbon nanofiber/oil blend [95]. Liu *et al.* used a liquid paraffin oil to obtain an homogeneous blend of UHMW-PE and oil with the help of an internal mixer [41]. Zhang *et al.* studied the nonisothermal crystallization of UHMW-PE/ Liquid paraffin blends elaborated in an internal mixer [43]. Moreover, from a literature more focused on PE-separators, it is reported that paraffinic, naphthenic or

aromatic oil can be used as diluent to process PE-separators [9]. In this study, it is also shown that oils with a high aromatic content contribute considerably to provide an oxidative stability to the separator. Moreover, in the literature of patents about PE-separators, the use of naphthenic oil is commonly reported [10,21,27]. Naphthenic oils are oils with less than 50 wt% of paraffin in a blend of paraffins, naphthenes, aromatics and alkenes [96]. In order to enhance the oxidative stability of the separator and to be the nearer to the industrial formulation, the naphthenic oil has been used during this thesis work. This naphthenic oil is the Edelex 946 kindly provided by shell and used as received. As described in its technical data sheet, the shell edelex 946 has a density of 0.906 g.cm^{-3} , with an aromatic content of 26 wt% and flash point at 220°C .

Edelex 946 has been characterized by TGA in our laboratory, this TGA analysis is presented in Figure 18.

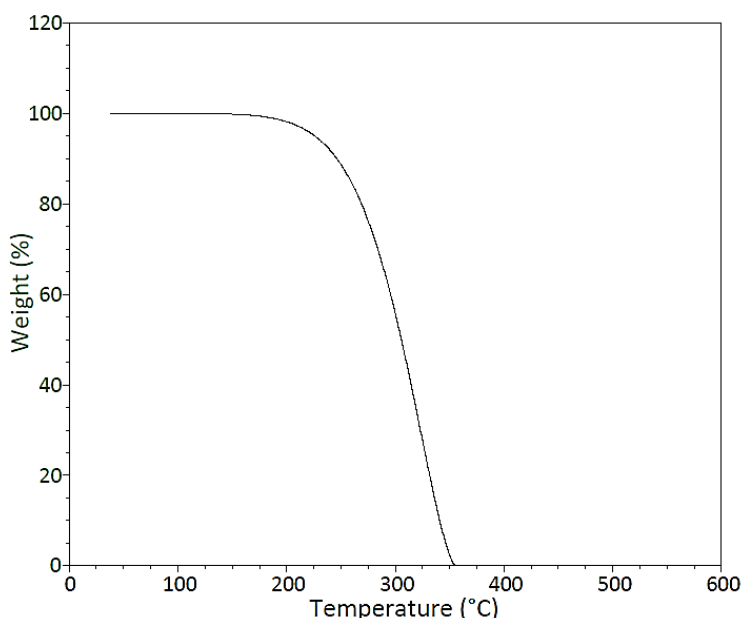


Figure 18: TGA analysis of the Edelex 946 naphthenic oil.

The degradation temperature of the Edelex 946 can be obtained from Figure 18 and is closed to 210°C . Thus, in order to ensure the thermal stability of the process oil, the temperature should not be higher than 210°C during processing of the PE-separators. Moreover, the pour point of the Edelex 946 is -27°C [97]. Thus, the Edelex 946 has a range of use between -20 to 210°C at the liquid state.

3.1.3 PRECIPITATED SILICA

First of all, it is important to define what the precipitated silica is. Silica or silicon dioxide (SiO_2), in the common language, can define sand, crystalline silica or amorphous silica (*e.g.* precipitated silica). This work of differentiation has been done by the INRS French institute (National Health and safety at work) directed by M.Ricaud in 2007 [98]. An overview of silica types provided by the ASASP (Association of Synthetic Amorphous Silica Producers) is shown in Figure 19 [99].

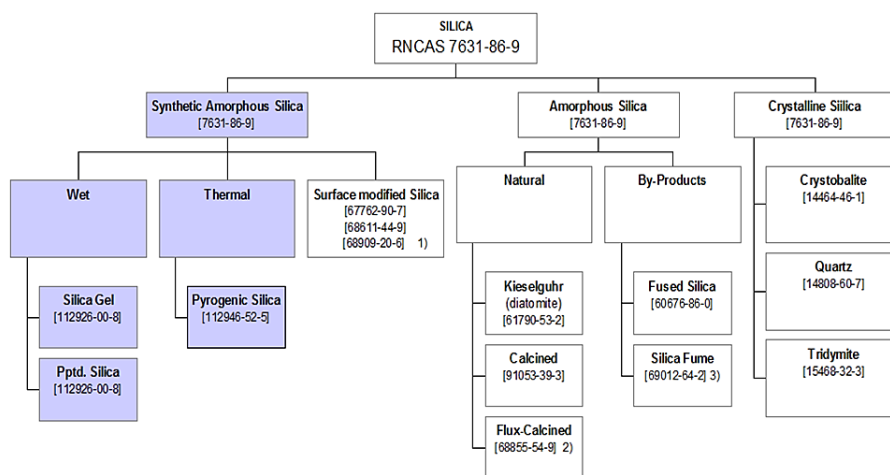


Figure 19: Overview from ASASP of silica types [99]

There are two ways to obtain synthetic silica, the wet process and the thermal process. The wet process can lead to the silica gel or the precipitated silica. The precipitated silica obtained is an amorphous powder which does not present any toxicity for the health [98]. The precipitated silica is used commonly in the tired industry, in toothpaste industry, in the animal nutrition sector and in the battery separator industry.

The precipitated silica is obtained by the precipitation of a solution of Sodium silicate (product of the reaction between sand and sodium carbonate). In presence of sulfuric acid, a glass of sodium silicate is obtained. Then, a reaction of precipitation between a solution of sodium silicate and sulfuric acid leads to the formation of precipitated silica. Afterward, steps of filtration, washing, drying, the agglomerates of precipitated silica are obtained. The precipitated silica obtained is composed of elementary particles forming aggregates which lead to agglomerates [98,100,101]. This multiscale structure of the precipitated silica is presented in Figure 20.

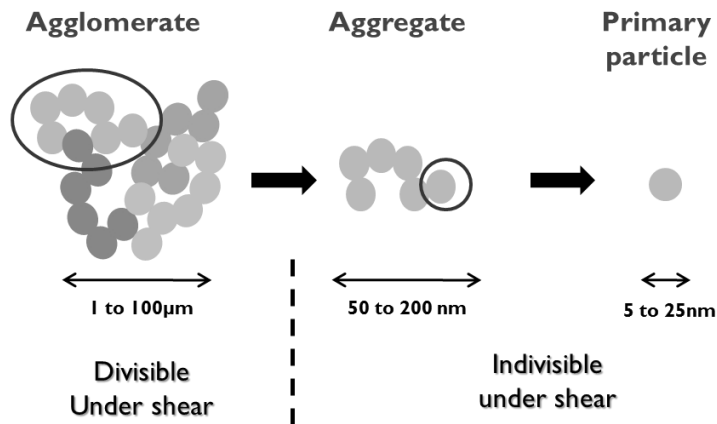


Figure 20: Multiscale structure of the precipitated silica

As it can be seen in Figure 20, during the process, agglomerates can be dislocated in aggregates but never into the primary particles.

In this thesis two types of precipitated silica have been used, a so called conventional precipitated silica versus a Highly Dispersible Silica (HDS) a grade supposed to be more dispersible than the conventional.

The grades of HDS precipitated silica have a smaller aggregates-aggregates cohesion compare to conventional grades of precipitated silica. This smaller cohesion between aggregates can be observed by measurements of fragmentation under ultrasonic waves.

This cohesion of the precipitated silica can be linked to the compactness of the precipitated silica. The more there are contacts between aggregates, the higher the agglomerates will be cohesive. The compactness and specific surfaces can be illustrated by Figure 21.

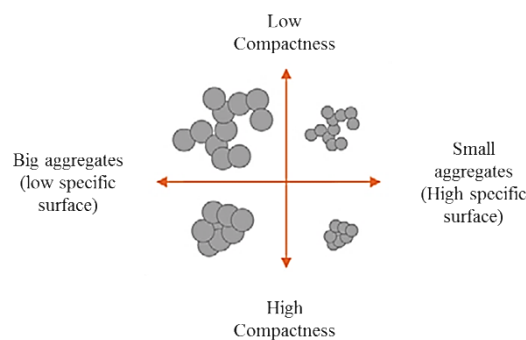


Figure 21: Illustration of the specific surface and compactness properties.
(Illustration extract from the thesis work of C.Fayolle [103])

Three grades of precipitated silica have been used in this thesis work: Zeosil®1165 (Z1165), Zeosil®175 (Z175) and Tixosil® 43B (T43B). The precipitated silica have been used has received and their characteristics are detailed in Table 3.

Grade	Z1165	Z175	T43B
Type	HDS	Conventional	HDS
Specific surface area BET (m ² /g)	150	157	140
Oil absorption DOA (ml/100g)	223	261	272
d ₅₀ (μm)	19.4	22.3	17
Water content (wt%) :	6.6	7.3	9.6

Table 3: Characteristics of precipitated used during the thesis work

3.2 TECHNIQUES USED

3.2.1 *PROCESSING AT MELTING STATE*

The industrial process is not entirely reproducible in the IMP laboratory. This study only focuses on the steps which may influence the structural properties of the membranes. Thus, in this work, there are three steps in the elaboration of PE-separator: the premix preparation, the mixing at the melting state and membrane shaping. During this work, two types of mixing process have been used: process in an internal mixer and the mixing process by extrusion.

3.2.1.1 **Processing in an internal mixer**

Some of the blends used in this work were elaborated in an internal mixer with contra-rotative rotors. The internal mixer used was a Haake Rheomix OS lab mixer equipped with roller rotors or banbury rotors. The volume capacity of the chamber equipped with roller rotors is 69 cm³ and 76 cm³ with the banbury rotors.

Before processing the batch, a premix is prepared in a mortar at room temperature. Polyethylene, precipitated silica and 50 wt% of the naphthenic oil are mixed together by hand in the mortar. This premix is called by the PE-separator manufacturer a “dry blend”. Then the premix is inserted in the internal mixer and 10 s after the rest of the naphthenic oil (50 wt%) is inserted.

Each batch is prepared at 165 °C with a rolling speed of 60 rpm during 12 min with a filling factor of 80 %. The blends were then cooled at room temperature. The Si/PE mass ratio varies from 0 to 4 (0 to 18 vol%) while the Oil/PE ratio was fixed to 7.5 for all these blends. Thus, it is really important to take into account the density of each component in order to keep the filling factor at 80 %.

The temperature of process is in the range of temperature defined by the melting point of polyethylene and the degradation temperature of the naphthenic oil. In order to confirm that there is no degradation of the polymer and the naphthenic oil during the process, TGA analyses at 165 °C during 50 min have been realized. These TGA analyses show that there is no degradation for the polyethylene and only 2 wt% of loss after 12 min for the naphthenic oil at 165 °C. Moreover, the loss of weight is only of 4 wt% at the end of the 50 min for the naphthenic oil. Thus, the polyethylene and the oil are considered stable during the process.

3.2.1.2 Processing by extrusion

The second kind of PE/Oil/Silica blends were prepared in a co-rotating extruder Leistritz ZSE18 with screw diameter: D of 18 mm, a barrel length L of 1.08 m ($L/D = 60$) and the barrel temperature was set at 180°C.

Two types of screw design were used, one called “screw without reverse elements” (*OCF*) and a second called “screw with 2 reverse elements” (*2CF*). For each design, three rotation speeds varying between 500 and 1100rpm and only one formulation, with mass ratios Si/PE of 2.5 ($\Phi_{Si} = 12.4$ vol%) and H/PE of 7.5, were used.

Before processing by extrusion, a premix is performed in a “kitchen aid” (a kitchen blender) at room temperature. A typical premix is prepared with 100 g of Polyethylene, 250 g of precipitated Silica and 375 g of naphthenic oil.

The premix is inserted in the first block of the extruder at a rate of 989 g/h. The rest of the naphthenic is inserted in the third block of the extruder (between 10D and 15D) with the help of a pump at a rate of 9.4 ml/min (511 g/h). Thus, the total feeding flow rate of the extruder is 1.5 kg/h.

At the end of the extruder, the melt blend goes through a circular die with a diameter of 1 mm, then the material is cooled under an air flow and finally cut into small granules by a granulator.

The screw designs are presented in Figure 22.

.

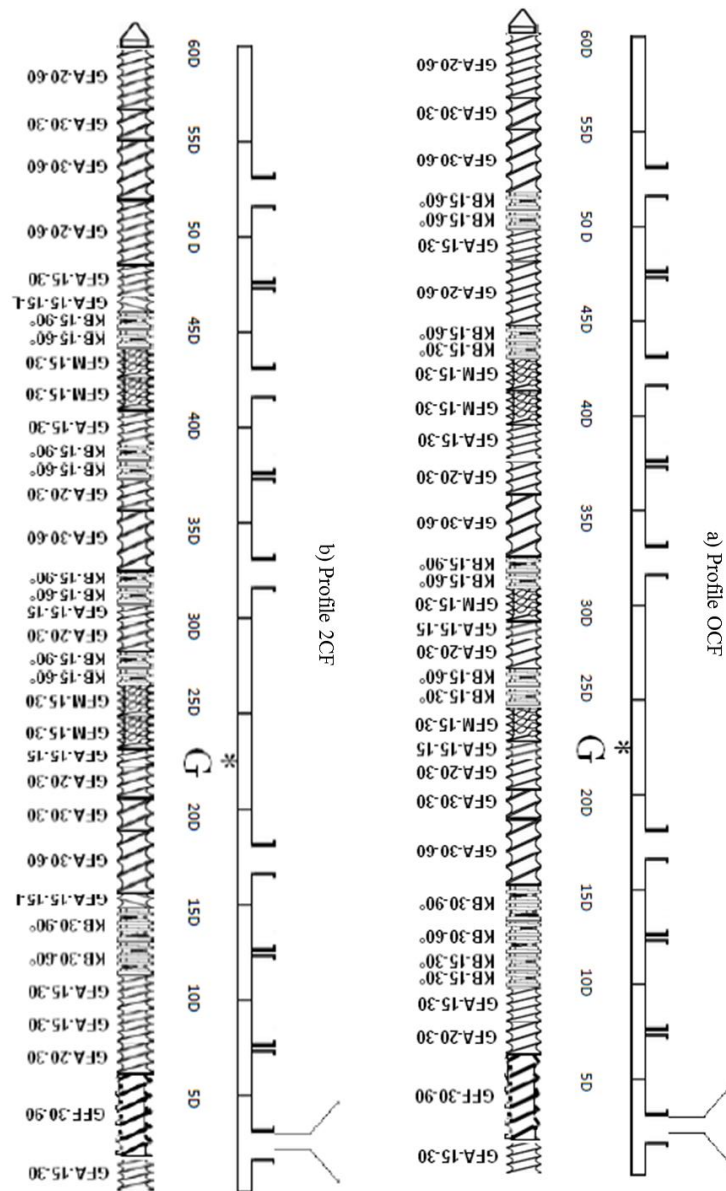


Figure 22: Extrusion profiles: a) Profile OCF and b) Profile 2Cf

3.2.2 PREPARATION OF MEMBRANES

3.2.2.1 Protocol of shaping under press

Around 8 g of material were used to elaborate films with a thickness equal to about 280 μm by molding samples in a laboratory press at 165 $^{\circ}\text{C}$ into a square mold of 15x15 cm with a thickness of 250 μm . The applied force profile was of 5×10^3 N during 1 min then 10^4 N during 2 min and finally during 10 min under 125×10^3 N. The membranes were then cooled at room temperature in the mold.

3.2.2.2 Protocol of process oil extraction

Some studies report the influence of the oil content in the final properties of the battery separator [48]. Industrial battery separators contain around 15 wt% of residual oil [7,8,104]. Because it is easier to totally remove the oil than to keep 15 wt% accurately, we decided to test the porosity and the resistivity of membranes without residual oil. In this part, a protocol to obtain 15 wt% \pm 3 wt% of oil will also be presented.

3.2.2.2.1 Oil extraction by soxhlet

The soxhlet extractor was first proposed by F.R Soxhlet in 1879 [105]. The soxhlet extractor is an automated batch extractor used for solid-liquid extraction. A scheme of soxhlet apparatus is presented in Figure 23.

A solvent of the liquid is heated and the vapor travels up to a condenser and immersed drop by drop the thimble which containing the sample. When the chamber is full, a siphon permit to clear the chamber and the solvent goes back to the distillation flask. Then, this cycle is repeated.

In order to extract the oil in the membrane, Isopropyl Alcohol (IPA with IUPAC name propan-2-ol) was used.

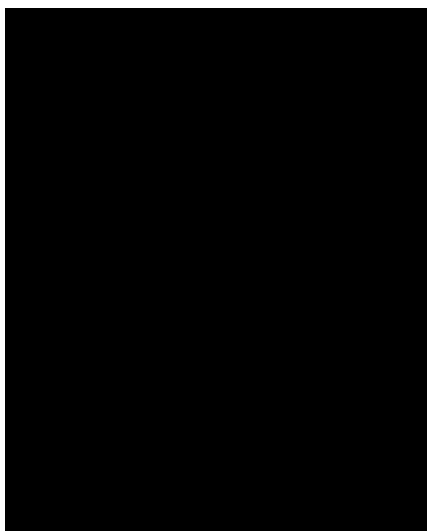


Figure 23: Conventional Soxhlet extractor (scheme adapted from [106])

After the extraction, membranes are dried in a vacuum oven at 80 °C during 2h. After this step a control by TGA is done. If the TGA analysis reveals that there is more than 1 wt% of oil in the membrane, another extraction by soxhlet is carried out. After a complete extraction and drying, there is less than 1 wt% of residual oil and around 3 wt% of IPA.

3.2.2.2.2 Oil extraction in a bath Oil/solvent

Classical industrial PE-separators have around 15 wt% of oil. In the present work, an empirical study has shown that the residual amount of oil after extraction in the membranes can be controlled.

In this study a sample of 0.1 g of membrane was immersed during 10 min in a blend of IPA and naphthenic oil. The sample was then dried in a vacuum oven at 83 °C during 2 hours. Finally a TGA analysis is used to determine the residual amount of oil in the membrane. The total volume of the blend was 50 ml and the weight percentage of naphthenic oil in the IPA/oil blend varies between 0 to 15 wt%. Moreover this test was also done on a membrane of 12x12 cm but in a volume of 800 ml. This high quantity of solvent is necessary to fully immerse the membrane without damage it and to be able to neglect the quantity of oil in the membrane. The membranes were elaborated in the internal mixer with a silica grade Z1165 and Si/PE = 2.5 and Oil/PE = 7.5. The results of this study are presented in Figure 24.

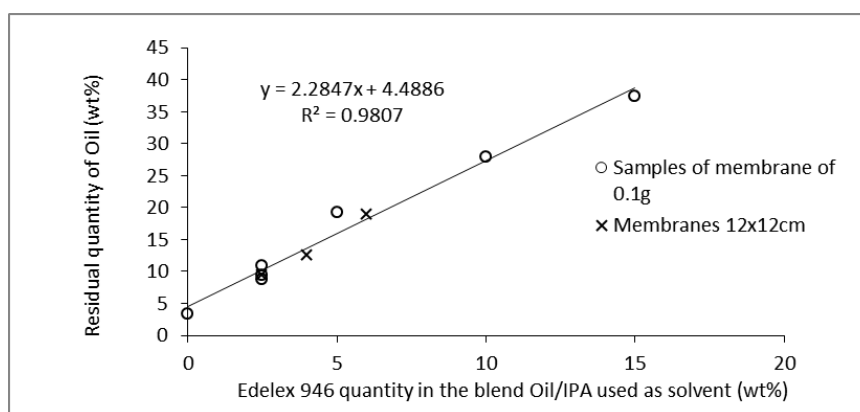


Figure 24: Correlation between residual quantity of oil in the membrane after extraction and the purity of the extraction bath

As it can be seen, the residual quantity of oil in the membrane can be easily controlled. Despite this good relationship, it is well known that the amount of oil in the membrane affects the properties of separators. Moreover, this extraction technique implies a strict control of the sample by TGA (ThermoGravimetric Analysis) after extraction to be sure of the residual quantity of oil. Moreover, the method used to control the residual quantity of oil in the membrane is using a quite huge amount of solvent. Having regards to those limitations, a full extraction of the oil by soxhlet has been preferred.

3.2.3 STRUCTURAL AND PHYSICOCHEMICAL CHARACTERIZATION OF MATERIALS

3.2.3.1 Thickness measurement

The measurement of the thickness of the separator is required to determine the electrical resistivity value. The thickness determination is carried out according to the Battery Council International (BCI) recommendations [107], using a model 49-56 digital micrometer from Testing Machines Inc..

A gauge with a circular upper contact foot of 9.5 mm in diameter exerts a pressure of 2.1 kPa on the sample. A measurement without separator is realized to calibrate the 0 mm thickness. Then, the sample is loaded under the gauge and an automatic measurement of the thickness of the membrane is performed with a precision of 1 μm . The backweb thickness of the separator is measured at the middle of each edge, each corner and at four points in the center. Then the average of the twelve measurements is used to define the thickness of membranes.

3.2.3.2 Thermal analysis

Thermogravimetric analysis (TGA) has been used to control the amount of each component in the membranes at different steps of the process. Moreover, DSC combined with TGA have been used to understand the influence of the naphthenic oil and precipitated silica on the UHMW-PE crystallization process.

3.2.3.2.1 TGA (*Thermogravimetric analysis*)

A TGA Q500 TA Instrument was used to determine the real composition of each membrane. Samples were heated from 30 °C up to 550 °C at a heating rate of 8 °C/min. The heating rate of 8 °C/min makes it possible to distinctly differentiate the weight loss of oil and the weight loss of polyethylene. Thus, the mass of polyethylene (m_{PE}), Oil (m_{oil}), silica (m_{Si}) and IPA (m_{IPA}) were obtained. The corresponding weight percentages of polyethylene ($PE_{wt\%}$), Oil ($Oil_{wt\%}$) and silica ($Silica_{wt\%}$) can be deduced with the help of the weight of the initial sample.

Besides, in some cases, In order to accurately determine the actual quantity of each material in the used DSC pans, these were perforated before proceeding to thermogravimetric analyses.

3.2.3.2.2 DSC (*Differential Scanning Calorimetry*)

Samples of membranes or raw materials were analyzed using a Pyris Diamond DSC instrument (Perkin Elmer). The sample was first heated from 30 °C up to 165 °C at a heating rate of 20 °C/min and maintained at this temperature for 2 minutes. This step is crucial for erasing and controlling the thermal history. Then, the sample was cooled down to 30 °C at a cooling rate of 10 °C/min in order to characterize the crystallization. Thereafter, the crystallization temperature (T_c) will be considered at the peak onset. Finally the sample was again heated up to 165 °C at 20 °C/min in order to obtain the melting enthalpy values of the blend (ΔHm_{Blend}) and the corresponding melting temperature (T_m) which will be taken at the peak maximum.

A DSC analysis has been done on the EDELEX 946 and has shown no variation on the baseline in this range of temperature. Thus, only the polyethylene provides some variation of the signal during the DSC experiment.

The DSC analysis, combined to the TGA experiment, is used to measure the crystallinity (χ_c) of the polyethylene in the blend. In order to determine the actual melting enthalpy corresponding to the polyethylene into the blend (ΔHm_{PE}), TGA results are used to normalize the melting enthalpy of the blend obtained by DSC by the amount of polyethylene:

$$\Delta Hm_{PE} = \frac{\Delta Hm_{Blend}}{PE_{wt\%}} \times 100 \quad [J/g] \quad \text{Equation 4}$$

The polyethylene crystallinity in the blend is calculated by the following equation with a value of the heat of fusion (ΔH_f°) of the purely crystalline polyethylene of 293 J/g [45]:

$$\chi_c = \frac{\Delta Hm_{PE}}{\Delta H_f^\circ} \quad \text{Equation 5}$$

3.2.3.3 Analysis of dispersion and distribution of the precipitated silica by microscopy.

3.2.3.3.1 Optical Microscopy

Two kinds of optical microscopy were used in this thesis work.

A combined transmitted and reflection visible light microscopy was used to qualitatively evaluate the dispersion of precipitated silica in membranes. A sample of membrane without oil was observed with a Leica M205A microscope at a magnification of x160.

A polarized light microscope was used to reveal the polyethylene crystallites. Under polarized light, only the crystalline phase can lead to some transmitted light. Thus, the crystallization of polyethylene during cooling can be followed [108]. This work was done with the help of a LEICA DM 2700M microscope and Mettler TOLEDO FP82HT hot stage. Thus, the isothermal crystallization of membranes at various temperatures (between 105 °C and 115 °C) has been studied. The intensity of the transmitted signal as recorded during the isothermal crystallization. When the intensity raised a plateau, the crystallization is considered as finished. A usual evolution of the intensity during the isothermal crystallization of membranes is presented in Figure 25.

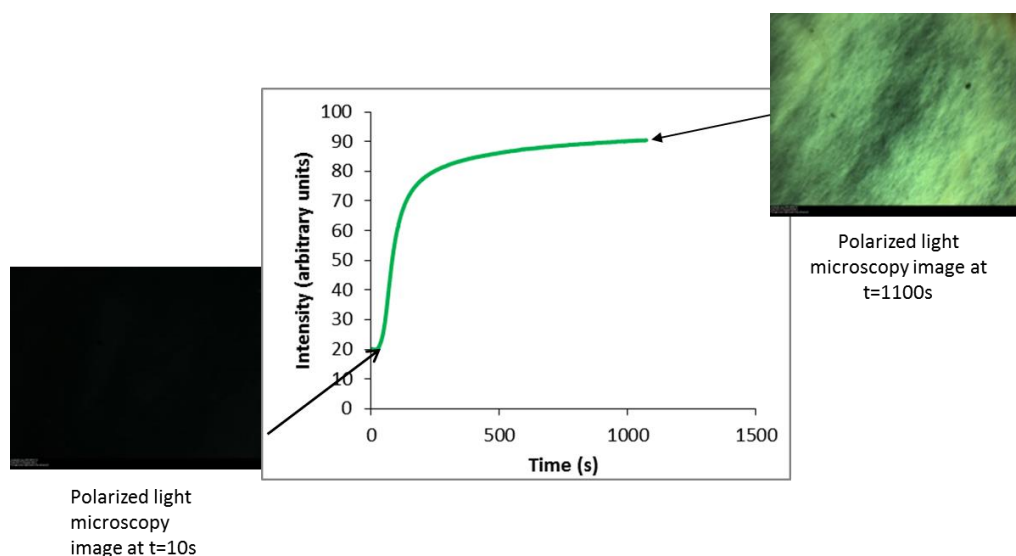


Figure 25: Evolution of the intensity during an isothermal crystallization at 108 °C of a membrane with Si/PE=2.5 and Oil/PE=7.5

After the experiment of isothermal crystallization, samples were analyzed by DSC and SEM analyses.

3.2.3.3.2 Scanning Electron Microscopy

Field emission scanning electron microscopy (SEM, Quanta 200Feg) was used to observe surfaces or fractured surfaces of membranes. In the case of fractured surfaces observations, the membranes were immersed in liquid nitrogen for 5 min prior to fracture. The samples prepared for SEM were coated by a layer of 10 nm of gold-palladium prior to imaging in order to limit static charging.

3.2.3.4 Membranes porosimetry

The porosity of membranes is a key parameter for the battery separator application. Thus, the measurement of the porosity of membranes was an essential part of this work. In this section, the measurements of porosity and associated equations will be presented.

3.2.3.4.1 Mercury porosimetry

Mercury intrusion porosimetry technique is based on the theory that a nonwetting liquid will only intrude the porosity under pressure [109–111]. Therefore, the mercury will only penetrate the pores if it is forced to do it. The surface tension (γ) between the sample and the mercury is approximated to 0.485 N.m⁻¹ and the contact

angle (ϑ) between the mercury and the sample is estimated to 140 °. The entry to pore spaces with a diameter D [μm] requires applying a pressure P [Pa] according to the following equation:

$$D = \frac{-4\gamma\cos\theta}{P} \text{ } [\mu\text{m}] \quad \text{Equation 6}$$

In the mercury intrusion porosimetry, the pores are assumed to be cylindrical, regular and interconnected. The data of intruded volume of mercury inserted versus the applied pressure are obtained and according to Equation 6 the pressures are converted to pores size.

A MICROMERITICS Autopore 9520 with penetrometers n°7 of volume V_{iHg} was used to obtain the pores size distribution and the porosity by mercury intrusion (ε_{Hg}). The membranes sample of around 100 mg were dried at room temperature during 1 day and then weighed and analyzed in the Autopore 9520. The porosity volume of the sample is equal to the volume of mercury having penetrated (V_{pHg}) which is different from the total volume of mercury inside the penetrometer V_{totHg} during the porosity measurement. Finally, ε_{Hg} can be defined as presented in Equation 1.

$$\varepsilon_{Hg} = \frac{V_{pHg}}{V_{bulk}} = \frac{V_{pHg}}{V_{iHg} - V_{totHg}} \quad \text{Equation 7}$$

Where V_{bulk} is the volume of the samples.

3.2.3.4.2 Porosimetry density kit

A density kit is a tool usually used to determine the density of sample. Another use of a density kit is to determine the porosity of a sample. Photography of the density kit used is presented in Figure 26. The use of the density kit to determine the porosity is inspired from the Battery Council International technical Manual [107].



Figure 26: Picture of the density kit used [112]

Two solvents were used with the density kit: Isopropyl Alcohol (IPA) and distilled water.

The isopropyl alcohol porosity (ε_{IPA}) was obtained with the use of a METTLER TOLEDO's density kit scales combined with a ML 303T analytical scale. First, a sample of diameter 24 mm was taken from membranes, then it was dried in a vacuum oven at 83 °C during one day and weighed just afterwards to obtain the dry weight w_1 . Then, the sample was immersed into IPA at room temperature during one hour and weighed into IPA, with the help of the density kit, in order to obtain the wet weight in isopropyl alcohol w_{ipa2} . The sample was then removed from the support and carefully cleaned from the excess of IPA with a tissue. After that, the sample was immediately weighed in air to obtain the IPA wet weight in air (w_{IPA3}). Then, ε_{IPA} is obtained from Equation 8:

$$\varepsilon_{ipa} = \frac{w_{ipa3} - w_1}{w_{ipa3} - w_{ipa2}} \quad \text{Equation 8}$$

The volumetric mass density is the density of the “skeleton” of the membranes. The volumetric mass density has to be distinguished from the bulk density. The bulk density is defined as the total dry mass (w_1) divided by the total volume of material (v_{bulk}), where v_{bulk} including the volume of pores (v_{pores}) in the bulk. The volumetric mass density (D_{vm}) is defined as m_{bulk} divided by the volume of material (v_m) as described in Equation 9.

$$D_{vm} = \frac{w_1}{v_m} = \frac{w_1}{(v_{bulk} - v_{pores})} \quad [g.cm^3] \quad \text{Equation 9}$$

There are two ways to obtain D_{vm} . The first one is to use the density of the raw materials used and their amount in the blend. The second way is to use a density kit with a liquid which saturates every pore in the membranes.

Thus, from the data obtained by TGA and the density of raw material, D_{vm} can be calculated as in Equation 10. Because the membranes contain only traces of IPA and oil, their amounts are not taken into account to obtain D_{vm} .

$$D_{vm} = \frac{m_{Si} + m_{PE}}{\frac{m_{Si}}{d_{Si}} + \frac{m_{PE}}{d_{PE}}} \quad [g.cm^3] \quad \text{Equation 10}$$

Further, by assuming that the porosity measurement with the help of the density kit is realized in a liquid (with a density d_{liq}) which saturates every pore in the membranes; three measurements are obtained: w_1 (dry mass), w_{liq2} (value obtained with the sample weighed immersed) and w_{liq3} (value obtained with the sample wet

and weighed in the air). If such a solvent exists, it is possible to obtain D_{vm} from Equation 11.

$$D_{vm} = \frac{w_1}{w_1 - w_{liq2}} \times d_{liq} \quad [g.cm^3] \quad \text{Equation 11}$$

The Water porosities were also obtained with the METTLER TOLEDO's density kit.

The same samples as for the isopropyl alcohol porosity measurement were used. The sample was dried into a vacuum oven at 83 °C during 1 day. Then the sample was immersed into boiling distilled water during 10 min and, soon after, placed into distilled water at room temperature for 1 min. Afterwards, the sample was weighed into distilled water with the help of the density kit, in order to obtain the wet weight in water w_{w2} . The sample was then removed from the support and carefully cleaned from the excess of water with a tissue. After that, the sample was immediately weighed in air to obtain the water wet weight in air (w_{w3}).

Two kinds of porosity were measured with the density kit in water, the wet water porosity (ε_{ww}) and the nonwet water porosity (ε_{nw}). When the membranes are fully immersed into water, ε_{ww} is the part of the membranes porosity which is wettable by water and ε_{nw} is the part which is nonwetable and where the pores are filled only by air. ε_{ww} is obtained from Equation 12 and ε_{nw} is obtained from Equation 13.

$$\varepsilon_{ww} = \frac{w_{w3} - w_1}{w_{w3} - w_{w2}} \quad \text{Equation 12}$$

$$\varepsilon_{nw} = \frac{w_1 - w_{w2} - (w_1/D_{vm})}{w_{w3} - w_{w2}} \quad \text{Equation 13}$$

3.2.3.5 Electrical resistivity and Tortuosity measurements

The electrical resistivity of battery separator is a key property of the membrane. Thus, the determination of the membranes resistivity was an important part of this work. Moreover, the resistivity determination combined with the porosity measurement gives information on the tortuosity of the membranes. The electrical resistivity measurement and the tortuosity determination will be detailed in this section.

3.2.3.5.1 Electrical resistivity (Palico system)

A Palico system was used to obtain the membranes electrical resistivity (ρ) as recommended by the Battery Council International (BCI) in the section BCIS-03B of the BCI battery technical manual [107]. A photography of the Palico system and a schema of the top view of the electrical connections are presented in Figure 27.

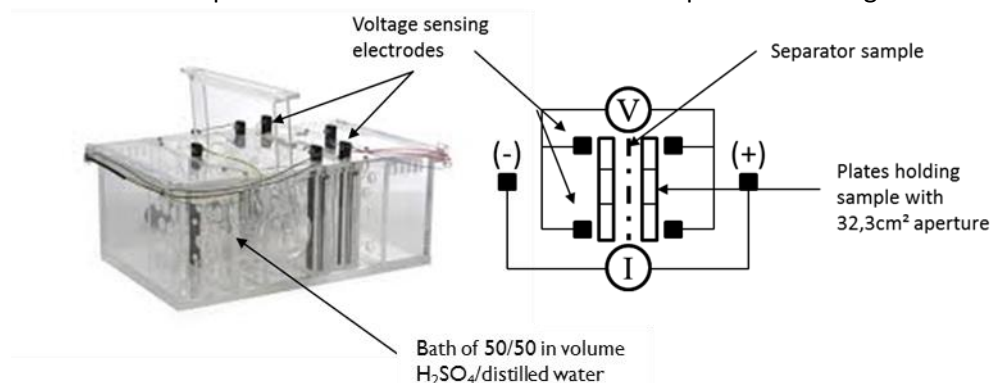


Figure 27: Photography of the Palico system and a schema on top view of the electrical connections

The Palico sends a 83 msec pulse of +100/-100 mA through the current delivery electrodes. Then, the response to the current is obtained by the voltage sensing electrodes. The difference in voltage drop, with and without a separator in the ionic current path, is used to calculate resistance of the separator.

The membrane samples of a minimum size of 120 mm x 120 mm with a thickness (e) were first immersed into boiling distilled water during 10 min. Afterward, the excess of water was removed carefully with a tissue and the sample was then immediately immersed in the electrolyte (a 50/50 blend in volume of water and sulfuric acid $d= 1.28 \text{ g.cm}^{-3}$) for 10 minutes at 27 °C. After soaking, the sample was transferred to the storage compartment of the Palico bath for 10 min at $26.7 \text{ °C} \pm 2.2 \text{ °C}$. Soon after, the sample was put in the measure compartment in order to obtain the electrical resistance ($R [\Omega]$) of the sample. The measurement cell is a disk with a surface area (A) of 32.26 cm^2 . The resistivity of the sample is obtained by Equation 14. In this equation, f is a correction factor between 0.96 and 1.03 which evolves linearly as function of the bath temperature.

$$\rho = \frac{R}{e} \times f \times A \quad [\Omega.m] \quad \text{Equation 14}$$

It is also important to notice that the terms “resistance of the separator” are generally used in the battery separator industry. In fact, the measured resistance is the resistance of the electrolyte inside the porous structure. The protocol of tortuosity determination is presented below.

3.2.3.5.2 Determination of Tortuosity

The tortuosity factor (τ) in microporous membranes is the ratio of the mean actual path of the ion in comparison with the direct distance [16]. The tortuosity can be expressed by:

$$\tau = \frac{l_s}{e} \quad \text{Equation 15}$$

In Equation 15, l_s is the ion path through the separator and e is the thickness of the membrane. Obviously, the tortuosity affects the resistivity of a battery separator. The Mac Mullin number is one way to obtain the tortuosity of a battery separator.

The Mac Mullin number is the ratio of the resistivity of the separator (ρ) on the resistivity of the electrolyte (ρ_e) [7,17,113] as described in Equation 16 where σ_e is the specific conductivity of the electrolyte. Moreover the Mac Mullin number is also equal to the ratio of the squared tortuosity divided by the porosity (ε) of the membrane. The mac Mullin number describes the relative contribution of a separator to the cell resistance. In the Mac Mullin number approach, the membranes are assumed to be fully wetted by the electrolyte.

$$N_m = \frac{\rho}{\rho_e} = \rho \times \sigma_e = \frac{\tau^2}{\varepsilon} \quad \text{Equation 16}$$

In the Palico system, the specific conductivity or the resistivity of the electrolyte is considered as known [107]. At 27 °C the resistivity of the electrolyte (Sulfuric acid/distilled water blend with $d = 1.26 \text{ g.cm}^{-3}$) is equal to $1.26 \text{ } \Omega.\text{cm}$ [107].

Thus, from Equation 14 and Equation 16 it is possible to obtain Equation 17.

$$\rho = \frac{\tau^2}{\varepsilon} \times \frac{1}{\sigma_e} \quad [\Omega.m] \quad \text{Equation 17}$$

Finally, with measurements of the resistivity and of the porosity, it is possible to obtain the tortuosity of the membranes. A good control of the temperature and of the density of the bath during the electrical resistivity measurements are extremely important to obtain an accurate value of the tortuosity of membranes.

RESUME DU CHAPITRE 3

Ce chapitre présente les matériaux, les procédés d'élaborations des membranes ainsi que les techniques de caractérisation utilisées au cours de ce travail de thèse.

Trois grades de polyethylenes ont été utilisés, un polyéthylène de ultra haute masse molaire (GUR 4150), un HDPE (HDT10) ainsi qu'un L-LDPE (TM50-U). Une huile de type naphténique (EDELEX 946) a été utilisé comme diluant. Pour finir trois grades de silice précipitée Solvay ont été utilisés : le grade Z1165, le grade T43 et le grade Z175.

L'élaboration des membranes se réalise en 4 étapes :

1. La préparation d'un prémix
2. Le mélangeage à chaud en mélangeur interne ou en extrusion
3. La mise en forme des membranes sous presse
4. L'extraction d'huile par soxhlet.

Les membranes sont ensuite caractérisées par des techniques d'analyses variées :

- Mesure d'épaisseur
- Analyses thermiques (DSC et ATG)
- Microscopie (Optique ou électronique)
- Porosimétrie (par intrusion au mercure et/ou en kit de densité)
- Résistance électrique (Système Palico)

4 INFLUENCE OF THE FORMULATION AND COOLING RATE ON THE CRYSTALLIZATION OF MEMBRANES

The crystallization of PE/blends has been studied in the literature. Moreover crystallization of UHMW-PE/mineral oil systems has been also well studied. This chapter presents the results of this thesis work focused on the crystallization of the UHMW-PE in UHMW-PE/oil and UHMW-PE/oil/precipitated silica systems.

4.1 INTRODUCTION

The unique properties of the UHMW-PE described in the literature are attributed at the very high molar mass of the UHMW-PE. In this work, in order to understand the impact of the molecular parameters of the UHMW-PE on its crystallization, other classical polyethylenes have been used: a HDPE (linear polyethylene) to understand the impact of the molar mass and a L-LDPE, a linear polyethylene with ethylene branches, to introduce the influences of branches. The influence of the cooling rate on the crystallization of polyethylene will be also discussed in this chapter. The main part of the following results have been already published in Polymer [114].

4.2 EFFECT OF THE FORMULATION ON THE UHMW-PE CRYSTALLIZATION

In this part of the chapter, the indirect or direct effect of the formulation on the UHMW-PE crystallization will be discussed.

4.2.1 *EFFECT OF THE FORMULATION ON THE COMPOSITION OF THE BLENDS AFTER PROCESS*

The first objective of this study was to observe a possible nucleating effect of the precipitated silica on the UHMW-PE. Thus, samples were formulated with a same ratio oil/PE and various Si/PE ratios using the Z1165 precipitated silica grade. Homogeneous PE/oil/Silica blends were prepared in an internal mixer (Haake™ Rheomix) using roller rotors. The samples were molten at 165 °C with a rolling speed of 60 rpm during 12 min and a chamber filling factor of 80 %. The blends were then cooled at room temperature. The Si/PE mass ratio varies from 0 to 3 while the oil/PE ratio was fixed to 7.5 for all these blends with silica. Exact formulations of the blends studied are presented below.

Si/PE (mass ratio)	Precipitated Silica (Z1165) (g)	UHMW-PE (g)	Oil Edelex 946 (g)
0	0.0	5.9	44.3
0.25	1.5	5.8	43.7
0.5	2.9	5.8	43.1
1.0	5.6	5.6	42.0
2.0	10.6	5.3	39.8
2.5	13.0	5.2	39.0
3.0	15.2	5.1	37.9

Table 4: Formulation of UHMW-PE/oil/precipitated silica blends elaborated

Nevertheless, it is important to notice that the oil/PE ratio in the *process samples* is not necessarily equal to the setpoint after process. In fact, during the process at 165 °C, PE and naphthenic oil are described as miscible, but after cooling, due to the phase separation, a loss of oil by exudation can happen. By looking at the sample just after the cooling, it is possible to notice that small quantities of oil exude from some blends. However, as shown in Figure 28, which shows the composition of the blends measured by TGA after process, the precipitated silica helps to avoid the oil exudation. Hence, from a mass ratio Si/PE of 2, the initial oil/PE ratio of 7.5 (represented with a dashed line in Figure 1) is maintained whereas, without silica, the oil/PE ratio after process falls down to only 2.3. Due to its intrinsic porous structure, the use of silica as filler to prevent exudation in blends is very helpful. In these formulations, the silica is crucial to keep all the oil inside the blend during and above all after cooling. Obviously, for a higher desired amount of oil, the necessary precipitated silica quantity should be higher. In Figure 28, it can be also seen that the measured Si/PE is slightly smaller than the desired Si/PE in the formulation. This diminution can be explained by the initial presence of water in the precipitated silica, which is lost during the mixing process at high temperature.

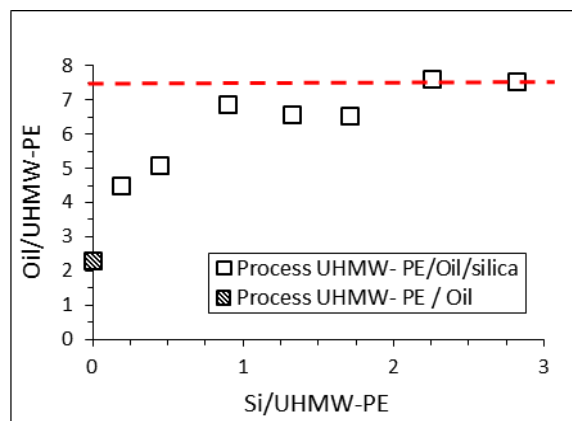


Figure 28: Variation of oil/PE weight ratio after process as a function of Silica/PE weight ratio inside the blend (dashed line is the oil/PE ratio before process).

Blends performed in an internal mixer are called “process sample” in this study. Using HDPE and L-LDPE, other process samples were performed in this work.

In order to obtain additional different ratios of dilution of PE in oil, other kind of samples called “suspension samples” have been prepared by simply mixing PE and oil in a mortar at room temperature, leading to suspensions of polyethylene powder with volume fractions of naphthenic oil (ϕ_{oil}) ranging from 0 to 0.9.

4.2.2 EFFECT OF THE FORMULATION ON THE UHMW-PE CRYSTALLIZATION

Figure 2 shows typical DSC results for the studied blends at a cooling rate of 10 °C/min and a heating rate of 20 °C/min. In Figure 2a, which corresponds to the re-crystallization after the first melting, the crystallization temperature is shifted to lower temperatures when increasing the oil/PE ratio. In the same way, as it can be seen in Figure 2b, T_m is also shifted to lower temperature with the increase of oil/PE ratio.

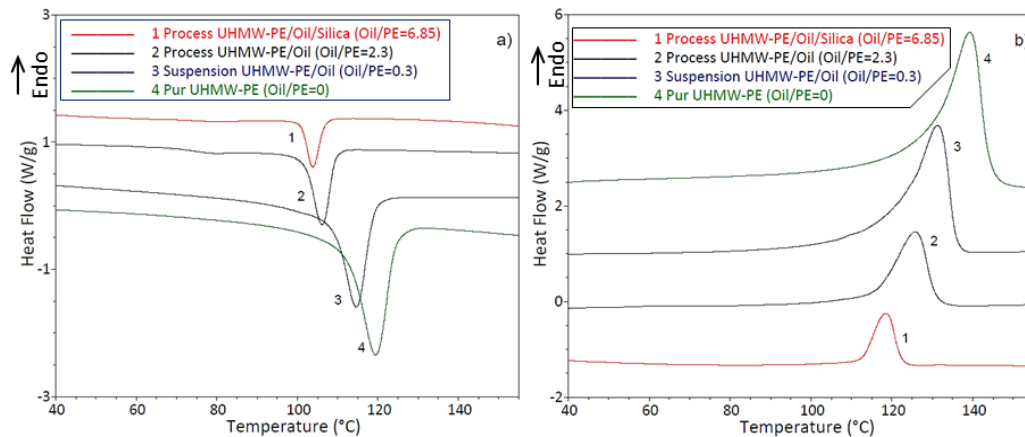


Figure 29: Example of DSC results: a) First cooling curves after melting b) Second heating curves.

These results are very similar to the diminution of crystallization temperature observed by Zhang *et al.* in UHMW-PE/ liquid paraffin systems [39]. It is important to keep in mind that the amount of polyethylene is not the same in each samples presented in Figure 29. Thus it is not possible to directly compare the crystallinity of each samples by the area developed under curves.

The melting temperatures of all studied samples are presented in Figure 30 as a function of their respective oil/PE ratio.

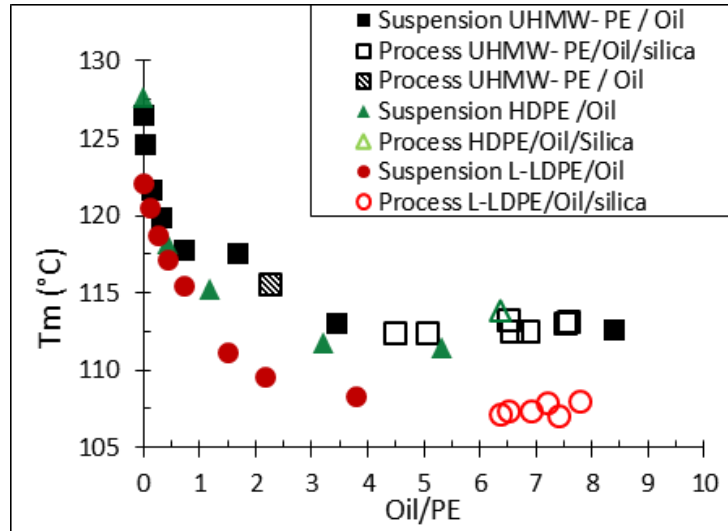


Figure 30. Melting temperature as a function of oil/PE weight ratio after process.

From Figure 30 it can be noticed that, for each of the three PE in blends, T_m decreases of about 15 °C and stabilize with increasing oil content, independently of the blending process and the presence or not of silica. Moreover, the lower melting temperature observed for L-LDPE is directly linked to its lower attainable crystal thickness due to the higher branches content [115,116]. Additionally, samples with HDPE or UHMW-PE are on the same curve which indicates that the crystal thickness in both of these polyethylenes is similar.

Furthermore, as shown in Figure 30, the samples with or without silica are on the same trend. Hence the amount of the silica appears to have no direct effect on the T_m diminution. Therefore, it is reasonable to consider that this T_m diminution is only connected to the PE dilution into naphthenic oil. From this viewpoint, the results can be analyzed in the framework of the Flory-Huggins theory already presented in part 2.1.2.2 (see Equation 1).

However, in Equation 1 the equilibrium melting temperatures are very fastidious to determine for each dilution. Therefore, it is convenient to modify this equation using the Gibbs-Thomson equation which relates the actual melting point and the crystalline lamella thickness (L):

$$T_m = T_{m,Eq} \left(1 - \frac{2\sigma}{\Delta H_f \rho_c L} \right) \quad \text{Equation 18}$$

where ρ_c is the crystal density (0.997 g.cm⁻³) and $\sigma = 8.3 \times 10^{-2}$ J.m⁻² is the specific surface energy of the crystalline lamella which remains quasi-independent of the diluent [117].

Considering now that, for a given studied PE, and because of the same cooling process for all the samples, the obtained crystalline lamellae are approximately of the same thicknesses L , the bracket in Equation 18 can be considered as nearly constant [118]. Therefore, Equation 1 becomes:

$$\frac{1}{T_m} - \frac{1}{T_m^0} = \frac{RV_u}{(1-A)\Delta h_u V_d} (\phi_{oil} - \chi\phi_{oil}^2) \quad \text{Equation 19}$$

$$\text{with: } A = \frac{2\sigma}{\Delta H_f^\circ \rho_c L}$$

In the present case, only the binary blend of PE and oil has to be taken into account for expressing ϕ_{oil} because the silica is an inert phase. Hence, ϕ_{oil} is obtained from the volume content of PE (V_{PE}) and the volume content of oil (V_{oil}) as described in Equation 20.

$$\phi_{oil} = \frac{V_{oil}}{V_{oil} + V_{PE}} \quad \text{Equation 20}$$

From Equation 19, it is obvious that the plot of $1/T_{m, Eq}$ versus ϕ_{oil} should be quadratic with a curvature linked to the interaction parameter value. These types of plot shown in Figure 4 for L-LDPE, HDPE and UHMW-PE, exhibit quasi linear evolutions (only very slight curvatures might be distinguished but much lower than for $\chi=0.5$). Therefore, the interaction parameter can be considered very close to 0 which is favorable for the dissolution. For comparison, it can be mentioned that, for PE/paraffin blends analogous to the blends studied in the present work, Chen and Wolcott obtained an interaction parameter of approximately 0.06 for PE [46].

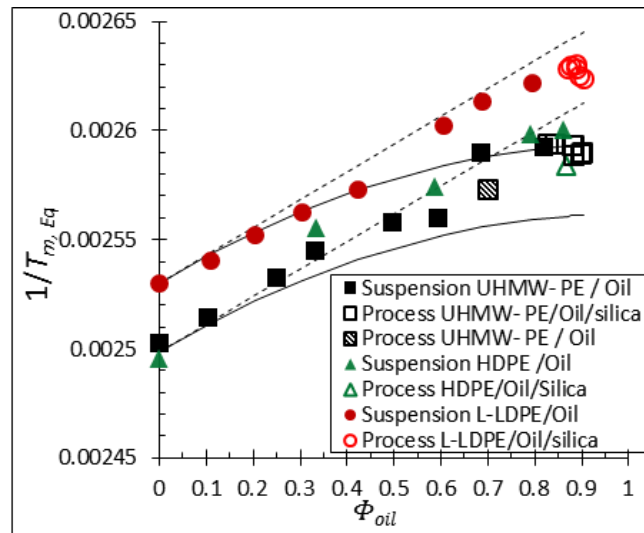


Figure 31: Inverse of melting temperature as a function of ϕ_{oil} (Lines serve as guide for eyes, dashed line for $\chi = 0$ and solid line for $\chi = 0.5$ in Equation 19).

As a result of the nature of the naphthenic oil, which is a blend of paraffins, naphthenes and aromatics [97], it is not possible to give an exact value of V_d . However, an equivalent molar volume of the diluent can be estimate by considering the slope values of the plots in Figure 31 that correspond to the prefactor of Equation 19. It must be pointed out that, using the parameters values previously given; the constant A varies only from 0.033 for HDPE and UHMW-PE to 0.047 for LLDPE. Thus, the ratio V_d/V_u is estimated from the slope values between $1.11 \times 10^{-4} \text{ K}^{-1}$ and $1.12 \times 10^{-4} \text{ K}^{-1}$. Hence, a ratio of ≈ 19 is obtained indicating that the equivalent molar volume of the diluent can be considered 19 times larger than the considered repeating unit volume of PE ($-\text{CH}_2-$). It can be concluded that, despite the several assumptions made to estimate this ratio, the obtained value appears quite consistent regarding the oil nature.

Concerning the crystallization analysis, in Figure 32, the crystallization temperatures of all studied samples are presented as a function of their respective ϕ_{oil} . Once again, for the three types of polyethylene, T_c decreases with the increase of oil content. The variation of T_c for the samples with UHMW-PE, HDPE and L-LDPE are respectively from 124 °C to 107 °C, from 121 °C to 106 °C and from 114 °C to 100 °C. Basically, T_c decreased of about 15 °C for each polyethylenes. Because the cooling rate is the same for all experiments, it can be considered in a first approximation that, the crystallization likely occur for similar quench depth (difference between the melting temperature in the polymer-oil blend and the actual temperature). Consequently this decrease of T_c is linked to the phase diagram of PE/oil and the $T_{m,Eq}$ decreasing when increasing ϕ_{oil} [46,119].

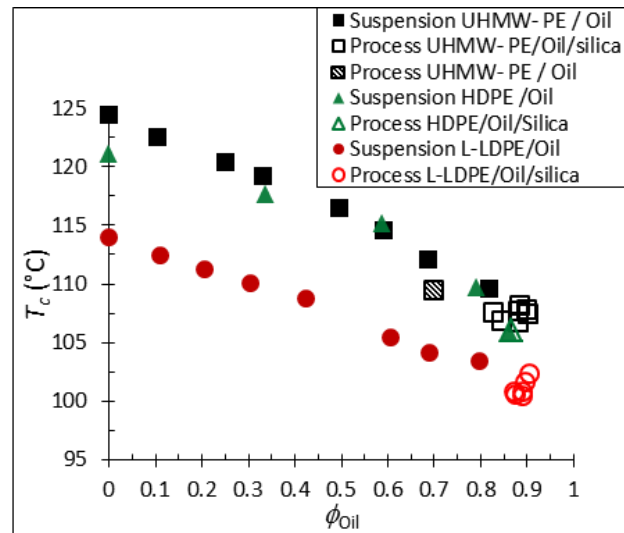


Figure 32: Crystallization temperature as a function of ϕ_{oil} .

As it can be seen in Figure 32, for samples with different weight ratios Si/PE, the crystallization temperature is almost the same. Moreover, for these samples, the volume fraction of oil varied only from 0.82 to 0.91. However, a nucleating effect of a filler on a polymer crystallization would induce an increase of the crystallization temperature at a same cooling rate [120]. Thus it appears that the silica have no nucleating effect on the UHMW-PE, HDPE or on the L-LDPE crystallization. In order to confirm this result, blends of precipitated silica / UHMW-PE without oil have been studied. The PE/ precipitated silica powder blends were simply prepared in a mortar at room temperature. Then, these blends were heated at 165 °C then cooled at room temperature two times. The final blends were analyzed by DSC and the results are shown in Figure 33. As it can be seen, the amount of silica does not have any effect on the crystallization temperature. Therefore it is clearly shown that, the precipitated silica has no nucleating effect on the UHMW-PE crystallization.

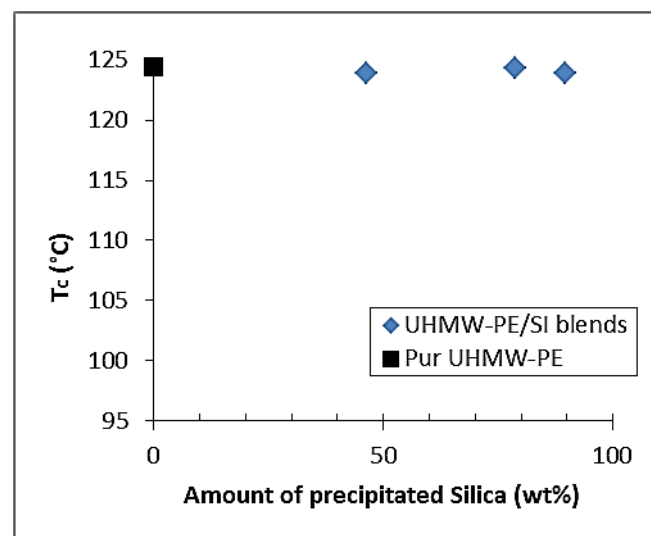


Figure 33: Crystallization temperature as a function of the amount of precipitated silica in UHMW-PE/Silica blends

As concerns the material properties after processing, it is obvious that the PE crystallinity obtained will be a crucial parameter. From our experiments, this crystallinity is analyzed on the basis of the second heating DSC curves (Figure 29b).

This crystallinity is obtained after renormalization of the peak enthalpies using Equation 4 to take into account the PE content in the DSC sample. Then, the PE crystallinity is calculated from Equation 5 .

Figure 34 shows the obtained crystallinity as a function of ϕ_{oil} for all samples. For the HDPE and the L-LDPE, there is absolutely no effect of the dilution into oil on their respective crystallinity. The samples of HDPE and L-LDPE have a crystallinity around

62.5 % and 43.5 % respectively. As expected, L-LDPE exhibits the lowest crystallinity due to the branches on the polymer chain [115,116]. Chen and Wolcott also observed that the dilution of HDPE in paraffin oil does not affect their crystallinity but they observed a slight diminution of crystallinity for L-LDPE/Paraffin oil blend [46]. However, for the UHMW-PE samples, there is obviously an influence of the dilution on the resulting polymer crystallinity.

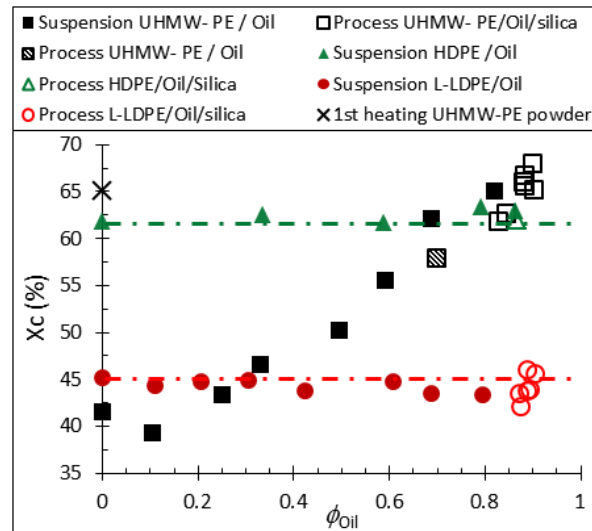


Figure 34: Crystallinity of polyethylene as a function of ϕ_{oil} .

Indeed, for UHMW-PE the crystallinity drastically increases from 40 to 65 % with the increase of oil content. This phenomenon is attributed to the ability of the solvent to provide the necessary mobility to the polymer chains leading to a more perfect crystallization. This necessary mobility is enough without diluent for classical melt PE (HDPE and LLDPE) but for the very long chains of UHMW-PE, the effect of the diluent is manifest. Process and suspension samples with or without silica are on the same trend which means that the crystallinity of UHMW-PE is directly governed by ϕ_{oil} regardless the presence of silica or the processing means. Although, by permitting higher content of oil in the blends for process samples, the precipitated silica permits to achieve indirectly a higher crystallinity than without silica. Indeed, due to its ability to absorb a large quantity of oil, the silica can retain this oil inside the material at ambient temperature while it is rejected by the PE itself because of the phase separation. In other words, the exudation of oil by the material at ambient temperature is avoided in presence of the silica. Therefore, during the process at high temperature and the following cooling, this excess of oil advantageously permits a more complete crystallization by providing even more mobility to the UHMW-PE macromolecules.

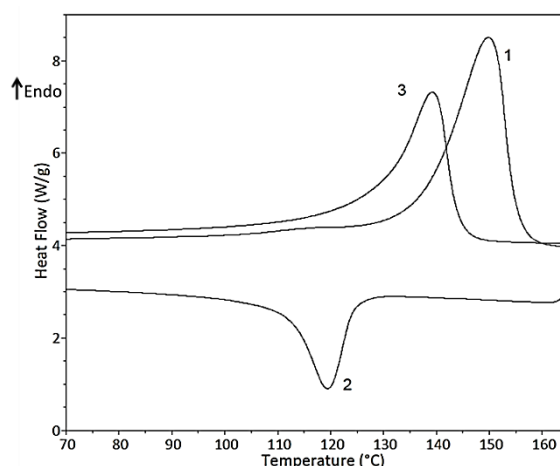


Figure 35: DSC curves for nascent power of UHMW-PE: 1) 1st heating; 2) 1st cooling; 3) 2nd heating.

In this respect, it can be added that the initial crystallinity of the nascent powder of GUR®4150 (UHMW-PE) determined by DSC was about 65 %. However, after one melting/recrystallization, the UHMW-PE crystallinity decreases to 40 % as it can be observed in Figure 35. This diminution of crystallinity after melting is commonly reported for pure UHMW-PE [87,121,122]. Indeed, the chain topology of nascent UHMW-PE powder is at low level of entanglements due to the crystallization of individual chains during the polymerization which prevents entanglement with neighbor chains [123,124].

To conclude, the formulation of UHMW-PE/oil/Silica blends prepared by thermally induced phase separation process is crucial to control the crystallinity and the properties of the resulting material. For the intended application, this is of primary importance because the crystallinity influences the durability of the PE-separator membrane. The results of the present study indicate that the amount of precipitated silica helps to keep naphthenic oil inside the UHMW-PE/oil/Silica blend during the TIPS process and to avoid exudation of oil after cooling at room temperature. However, the precipitated silica appears to have no nucleating effect on the UHMW-PE crystallization.

Moreover, UHMW-PE crystallinity is controlled by the amount of oil present in the blend. With the increase of the oil content, there is an increase of UHMW-PE crystallinity which permits to, at least, recover the initial crystallinity UHMW-PE nascent powder.

4.3 EFFECT OF TEMPERATURE CONDITIONS ON THE CRYSTALLIZATION OF UHMW-PE SAMPLE.

In this section of the chapter, the influence of the temperature conditions during the crystallization will be presented. First, the influence of a higher cooling rate than 10 °C is investigated. Then, isothermal crystallization of membranes are presented and discussed.

4.3.1 INFLUENCE OF THE COOLING RATE ON THE MEMBRANES CRYSTALLIZATION

Same samples as before are used for this study. Blends of UHMW-PE/oil/precipitated silica with silica grade Z1165, GUR®4150 as UHMW-PE and Shell Edelex 946 as oil have been studied. After the DSC analysis with a cooling rate of 10°C and before the TGA analysis, another round of DSC analysis is performed. The samples were first heated from 30 °C up to 165 °C at a heating rate of 20 °C/min and maintained at this temperature for 2 minutes. This step is crucial for erasing and controlling the thermal history. Then, the sample was cooled down to 30 °C at a cooling rate of 50 °C/min in order to characterize the crystallization. Thereafter, the crystallization temperature (T_c) will be considered at the peak onset. Finally, the sample was again heated up to 165 °C at 20 °C/min in order to obtain the melting enthalpy values of the blend ($\Delta H_{m_{Blend}}$). Thus, with this second protocol of DSC, it is possible to compare the effect of cooling rates of 10 °C/min and 50 °C/min on the crystallization of membranes. As evoked before, higher cooling rates should induce lower crystallization temperatures of the UHMW-PE. Xiang *et al.* showed that an increase of the cooling rates induces a small decrease (around 4 %) of the crystallinity of HDPE in HDPE/carbon nanotubes systems [125].

In Figure 36 a), the crystallization temperatures of samples are presented as a function of their respective ϕ_{oil} for the two cooling rates, 10 °C/min and 50 °C/min.

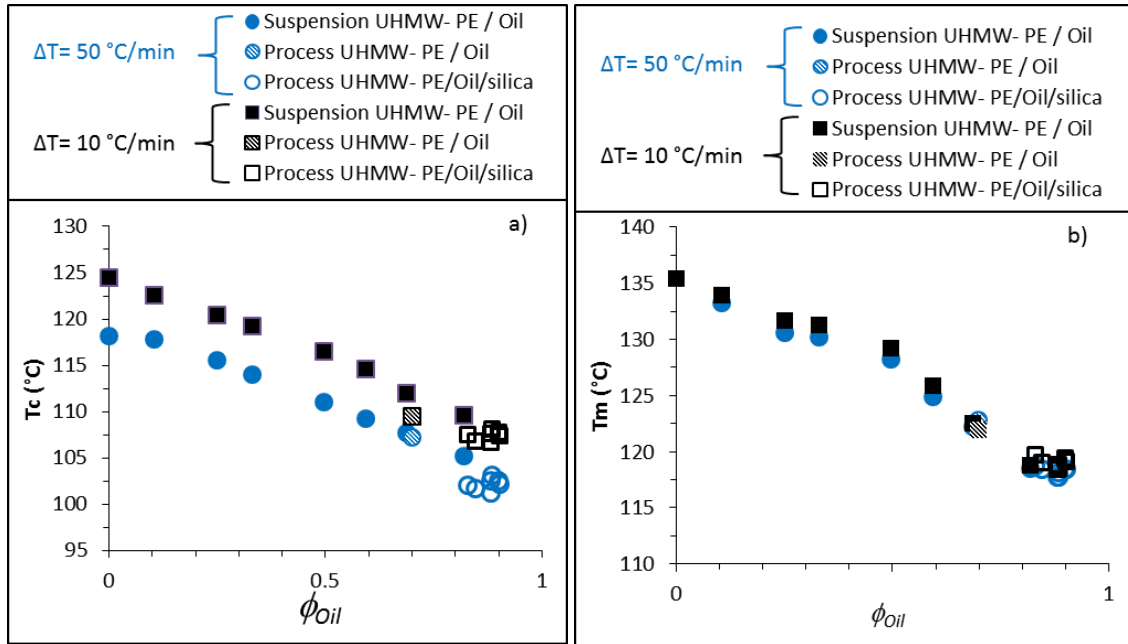


Figure 36: a) Crystallization temperature for blends with UHMW-PE analyzed at two different cooling rates, 10 °C/min and 50 °C/min. b) Melting temperature for blends with UHMW-PE analyzed at two different cooling rates, 10 °C/min and 50 °C/min.

As expected, the crystallization temperature decreases with an increase of the cooling rate. For each samples, a decrease of the crystallization temperature of around 7 °C can be observed when the cooling rates increases from 10 °C/min to 50 °C/min. These results are in agreement with the work of Zhang *et al.* They found a difference of 5 °C between cooling rate of 10 °C/min and 30 °C/min for UHMW-PE/liquid paraffin oil with 10 wt% of UHMW-PE [119]. Liu *et al.* also observed a decrease of the crystallization temperature of around 6 °C with an increase of the cooling rate from 0.2 °C to 5 °C in UHMW-PE/liquid paraffin oil blends. However, as it can be seen in Figure 36 b), this decrease of the crystallization temperature with the increase of the cooling rate is not associated to a decrease of the melting temperature. Melting temperature of samples is the same ± 1 °C after a cooling at 10 °C/min and at 50 °C/min. Thus, according to Equation 18 the same melting temperatures indicate the formation of crystals of polyethylene with the same size in the blend for both cooling rates. However, it does not provide information about the crystallinity of UHMW-PE in membrane. It is necessary to normalize the enthalpy of fusion of blends by the amount of polyethylene in blends and the enthalpy of the heat of fusion (ΔH_f°) of the purely crystalline polyethylene to obtain the crystallinity of sample. These results of crystallinity are presented in Figure 37.

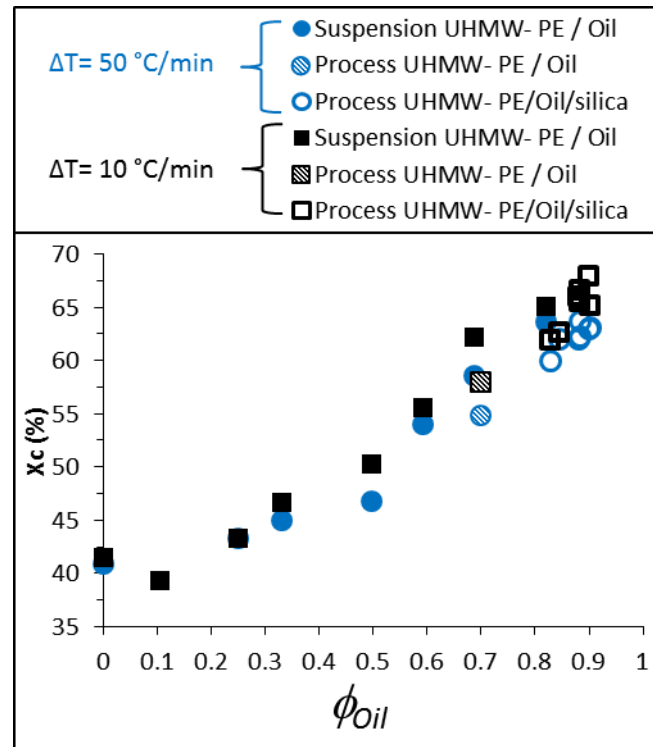


Figure 37: Crystallinity for blends with UHMW-PE analyzed at two different cooling rates, 10 °C/min and 50 °C/min.

Once again, the precipitated silica appears to not have any effect on the crystallinity. Which is almost the same for each sample whether for a cooling rate of 10 °C/min or 50 °C/min. A small difference of crystallinity, around 3 % can be observed when the volume fraction of oil is higher than 0.6. Even if these 3 % of crystallinity variation are not really significant regarding the accuracy of the measurement of about 2 %, it could be admitted that, at high dilution of the UHMW-PE in oil, the cooling rate have a very small impact on the crystallinity. However at small dilution, the mobility of chains is already really low in the blends. Thus, the cooling rate does not influence the crystallinity of samples for low contents of oil.

To conclude, as expected the cooling rate has an influence on the crystallization temperature of UHMW-PE in membranes. This crystallization temperature decreases of 7 °C when the cooling rate increases from 10 °C/min to 50 °C/min. However, an increase of the cooling rate from 10 °C/min to 50 °C/min has almost no impact on the crystallinity of samples.

The influence of the temperature on isothermal crystallization of membranes is presented in the next section.

4.3.2 INFLUENCE OF THE TEMPERATURE ON THE ISOTHERMAL CRYSTALLIZATION OF MEMBRANES

Nonisothermal or Isothermal crystallization of UHMW-PE/liquid paraffin oil systems have been widely studied in the literature [41,126,127]. Using isothermal crystallization, the formation of the superstructure as spherulite or shish-kebabs can be followed using optical microscopy with polarized light [116,127]. Bustos *et al.* observed the formation of spherulite with a diameter of 30 μm to 10 μm for several polyethylenes in isothermal crystallization conditions [128]. From a very dilute solution of 2 wt% of UHMW-PE in “decalin” (or decahydronaphtalene oil), Ohta *et al.* obtained isolated spherulite with a diameter of 80 μm [129].

Therefore, two membranes with a thickness of 100 μm were prepared. One of these membranes is UHMW-PE/oil blend and the other is UHMW-PE/oil/precipitated silica blend with respectively $\phi_{oil} = 0.53$ and $\phi_{oil} = 0.85$. The precipitated silica grade T43B has been used in this study. Each membrane has been cut into small samples of 1 cm^2 and heated at 165 $^{\circ}\text{C}$ for 5 min in a Mettler TOLEDO FP82HT hot stage. Then, samples are cooled rapidly to the desired temperature for isothermal crystallization. The isothermal crystallization is then followed using a polarized light microscope and recording the transmitted light. When the light intensity is stabilized, the crystallization process is considered as finished. The samples were kept at the temperature of isothermal crystallization during 5 hours. The crystallization temperatures were adapted to the blend studied. Thus, the crystallization temperatures were lower for the system with the higher volume fraction of oil (Si/UHMW-PE/oil blend).

One sample of each membrane is also quenched in an ice bath. In this section, quenched samples are compared with the isothermal crystallization samples even if they are crystallized under non-isothermal conditions at a fast cooling rate. However, the use of these quenched samples is helpful to understand the crystallization process under the conditions.

Each sample is analyzed by DSC and TGA in order to obtain the melting temperature and the crystallinity after the crystallization. The samples is first heated at 20 $^{\circ}\text{C}/\text{min}$, then cooled at 10 $^{\circ}\text{C}/\text{min}$ and a second heating run at 20 $^{\circ}\text{C}/\text{min}$ is performed. This program allowed comparing crystallization temperature and crystallinity between isothermal crystallization and controlled nonisothermal crystallization.

A polarized light microscopy picture is presented in Figure 38. This photo is really representative of the samples with or without precipitated silica studied in this thesis work. As it can be seen, none spherulitic superstructure can be distinguished.

There is no spherulite in membranes crystallized at quiescent conditions (without shear) or they are too small to be observed by optical microscopy. Zhang *et al.* also do not observed spherulitic structure in UHMW-PE/liquid paraffin oil blends during nonisothermal crystallization [43]. This single dimensional crystal growth can be related to the structure of lamellae loosely connected by tie evoked before.

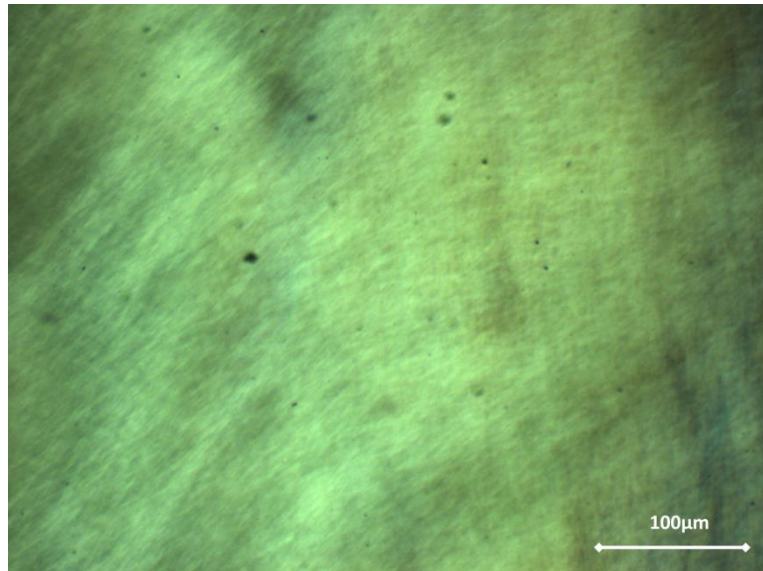


Figure 38: Optical microscopy using polarized light of UHMW-PE/oil/precipitated silica blend with $\phi_{oil} = 0.85$ after isothermal crystallization at 110 °C.

The melting temperatures obtained by DSC are presented in Figure 39. First of all, the difference of melting temperatures between membrane with and without precipitated silica can be explained by the difference of dilution state of the UHMW-PE. As presented before for non-isothermal crystallizations, the melting temperature depends on the volume fraction of oil in the blends as defined in Equation 20. The melting temperature decreases with the increase of the volume fraction of oil.

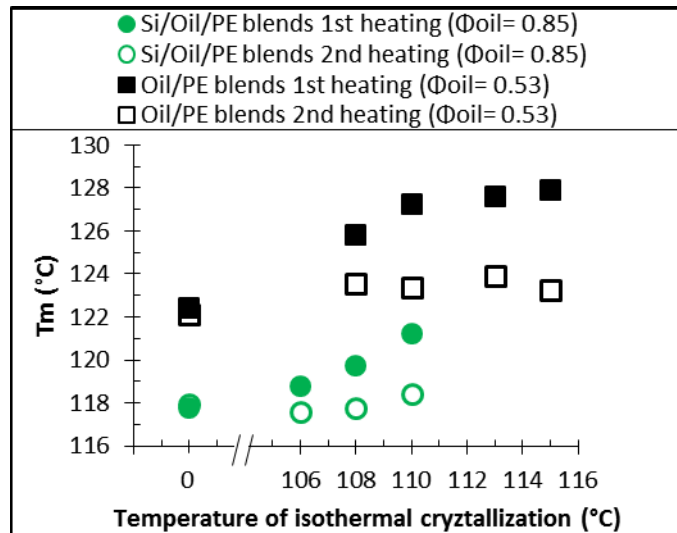


Figure 39: Melting temperature for the first heating and second heating for different isothermal temperature crystallizations (0 is for quenching in ice bath and must rather be considered as non-isothermal crystallization at high cooling rate)

As it can be seen in Figure 39, the melting temperatures obtained on the first heating and the second heating is the same for samples quenched in an ice bath. Thus, the nonisothermal crystallization in the ice bath can be assimilated to the results obtained with a cooling rate of 10 or 50 °C/min in the section 4.3.1.

Moreover, for both type of samples, the melting temperature, obtained after isothermal crystallization, increases with increasing the temperature of isothermal crystallization. Indeed, the higher is the crystallization temperature, the thicker are the obtained crystallites and the higher is the melting point. Furthermore a controlled nonisothermal recrystallization after the first melting to melting temperatures equal to this obtained after nonisothermal crystallizations (ice bath or 50 °C/min). This means that an isothermal crystallization lead to crystals with a higher thickness than a nonisothermal crystallization, whatever the cooling rate.

Once again, a higher thickness of crystal does not necessary mean a higher crystallinity in membranes. The crystallinity of the samples after isothermal crystallization and nonisothermal crystallization at 10 °C/min are presented in Figure 40.

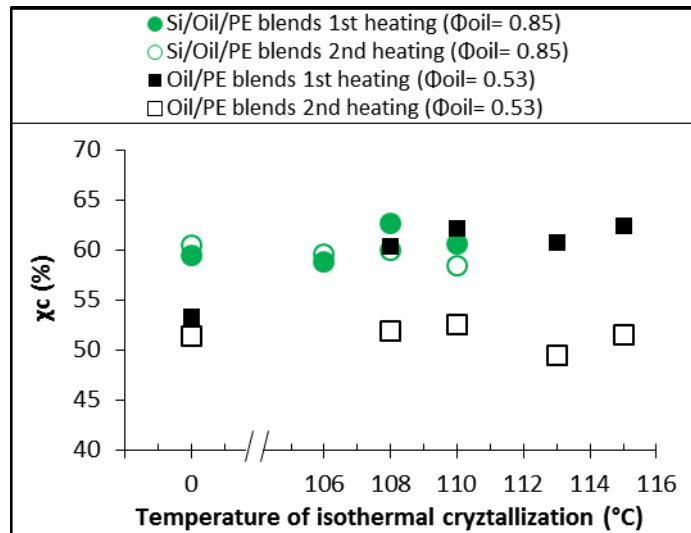


Figure 40: Crystallinity for the first heating and second heating for different isothermal temperature crystallization (0 is for quenching in ice bath and must be considered as non-isothermal crystallization at high cooling rate)

In Figure 40, it can be seen that for all UHMW-PE/oil blends (blends with $\phi_{oil} = 0.53$), the crystallinity after isothermal crystallization is around 60 % and decreases after melting and nonisothermal recrystallization to around 51 %.

Moreover, an isothermal or a nonisothermal crystallization lead to a same crystallinity of UHMW-PE in membranes. Once, again the crystallization in the ice bath induces the same results than the nonisothermal crystallization at 50 °C/ min or even at 10 °C/min. Thus, the crystallinity results obtained in DSC for studied membranes at moderately cooling rates can be extended to very high rate of cooling rates to 50 °C/min.

To conclude, for blends with a high value of ϕ_{oil} (around 0.8), the chains of UHMW-PE have enough mobility to reorganize themselves and to achieve the crystallization. Again, for membranes, these high volume fractions of oil are obtained only in presence of precipitated silica which keeps the oil in the blend during the crystallization. Moreover, for blends with low amounts of oil (typically ϕ_{oil} inferior to 0.6), the isothermal crystallization leads to a higher crystallinity than nonisothermal crystallization. During the isothermal crystallization, even if the mobility of the chains of UHMW-PE is not very high, they have enough time to reorganize themselves to complete the crystallization. However, during nonisothermal crystallization, these chains of low mobility do not have enough time to finish the crystallization.

4.4 CONCLUSION

In this study, the influence of the formulation of membranes on their crystallization has been discussed as well as the impact of the temperature conditions during crystallization. First of all, the results of the first part of this study indicate that the amount of precipitated silica helps to avoid exudation of naphthenic oil in UHMW-PE/oil/Silica blend during and after the TIPS process. However, the precipitated silica appears to have no nucleating effect on the UHMW-PE crystallization. Moreover, UHMW-PE crystallinity is controlled by its dilution in the naphthenic oil. With the increase of the oil content, there is an increase of UHMW-PE crystallinity from 40 % to 65 %. Experiences of non-isothermal or isothermal crystallizations have shown that this increase of crystallinity is due to a better mobility of chains of UHMW-PE during crystallization. The excess of oil advantageously permits a more complete crystallization by providing even more mobility to the UHMW-PE macromolecules during non-isothermal crystallization at high cooling rate.

This increase of crystallinity due to naphthenic oil and precipitated silica should have, in terms of application of the material as a battery separator, a beneficial impact on the chemical oxidation resistance in a sulfuric acid environment and the effect on the mechanical properties of the separator should be notable. To conclude, this study shows that the Si/PE weight ratio and the oil content are both governing factors for battery separator performances. They both permit to increase the crystallinity of UHMW-PE, the oil content directly by providing mobility to UHMW-PE chains and the Si/PE ratio indirectly by maintaining higher oil content in the blend.

RESUME CHAPITRE 4

Dans cette étude, l'influence de la formulation des membranes et des conditions de température sur la cristallisation y sont discutés. Dans un premier temps, cette étude met en évidence le fait que la silice précipitée permet d'éviter l'exsudation d'huile dans le mélange UHMW-PE/ huile/silice pendant et après la séparation de phase. De plus la silice précipitée n'a pas d'effet nucléant sur la cristallisation de l'UHMW-PE. La cristallinité de l'UHMW-PE est contrôlée par sa dilution dans l'huile. Avec l'augmentation de la quantité d'huile dans le mélange, on constate une augmentation de 40 à 65 % de la cristallinité de l'UHMW-PE. Des expériences de cristallisation en isotherme ou non-isotherme ont montré que l'amélioration de la mobilité des chaînes de polymère au cours de la cristallisation est responsable de l'augmentation de cristallinité de l'UHMW-PE. Une dilution plus importante de l'UHMW-PE dans l'huile permet de terminer la cristallisation en apportant une meilleure mobilité des chaînes de l'UHMW-PE lors d'une cristallisation à haute vitesse de refroidissement.

Cette augmentation de la cristallinité est un bénéfice pour l'application séparateur de batterie car elle devrait permettre d'apporter une meilleure résistance à l'oxydation. Une augmentation de certaines propriétés mécaniques (comme la résistance à la rupture) devrait également être observée.

Pour conclure, cette étude a montré que la quantité de silice et la quantité d'huile sont des facteurs contrôlant la cristallinité de l'UHMW-PE. La quantité d'huile directement en améliorant la mobilité des chaînes d'UHMW-PE et la silice indirectement en permettant de maintenir une quantité d'huile élevée dans le mélange.

5 INFLUENCE OF THE FORMULATION ON THE POROSITY AND ON THE ELECTRICAL RESISTIVITY OF MEMBRANES

In this chapter the influence of the formulation on the porosity development and on the electrical resistivity of the studied membranes is discussed. The first part presents the effect of the amount of silica on the properties of the PE-separators. The second part of the chapter discusses of how the dispersion and the distribution of the precipitated silica influences the properties of polyethylene membranes. Different hypotheses related to the effect of the dispersion state of the precipitated silica are presented and discussed. Finally, the efficiency of different grades of precipitated silica for PE-separator application is discriminated.

5.1 INFLUENCE OF THE PRECIPITATED SILICA AMOUNT ON THE MEMBRANES POROSITIES

As presented before, the amount of precipitated silica has a strong impact on mechanical and electrical properties of the PE-separators. In this part of the chapter, the effect of the amount of silica on the properties of membranes is investigated. In this study, the three grades of precipitated silica (Tixosil® 43B, Zeosil® 1165 and Zeosil® Z175) were used. However, similar results concerning the influence of the silica amount on the membranes properties have been obtained with these three grades. Thus, in order to make this chapter easier to read, only the results obtained with the grade Tixosil® 43B will be discussed. The results obtained with the grade Zeosil® Z175 and the grade Zeosil® 1165 will be presented in the appendix to avoid useless repetitions in the text.

5.1.1 *SAMPLES PREPARATION*

The ultrahigh molecular polyethylene GUR®4150 and the naphthenic Oil, Shell Edelex Oil 946 were used to produce all samples. The grades of precipitated silica were: the Tixosil® 43B (T43B), the Zeosil® 1165 (Z1165) and the Zeosil® 175 (Z175). All the precipitated silica have a density d_{Si} of 2.1 g.cm⁻³.

The PE/Oil/Silica blends were prepared in an internal mixer (Haake™ Rheomix) with Banbury rotors. Samples were prepared at 165 °C with a rolling speed of 200 rpm during 12 min and a filling factor of 80 %. Blends were then cooled down at room temperature. The Si/PE mass ratio varied from 0 to 4 (Φ_{Si} from 0 to 18.5 vol%) while the Oil/PE mass ratio was fixed to 7.5 for all these blends with silica.

Then, around 8 g of material were used to elaborate films with a thickness equal to about 280 μm by molding samples in a laboratory press at 165 $^{\circ}\text{C}$ into a square mold of 15x15 cm with a thickness of 250 μm . The applied force was 5×10^3 N during 1 min, then of 10^4 N during 2 min and finally of 125×10^3 N during 10 min. The membranes were then cooled at room temperature.

Then, a soxhlet extraction at 83 $^{\circ}\text{C}$ with IPA during 1 day was used to extract the process oil from the membranes in order to liberate the porosity.

Finally, the membranes were dried in a vacuum oven at 80 $^{\circ}\text{C}$ before analysis. After this step, there was less than 1 wt% of residual Oil and around 3 wt% of residual IPA in these membranes.

5.1.2 INFLUENCE OF THE SILICA AMOUNT ON THE POROSITY OF THE MEMBRANES

First of all, in a lot of studies, alcoholic solvents such as ethanol or IPA were used to measure the porosity of PE-membranes [41,130–132]. In the present study, the chosen alcoholic solvent was IPA. Nevertheless, to ensure that this can be a reliable way for measuring the total porosity of the membranes, the accessibility of this total porosity by IPA as the pore filling liquid is required. Furthermore, mercury intrusion porosimetry has shown to be a reliable method to determine the full membranes porosity [133,134]. Thus, the comparison between ϵ_{Hg} (porosity accessible to mercury) and ϵ_{IPA} (porosity accessible to IPA) is necessary to verify the penetration of the total porosity by the IPA. In Figure 41, this comparison is presented for samples elaborated in the internal mixer with the grade T43B as the precipitated silica.

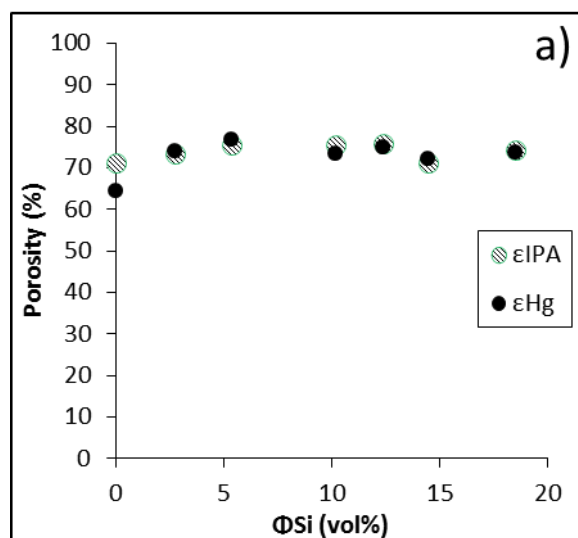


Figure 41: Comparison of ϵ_{Hg} and ϵ_{IPA} for samples produced in the internal mixer with the grade of precipitated silica T43B as a function of the volume fraction of silica in the formulation of the membranes.

As shown in Figure 41, ε_{Hg} and ε_{IPA} are equal for each sample with precipitated silica in the formulation. This means the assumption that IPA is a solvent which fully wet the porosity of the membranes is now verified, and ε_{IPA} can be considered as their total porosity. Additionally, this result involves that IPA can be considered as a liquid which verifies the conditions of Equation 13 and thus can be used to determine D_{vm} (which is the density of the “skeleton” of the membrane composed of precipitated silica and UHMW-PE). Therefore, two ways are suitable to determine D_{vm} : the first with the TGA analysis and the second with the density kit with the use of IPA as the wetting liquid. From this double check, two values of D_{vm} with less than 1 % of difference were determined. This result is crucial to avoid errors in the assessment of ε_{nw} with Equation 13. Moreover, from Figure 41, it can be also noticed that the total porosity of the membranes, around 70 %, does not depend on the amount of precipitated silica in the blend. A porosity value around 70 % is expected for industrial PE-separators [7] and Liu et al. have already reported a porosity of 60 % for UHMWPE/Oil membranes with 75 vol% of oil (without precipitated silica) [41]. As mentioned before, the formation of the porosity is due to the phase separation between UHMW-PE and naphthenic oil during the cooling after the processing [36,114]. However, some studies reported that the precipitated silica amount has a strong effect on the PE-membranes porosity [9,135,136]. Nevertheless, it must be mentioned that in these studies, the porosity was not measured using an alcoholic liquid. Thus, it appears relevant to compare ε_{IPA} with the two porosities measured using water as the penetrant liquid, namely, ε_{ww} (porosity wettable to water) and ε_{nw} (porosity nonwettable to water). This comparison is presented in Figure 42.

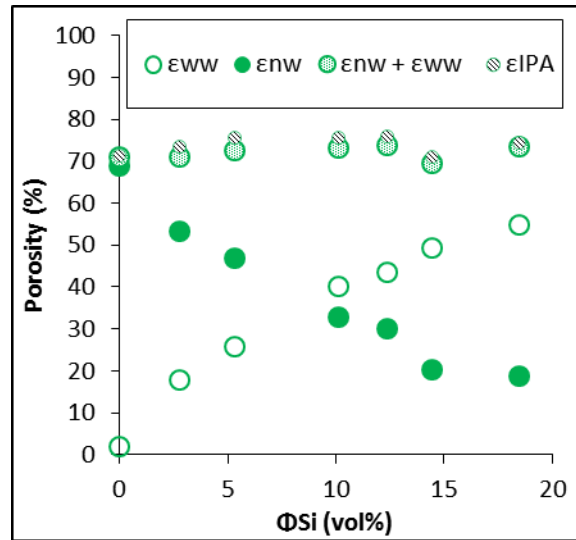


Figure 42: Comparison of water porosities and IPA porosity for samples processed using the internal mixer with the T43 grade of precipitated silica as a function of the volume fraction of silica in the formulation of the membranes.

Figure 42 highlights two significant results. The first one is that $\varepsilon_{ww} + \varepsilon_{nw}$ are always equal to ε_{IPA} . It confirms that the used procedure for the water porosities determination is highly accurate. The second is that ε_{ww} is always inferior to ε_{IPA} . This implies that all the membranes are not completely wettable by water. Moreover, as it can be seen, the more there is precipitated silica inside the blend, the more ε_{ww} increases. Furthermore, an increase of the precipitated silica amount does not mean an increase of the total membrane porosity but only an increase of the part of porosity wettable by water, the total porosity being governed by the solely oil amount. Thus, this increase of ε_{ww} with the increase of Φ_{Si} leads to the hypothesis that the fraction of porosity non wettable by water is free of highly hydrophilic precipitated silica and therefore not accessible to aqueous liquid. In that regard, as it can be seen on SEM analysis (Figure 43), some pores areas are not coated by precipitated silica. In Figure 43.b) ($\Phi_{Si}=5$ vol%) only a small part of the UHMW-PE is coated by precipitated silica. As expected, a bigger part of the membranes is coated by precipitated silica when the amount of precipitated silica is higher as shown by Figure 43.a) ($\Phi_{Si}=12.4$ vol%). Thus, the increase of the precipitated silica content in the blends leads to a better surface coating of hydrophobic PE fibrils improving the water wettability of the membranes.

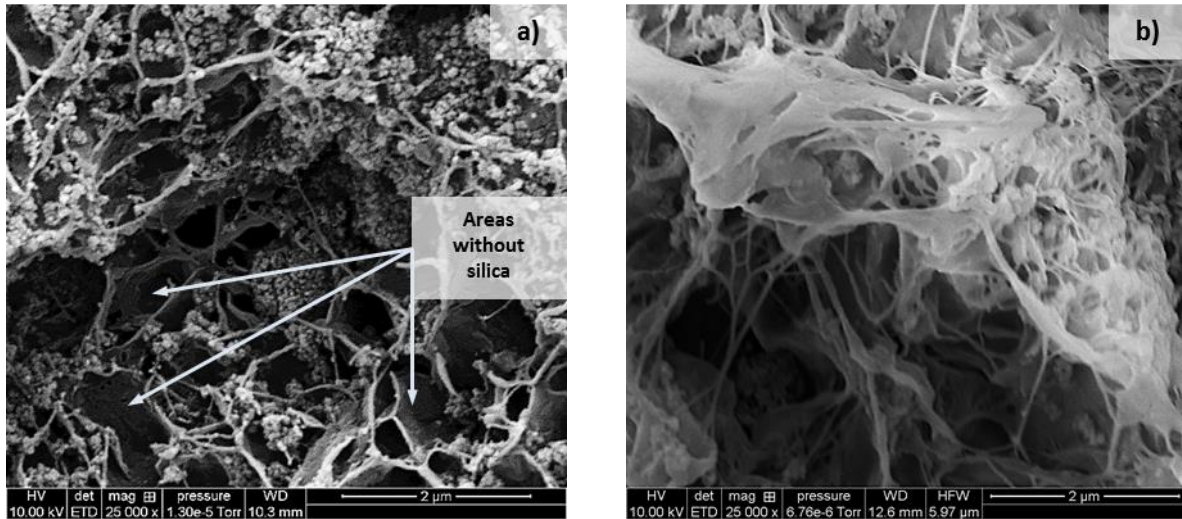


Figure 43: SEM analysis of an internal mixer membrane a) with $\Phi_{Si}=12.4$ vol% and b) with $\Phi_{Si}=5$ vol%.

Thus, regarding the hypothesis that the porosity free of precipitated silica is not accessible to aqueous liquid, it is possible to introduce an empirical parameter α characteristic of the dispersion/distribution quality of the silica inside the porous structure of the membranes:

$$\alpha = \frac{\varepsilon_{ww}}{\varepsilon_{total}} \quad \text{Equation 21}$$

Where ε_{total} is the total amount of porosity in the membrane and which can be assimilated to ε_{IPA} .

This parameter α is defined between 0 and 1: 0 for an inefficient dispersion of the mineral filler and 1 for the most efficient dispersion. As it will be seen in the next section of this chapter, the most efficient dispersion is obtained when all the pores are coated by silica. The parameter obtained α for all samples processed by internal mixer is shown in Figure 44.

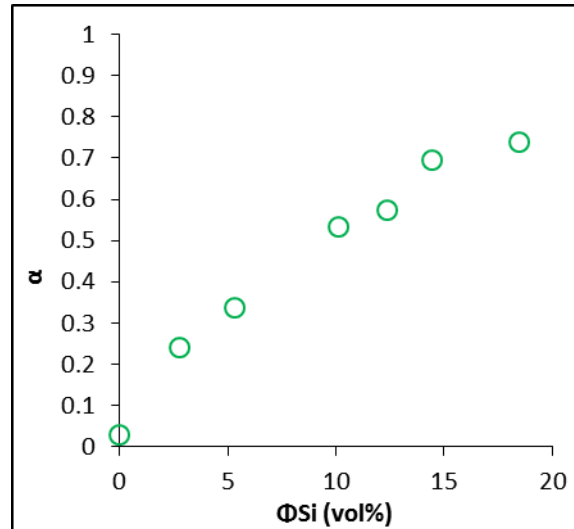


Figure 44: The parameter α as a function of the precipitated silica volume fraction in the formulation of the membranes before process for samples processed by internal mixer with the precipitated silica T43B.

As expected, the parameter α increases with the increase of the precipitated silica volume fraction. Nevertheless, for these samples processed by internal mixer, where the formulation varies, this parameter α does not provide a lot of supplementary information.

The amount of silica appears to have also an effect on the diameter of the pores. The evolution of the diameter of pores is not easy to highlight in SEM analysis but could be seen more easily with a pore size distribution obtained by mercury intrusion porosimetry. A pore size distribution obtained by mercury porosimetry is presented in its usual form in Figure 45, for samples elaborated thanks to the internal mixer with the T43B grade.

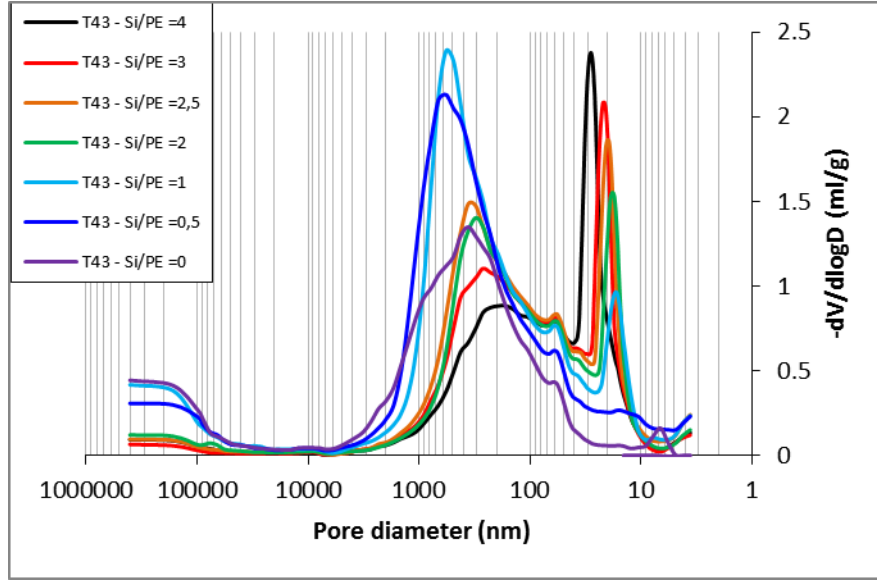


Figure 45: Differential pore size distribution for samples elaborated thanks to the internal mixer with the grade T43 of precipitated silica.

In Figure 45, the increase of the Si/PE mass ratio in the formulation of membranes has several effects on the differential pore size distribution of the studied membranes. In fact, it is not so obvious to compare the different curves because the y-axis is in ml/g and the density of each sample is not the same. Thus, another representation is necessary in order to compare the porosity of these samples. In a paper, focus on the comparison between different presentations, Meyer and Klobes proposed different representations of pores distribution for porous materials [137]. One of the representation is presented as the “incremental pore volume” defined by $D(d_i) = -\Delta V_i$, with d_i the diameter of the pores i superior than the diameter of the pore d_{i-1} , and $\Delta V_i = V_i - V_{i-1}$. However, this definition of the incremental pore volume the unit of ΔV_i is still in ml/g . In order to compare these samples, the best representation is the contribution of each pore to the total porosity of each sample. This contribution on the total porosity of the pores with a diameter superior or equal to d_i to the porosity (ε_i) can be connected to V_i as written in Equation 22:

$$\varepsilon_i = \frac{v_i}{\sum V_i + 1/D_{vm}} \quad \text{Equation 22}$$

Thus, it is possible to obtain $\Delta\varepsilon_i$ from Equation 23

$$\Delta\varepsilon_i = \varepsilon_i - \varepsilon_{i+1} \quad \text{Equation 23}$$

Moreover, using Equation 24, it is possible to normalize ε_i by ε_{Hg} to obtain a normalization by the total amount of porosity of each membranes.

$$\Delta\epsilon_i (\%) = \frac{\Delta\epsilon_i}{\epsilon_{Hg}} \times 100 \quad \text{Equation 24}$$

Nota bene: It is important to notice that $\Sigma\epsilon_i = \epsilon_{Hg}$.

This incremental porosity in percentage ($\Delta\epsilon_i (\%)$) represents the contribution of the pores with a range of diameters $d_{i-1} - d_i$ on the total amount of porosity.

Finally, it is possible to represent an incremental porosity in percentage as function of the pores diameter of studied samples as it shown in Figure 46.

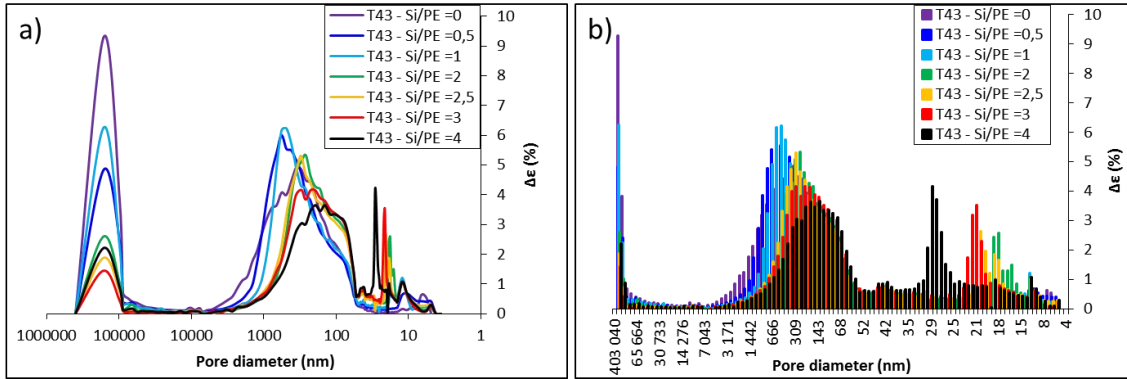


Figure 46: a) Incremental porosity in percentage as function of the diameter of the pores and b) Incremental porosity as function of diameter of the pores with a non-linear axis obtained in porosimetry by mercury intrusion. Membranes with a mass ratio H/PE=7.5 using the grade T43B of precipitated silica for different Si/PE mass ratios.

As it can be seen in Figure 46, the Si/PE mass ratio has an effect on the incremental porosity distribution. First, three kinds of pores can be distinguished. The first kind are large pores of around 100 μm size. These pores could be assimilated to bubbles of air presents in the membranes of 250 μm . The second kind of pores is a massif of pores with diameter between 4 μm and 50 nm in the membranes. These pores could be assimilated to the pores observed in SEM analysis of the studied membranes and will be defined as pores of the membranes. The third kind of pores is represented by a peak around 20 nm. These pores are due to the porous structure of the precipitated silica. They represent the *inter* and *intra* porosities of aggregates of the porous structure of the precipitated silica. As it can be seen in Figure 47, this peak is already present in the porosimetry analysis of the grade of precipitated silica T43B.

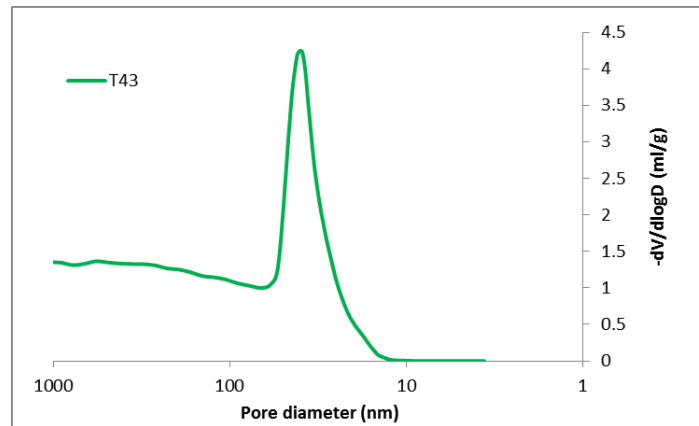


Figure 47: Differential pore size distribution for grade of precipitated silica T43B obtained by porosimetry by mercury intrusion

The Si/PE mass ratio has an influence on the three kinds of pores. When the Si/PE mass ratio increases, the amount of pores described as “bubbles” inside the blends decreases. When the Si/PE ratio increases, the diameter and the amount of the pores of the membranes decreases. However, there are two effects of the increase of the Si/PE mass ratio on the peak of porosity attributed to the porous structure of silica. The first is that the amount of porosity attributed to the precipitated silica compared to the total porosity ($\Delta\epsilon_{Si}$ (%)) increases as it can be seen in Figure 46b and in Figure 48a . The second is that the mean diameter of the porosity attributed to the aggregates of precipitated silica increases. Then, it is obvious that an increase of the amount of precipitated silica inside the blend increases the amount of porosity attributed to the precipitated silica. However, it is more complicated to explain the increase of the mean diameter of the porosity attributed to precipitated silica. This increase of the mean diameter of the peak attributed to the silica could be also due to an increase of the inter-aggregates porosity inside the blend. It could be due to the presence of agglomerates which were not divided into aggregates, which leads also an increase of the *inter*-aggregates porosity.

The increase of the porosity attributed to the peak of the precipitated silica could be linked to the increase of the porosity accessible to water. In Figure 48b, it can be seen that the increase of the porosity wettable to water is associated with an increase of the amount of porosity of the peak attributed to the precipitated silica. Thus, it is reasonable to formulate the hypothesis that the porosity accessible to water is linked to the increase of the porosity of the peak attributed to the precipitated silica. This hypothesis is sometimes presented in papers but without any proof [7,9]. However, because $\Delta\epsilon_{Si}$ (%) and ϵ_{ww} both increase with the amount of silica in blends, it is not possible to clearly ascertain whether the increase of ϵ_{ww} is due to the increases of $\Delta\epsilon_{Si}$ (%).

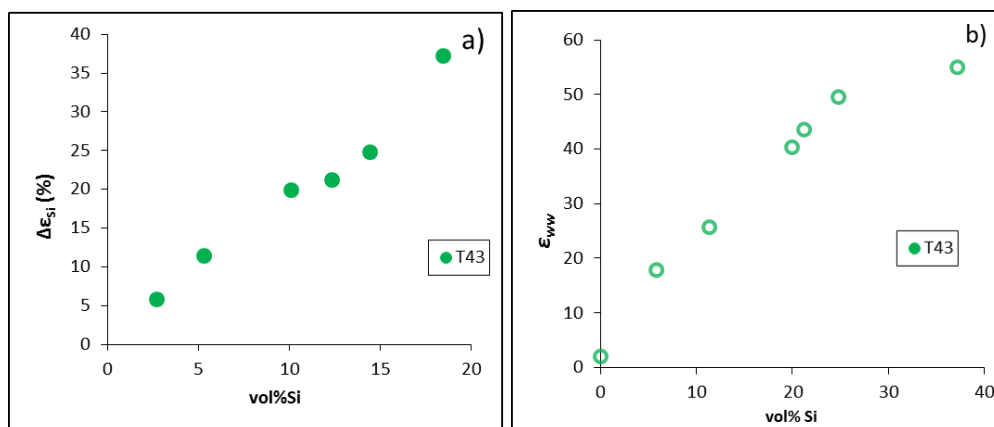


Figure 48: a) Porosity attributed to the peak of silica observed in mercury intrusion porosimetry as a function of the amount of precipitated silica in the formulation before process of membranes. b) Porosity accessible to water as a function of the porosity attributed to the peak of silica observed in mercury intrusion porosimetry.

To conclude, the increase of silica amount in the formulation of membranes has several effects on the porosities of the studied membranes. The increase of the silica amount does not influence the total porosity of the membranes which is nearly constant for the same oil/PE mass ratio. However, the porosity accessible to water increases when the amount of silica increases in the membranes. Moreover, there are two hypotheses which could explain the increase of the porosity accessible to water when the amount of precipitated silica increases. The first hypothesis is that ϵ_{ww} represents the pores “coated” with the precipitated silica inside the blend. Thus, an empirical parameter α has been introduced to qualitatively describe the dispersion/distribution of the precipitated silica inside the pores of the studied membranes. This parameter α represents the proportion of porosity reachable by water and is defined between 0 and 1: 0 for inefficient dispersion and 1 for the most efficient dispersion. The second hypothesis is that the porosity accessible to water could be linked to the increase of the porosity of the peak attributed to the precipitated silica. However, it is not possible to confirm one of these two hypotheses with the membranes elaborated in the internal mixer because of the high variation of the silica amount in the membranes.

5.1.3 INFLUENCE OF THE SILICA AMOUNT ON THE MEMBRANES ELECTRICAL RESISTIVITY

The electrical resistivity of membranes elaborated thanks to the internal mixer with the silica grade T43B is presented in Figure 49. In this figure, the electrical resistivity

value of the sample with $\Phi_{Si} = 0$ vol% was removed consciously because of its resistivity too high to be correctly measured by our device.

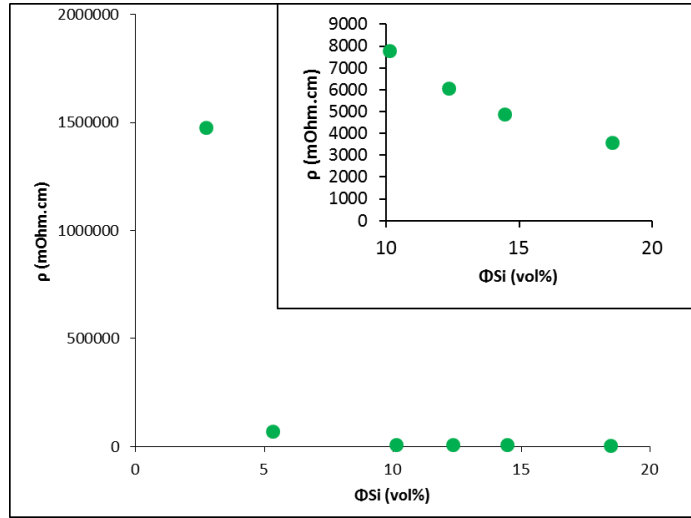


Figure 49: Electrical Resistivity of membranes with the grade of precipitated silica T43B as a function the amount of silica (before process). A focus on membranes with more than 10 vol% (Si/PE=2 mass ratio) of silica in the insert

Obviously, the electrical resistivity of the membranes varies a lot with the volume fraction of precipitated silica. The electrical resistivity varies from 1.5×10^6 mΩ.cm to 3.5×10^3 mΩ.cm when the volume fraction of precipitated silica varies from 2.7 to 18.5 (respectively Si/PE= 0.5 and Si/PE= 4 mass ratios). Between 5 vol% and 10 vol% of precipitated silica in the formulation, there is a significant drop of the electrical resistivity from 68 000 to 7 800 mΩ.cm. Then, the decrease of the electrical resistivity with the increase of the volume fraction of silica is smoother between 10 vol% and 18 vol% of precipitated silica. The electrical resistivity decreases from 7 800 to only 3500 mΩ.cm between 10 and 18 vol% of precipitated silica. Furthermore, it is appropriate to assume that the electrolyte will have the same behavior as the distilled water with respect to the water wettability of the porosity. Unfortunately, because of the electrolyte nature (acid sulfuric/water 50/50) it is not possible to measure directly the porosity of membranes accessible to the electrolyte without damage the density measurement device. Besides, the electrical resistivity ρ can be expressed as in Equation 17, where σ_{el} is the electrolyte conductivity (S.m), τ is the membrane tortuosity defined by the ratio between the actual path through the membrane and the straight line, and ε is the membrane porosity.

$$\rho = \frac{\tau^2}{\varepsilon} \times \frac{1}{\sigma_{el}} \quad [\Omega.m]$$

Equation 17

Nevertheless, in Equation 17, it is assumed that ε is the total porosity of the membrane. However, as discussed before the electrolyte will have the same behavior as the distilled water. Thus, ε should be replaced by ε_{ww} in Equation 17 to account only for accessible porosity by sulfuric acid. Moreover, the tortuosity can be deduced from Equation 10. This tortuosity is presented in Figure 50 for each sample processed by internal mixer with the grade T43B.

In Figure 50, the tortuosity of membranes is shown to vary a lot with the volume fraction of precipitated silica. Between $\Phi_{Si} = 2.7$ vol% and $\Phi_{Si} = 10.1$ vol%, there is a significant drop of the tortuosity from 18 to 2. Then between $\Phi_{Si} = 10.1$ vol% and $\Phi_{Si} = 18.5$ vol%, the tortuosity decreased slowly from 2 to 1.6. Thus, this high variation of tortuosity will lead to a non-linear relation if ρ is plotted as a function of $1/\varepsilon_{ww}$ as proposed by Equation 17.

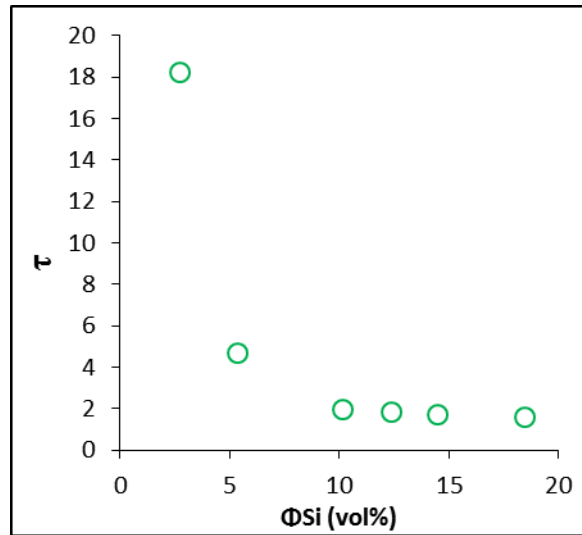


Figure 50: Tortuosity of samples processed by internal mixer with grade T43B as a function of the volume fraction of precipitated silica T43B in the formulation (before process).

To conclude, the increase of the Si/PE mass ratio leads to a decrease of the electrical resistivity and of the tortuosity of membranes. These decreases are really important for precipitated silica amount between 0 vol% and 10.1 vol% and become lower between 10.1 and 18.5 vol% of precipitated silica. These decreases are linked to the increase of the porosity wettable by water: Two hypotheses have been proposed to describe how the precipitated silica makes the porosity wettable: The first is a coating of the pores by the precipitated silica. The second is that the porosity attributed to the porous structure of the precipitated silica is directly responsible of the wettability of the membranes. However, with this study it is not possible to verify one of the two hypotheses proposed. As evoked before, the same conclusions have

been obtained for the membrane elaborated with the grades of precipitated silica Z175 and Z1165. Figures of porosity profiles and electrical resistivity for these membranes are presented in appendix.

Up to this point, in this study, we only discussed the influence of the silica amount on porosity with the help of samples processed by internal mixer. However, it is interesting to discuss the effect of the processing itself, and particularly, to ascertain whether the α parameter previously introduced can be relevant. Indeed, samples with different process settings and different silica grades can lead to different values of the parameter α or different value of $\Delta\epsilon_{Si}$ (%) for a same Si/PE mass ratio.

5.2 DISCRIMINATION OF SILICA GRADES ON THEIR EFFICIENCY FOR LEAD-ACID BATTERY SEPARATOR APPLICATION

The aim of this study is to understand the role of the precipitated silica on the wettable part of the porosity of the studied membranes. Thus, three grades of precipitated silica were used to understand the effect of each grade on the porosity and on the electrical resistivity of membrane. Moreover, the pertinence of each grade of precipitated silica for the battery separator application will be discussed.

5.2.1 SAMPLES OF THE STUDY

To characterize the influence of the process and of the precipitated silica grade, a comparison of all samples with the same initial UHMW-PE, oil and precipitated silica contents ($\Phi_{Si} = 12.4$ vol%, Si/PE = 2.5, oil/PE=7.5 mass ratio) was carried out. For each of the three precipitated silica grades (Z175, Z1165 and T43B), one sample was obtained from internal mixer and three samples were obtained for each extrusion screw profiles *OCF* and *2CF* (with a rotation speed v of 500, 800 and 1100 rpm). The measured porosities, the parameter α and the D_{vm} determinations for the studied membranes are presented in Table 5. The porosimetry by mercury intrusion has been carried out for the samples made with the screw profile *OCF* and the grades of the precipitated silica Z175 and Z1165. The obtained $\Delta\epsilon_{Si}$ (%) values are presented for these membranes.

Process type	Si grade	v (rpm)	ε_{ww}	ε_{IPA}	α	$\Delta\varepsilon_{si}$ (%)	D_{vm}
<i>OCF</i>	Z175	500	0.386	0.721	0.54	19.8	1.42
<i>OCF</i>	Z175	800	0.376	0.724	0.52	19.3	1.50
<i>OCF</i>	Z175	1100	0.378	0.719	0.53	18.6	1.50
<i>I.m.</i>	Z175		0.398	0.750	0.53	21.5	1.58
<i>2CF</i>	Z175	500	0.344	0.689	0.50		1.49
<i>2CF</i>	Z175	800	0.379	0.704	0.54		1.56
<i>2CF</i>	Z175	1100	0.372	0.691	0.54		1.40
<i>OCF</i>	Z1165	500	0.441	0.713	0.62	19.8	1.48
<i>OCF</i>	Z1165	800	0.423	0.712	0.59	19.4	1.47
<i>OCF</i>	Z1165	1100	0.435	0.721	0.60	20.0	1.56
<i>I.m.</i>	Z1165		0.445	0.755	0.59	24.0	1.61
<i>2CF</i>	Z1165	500	0.379	0.683	0.56		1.45
<i>2CF</i>	Z1165	800	0.379	0.694	0.55		1.48
<i>2CF</i>	Z1165	1100	0.379	0.690	0.55		1.48
<i>OCF</i>	T43	500	0.449	0.681	0.66		1.53
<i>OCF</i>	T43	800	0.431	0.679	0.63		1.42
<i>OCF</i>	T43	1100	0.428	0.692	0.62		1.52
<i>I.m.</i>	T43		0.436	0.759	0.57	21.2	1.56
<i>2CF</i>	T43	500	0.400	0.683	0.59		1.54
<i>2CF</i>	T43	800	0.394	0.718	0.55		1.61
<i>2CF</i>	T43	1100	0.392	0.710	0.55		1.62

Table 5: Porosity measurement by water and IPA as probes of each sample (I.m. stands for samples processed by internal mixer).

5.2.2 DISPERSION OF PRECIPITATED SILICA IN MEMBRANES

The dispersion and the distribution of precipitated silica in membranes have been investigated by SEM analysis. The surfaces of the membranes performed with the screw profile *OCF* are presented in Figure 51. As expected and regarding the very high amount of precipitated silica in these membranes, the agglomerates and the aggregates of silica appear to be well distributed in the membranes for each silica grade. However in this figure, it is possible to notice some differences of the dispersion state between the silica grades mixed at the same speed. First, there is a significant difference between the conventional grade of precipitated silica (Z175) and the highly dispersible silica grades (Z1165 and T43B). The elaboration of membranes in extrusion with the screw profile *OCF* makes it possible to achieve a more advanced dispersion state (smaller agglomerates) with grade T43B and Z1665

than with the grade Z175. However, it is not possible to clearly distinguish a difference of the dispersion state between membranes with Z1165 and T43B in our conditions. Moreover, the high amount of silica in the membranes does not allow obtaining clear boundaries between particles of precipitated silica. Thus, the determination of the size of precipitated silica agglomerates in blends by image analysis is highly dependent of the selected contrast limit. Furthermore, for the same reason, it is not possible to distinguish the effect of the screws rotation speed on the dispersion state of precipitated silica when this speed increases from 500 rpm to 1100 rpm.

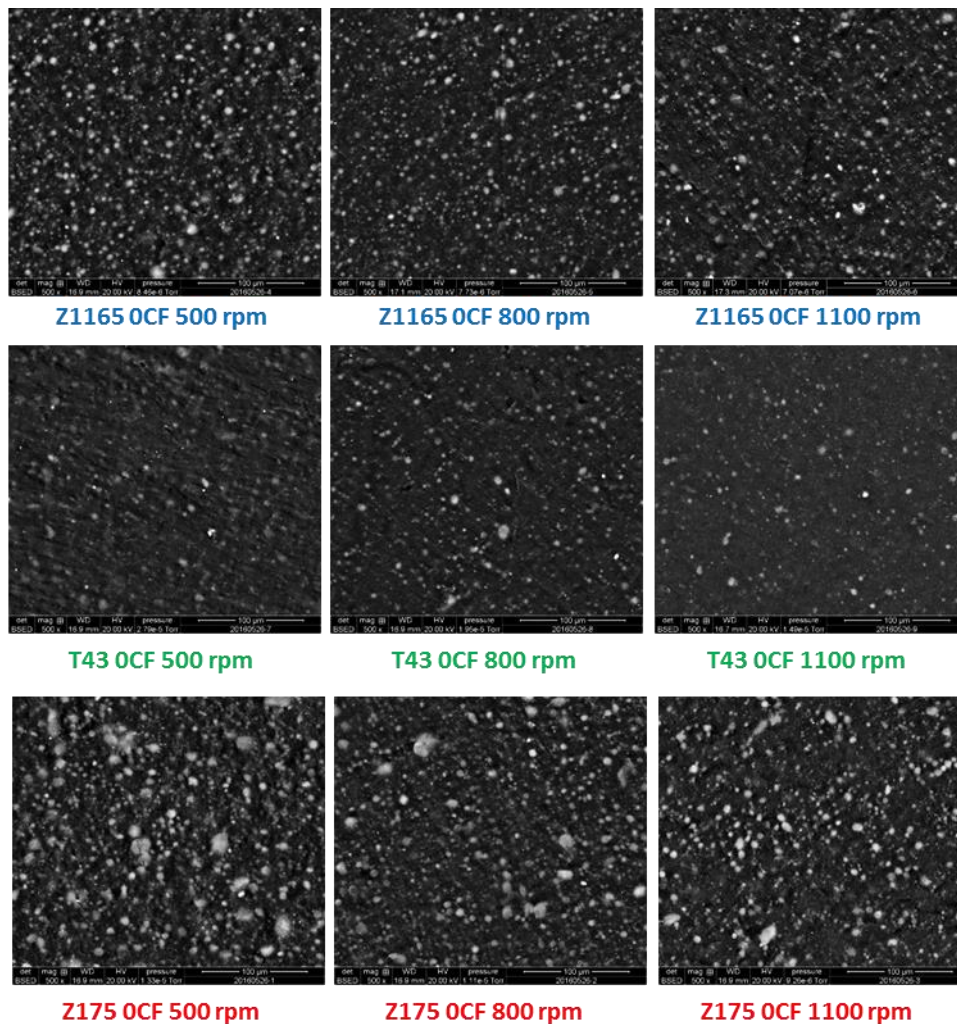


Figure 51: SEM analyses of the surfaces of the membranes elaborated in extrusion with the screw profile *OCF* and for the three grades of precipitated silica (the line in the SEM analyses represents 100 μm)

The effect of the screw design on the dispersion state of precipitated silica is presented in Figure 52 for the grade Z1165. As it can be seen, the use of the screw design *2CF* appears to lead to a little more advanced state of dispersion of the precipitated silica agglomerates especially for a rotation speed of 1100 rpm. However, for a same rotation speed of the screws, it is really difficult to observe a change of the size of the agglomerates between the use of the two screw profiles due to the amount of precipitated silica in membranes. Furthermore, it is also really tricky to estimate the effect of the rotation speed of the screws of the profile *2CF* on the dispersion state of dispersion of precipitated silica with these SEM analyses. Moreover, it is also really difficult to identify a difference of the distribution of precipitated silica between membranes elaborated with the profile *OCF* and the samples elaborated with the profile *2CF*.

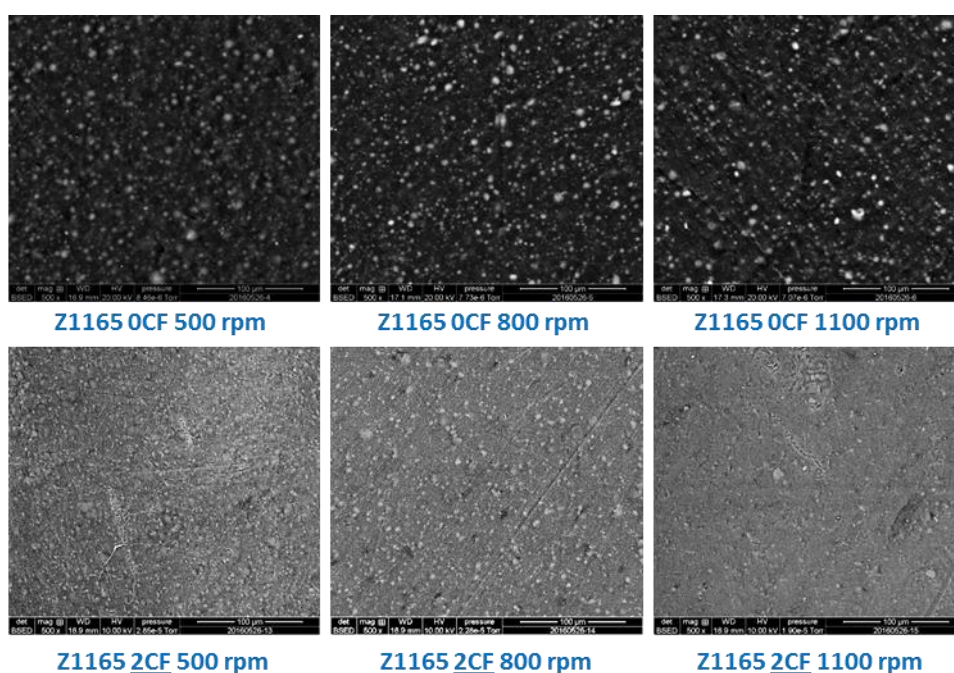


Figure 52: SEM analyses of the membranes elaborated in extrusion with the screw profiles *OCF* (up) and *2CF* (bottom) for grade of precipitated silica Z1165 (the line in the SEM analyses represent 100µm).

To conclude, the *SEM* analyses of membranes help to estimate the state of dispersion and distribution of the precipitated silica inside the membranes elaborated by extrusion. For each grade, the precipitated silica appears to be well distributed in membranes. However, the use of a HDS grade of precipitated silica (T43 and Z1165) leads to smaller aggregates after extrusion than the use of conventional grade (Z175). Moreover, because of the high amount of the precipitated silica, it is not possible to observe a difference of dispersion quality when the rotation speed of the screws is increased from 500 rpm to 1100 rpm. For the same reason, it appears that

the use of the screw design *OCF* and the use of the screw design *2CF* lead to almost the same dispersion state of the studied grades of precipitated silica.

5.2.3 POROSITY AND ELECTRICAL RESISTIVITY OF SAMPLES

As it can be seen in Table 5, different processing conditions lead to slightly but noticeably different porosities. ε_{IPA} varies from 0.76 (*int. mixer T43B*) to 0.68 (*OCF 800 T43* and *OCF 500 T43*) and ε_{ww} from 0.45 (*OCF 500 T43* and *I.m Z1165*) to 0.34 (*2CF Z175 1100*). Moreover, samples have slightly but noticeably different D_{vm} . This small difference of D_{vm} comes from small change in the formulation of the membrane after process. The process by extrusion leads to a variation of the silica amount and of the polyethylene amount of ± 2 wt% in the formulation of the membranes after processing. But, when the oil is extracted, this variation is artificially increased because the precipitated silica becomes very abundant in comparison with the polyethylene. Then, the more precipitated silica in the blend, the higher is D_{vm} . However, as presented before, the amount of silica has an impact on the amount of porosity wettable by water. Thus, it appears relevant to observe the influence of D_{vm} on the wettable porosity of the membranes as presented in Figure 53.

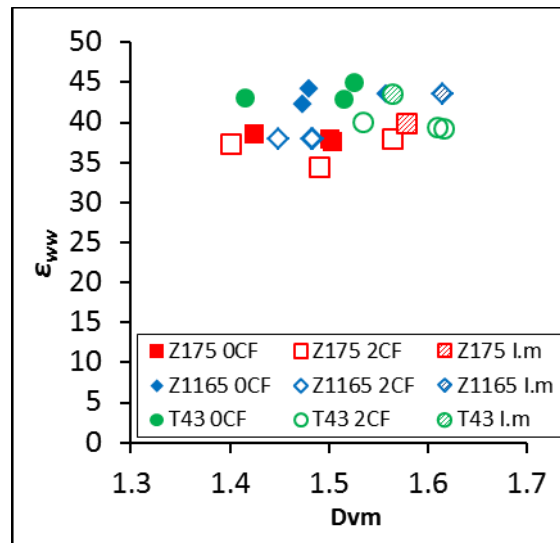


Figure 53: Wettable porosity of studied membranes as a function of the density of the “skeleton” of the membranes (density of the bulk considered without porosity)

As it can be seen in Figure 53, if all samples are considered, there is no obvious relationship between D_{vm} and ε_{ww} . Then, it can be concluded that this small variation of D_{vm} is not the principal parameter which influences the amount of the wettable porosity of the studied membranes.

Thus, it is interesting to notice that the process conditions have an influence on the total porosity of the membranes, as already reported for membranes made of PE/Oil blends [41,49,138]. Moreover, there is no obvious relation between ε_{ww} and ε_{IPA} which means that the processing conditions does not affect in the same way the wettable porosity and the total porosity. However, as discussed before, ε_{ww} can be directly linked to the precipitated silica dispersion quality. Thus, different process conditions could lead to different qualities of precipitated silica dispersions inside the pores which certainly lead to diverse membranes electrical resistivity. However, for the samples elaborated by extrusion and analyzed by mercury intrusion porosimetry, there are no obvious relationship between the amount of porosity attributed to the precipitated silica and ε_{ww} or the parameter α . If a focus is made on samples “Z175 OCF 800 rpm” and “Z1165 OCF 800 rpm”, it can be seen that these two samples have the almost the same $\Delta\varepsilon_{Si}$ (%), respectively 19.3 % and 19.4 %. However, these two samples have a different ε_{ww} (respectively 0.376 and 0.423) and they also have different α (respectively 0.52 and 0.59). The same approach can be done between samples “Z175 OCF 500 rpm” and “Z1165 OCF 500 rpm” which have the same $\Delta\varepsilon_{Si}$ (%) and different ε_{ww} and α . Moreover, as presented in Figure 54a, the Incremental porosity of samples elaborated with the screw profile OCF and with precipitated silica Z175 or Z1165 are almost the same. Furthermore, as it can be observed in Figure 54b, the Incremental porosity of samples Z175 OCF 800 rpm” and “Z1165 OCF 800 rpm” are extremely similar.

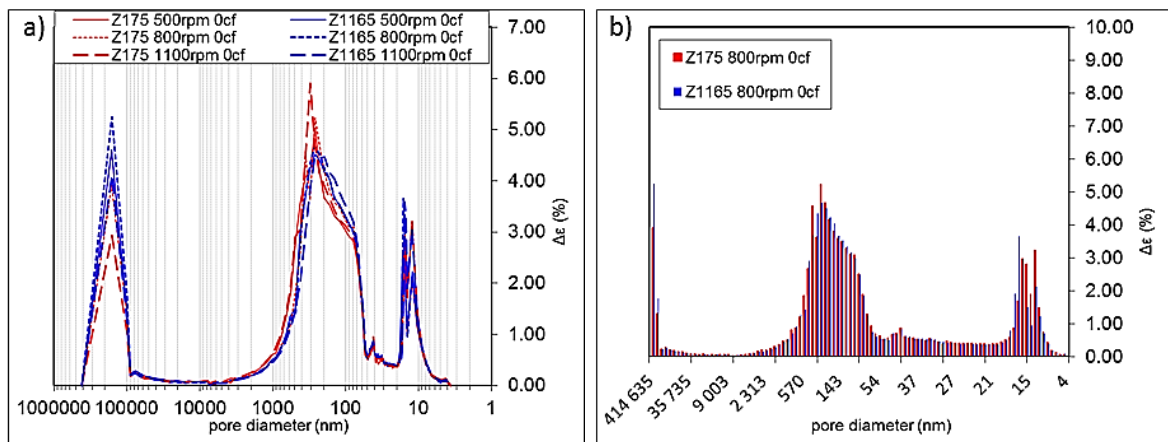


Figure 54: a) Incremental porosity as function of the diameter of the pores
 b) Incremental porosity as function of the diameter actually obtained in porosimetry by mercury intrusion for samples “Z175 OCF 800 rpm” and “Z1165 OCF 800 rpm”.

Thus, it is obvious that the porosity profile of the membrane is linked to the total porosity of membranes. However, the amount of porosity of the peak attributed to the porous structure of precipitated silica is not correlated to the porosity wettable by water.

Thus the hypothesis that ϵ_{ww} represents the pores “coated” with precipitated silica inside the blend appears to be the best hypothesis. An illustration of this hypothesis is proposed in Figure 55.

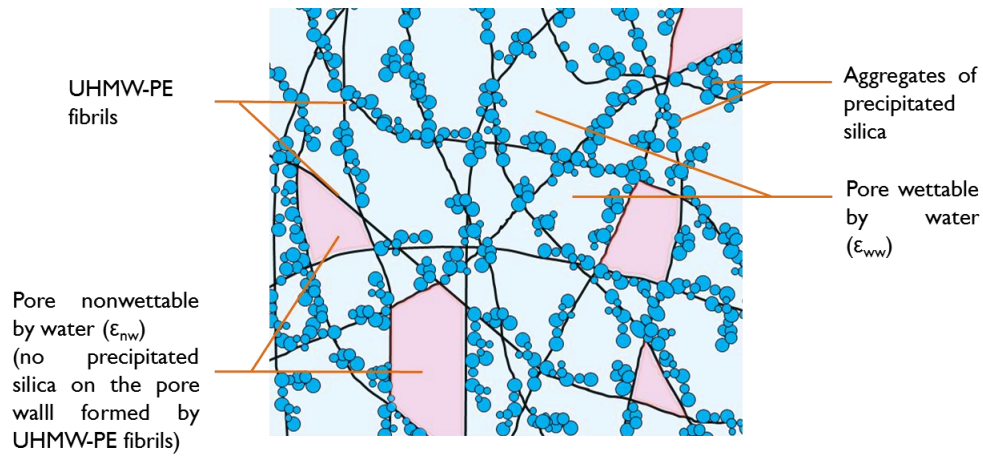


Figure 55: Illustration of the coating of UHMW-PE fibrils by precipitated silica which make wettable the pores formed by the network UHMW-PE fibrils.

In this regard, a comparison of the samples electrical resistivity is presented in Figure 56 as a function of $1/\epsilon_{ww}$ and as a function of α . Obviously, there is a strong effect of the process and of the precipitated silica grade on the membranes electrical resistivity. The resistivity almost doubles for samples with the grade T43B and varies from 3700 mΩ.cm (OCF 500rpm) to 6000 mΩ.cm (int. mixer) whereas all samples have the same formulation. There is also a large variation of ρ for the two other precipitated grades of silica as a function of the process used.

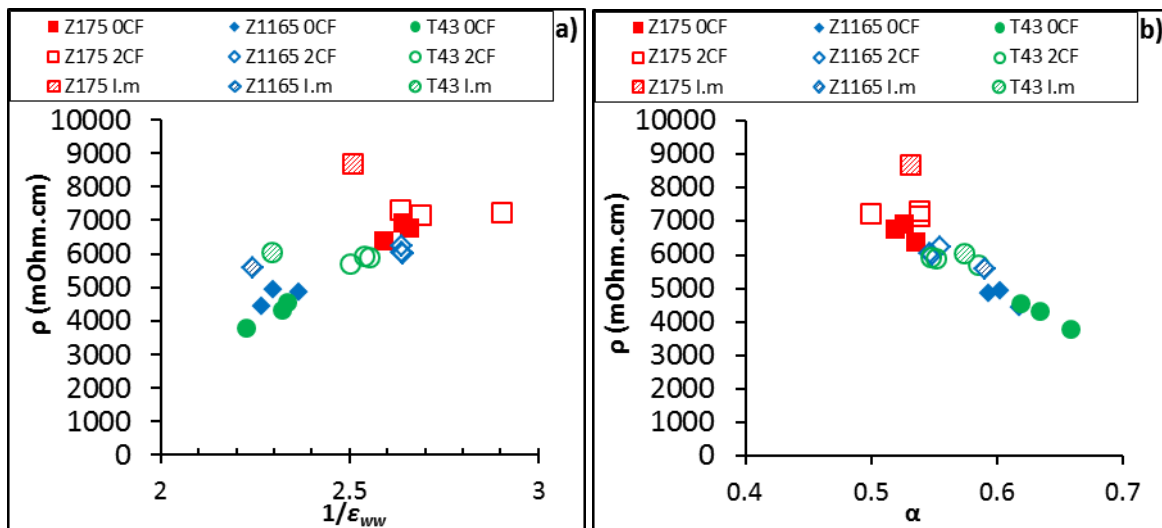


Figure 56: a) Electrical resistivity ρ of all samples of the same formulation. (a): as a function of $1/\epsilon_{ww}$, (b): as a function of α

From Figure 56b, it can be noticed that the closer α is to 1, the more the electrical resistivity decreases. Moreover, α appears to be a judicious parameter to discriminate the influence of each processing methods on ρ for membranes having the same initial component amount. Furthermore, with the parameter α , it is easier to discriminate the efficiency of the precipitated silica dispersion for decreasing the electrical resistivity: the grade T43B appears to be the best followed by the grade Z1165 and then the grade Z175. Likewise, the process effect can be discriminated: extrusion with *OCF* profile appears to be the best, followed by the internal mixer and the *2CF* profile which are difficult to distinguish.

Moreover, the parameter α appears to be more appropriate than $1/\epsilon_{ww}$ to describe the variation of electrical resistivity (ρ). Indeed, as discussed before, the tortuosity and the porosity play important roles on the electrical resistivity of the separator. Thus, the parameter α could be a relevant way to comprise the tortuosity and the porosity in a unique factor. Hence, it appears judicious to compare the variations of τ as a function of ϵ_{ww} and as a function of α . This comparison is presented in Figure 57.

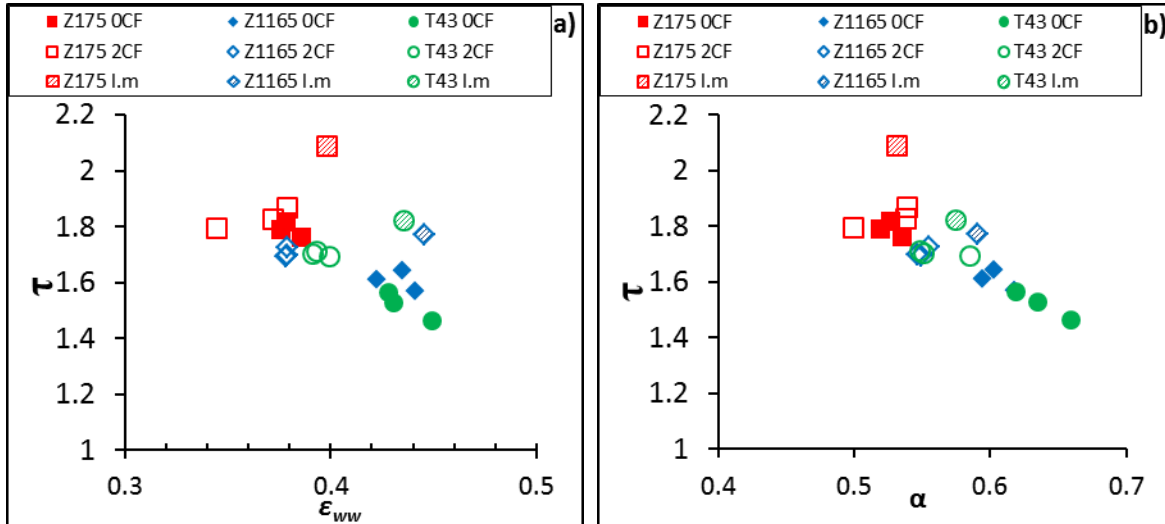


Figure 57: Comparison of the tortuosity as function of ϵ_{ww} (a) and as a function of α (b)

From Figure 57, it can be concluded that, when expressed as a function of the parameter α , the tortuosity values lay on a unique curve differently to the results shown as a function of ϵ_{ww} . Thus, the parameter α appears more reliable to discriminate the efficiency of a process or of a precipitated silica grade on the electrical resistivity of membranes.

To conclude, obviously, ρ depends on the path taken by an ion from one electrode to the other and this path is not straight through the membrane. This means that the membranes tortuosity is not equal to 1 and τ depends on the global porosity, the pores size and shape [7,8,16] and also on the water wettability of the porosity as

described in this study. All these characteristics of the membrane porosity may be affected by the process, but it has been demonstrated that ϵ_{ww} is affected by both the process and by the grade of the precipitated silica. Moreover, the parameter α appears to be extremely relevant to compare the efficiencies of processes and precipitated silica grades for samples with the same component amounts.

5.3 CONCLUSION

In this study, the roles of the precipitated silica and of the porosity have been clarified. It has been shown that the amount of precipitated silica has a strong impact on the water wettable porosity of membranes but no real effect on the total porosity which is mainly controlled by the oil amount. By coating the pores of the PE-separators, the precipitated silica permits to make the porosity wettable by the electrolyte. This influence on ϵ_{ww} leads to an indirect control of the membranes electrical resistivity by the amount and the dispersion quality of the precipitated silica. An empirical parameter α , defined by is the ratio between the water wettable porosity and the total porosity, has been introduced. This parameter is particularly relevant to compare the effect of the process or of the precipitated silica grade on the electrical resistivity for samples with the same quantities of oil, PE and precipitated silica. For example, in the case of the process described in the present study, the grades of precipitated silica can be sorted by their efficiency as following: T43 > Z1165 > Z175. As a perspective, it is also important to notice that the use of this parameter α is limited. Indeed, for membranes where $\alpha = 1$ ($\epsilon_{ww} = \epsilon_{IPA}$), the parameter α is no longer useful to compare membranes and only a measure of the electrical resistivity will permit to compare these fully wettable membranes. Nevertheless, in this case ($\alpha = 1$), all the silica can be considered completely efficient so that it becomes unnecessary to make efforts to improve even more its dispersion in membranes. For membranes with $\alpha = 1$, some possibilities for decreasing the electrical resistivity are to increase the porosity or decrease the tortuosity of the porous morphology.

RESUME CHAPITRE 5

Dans cette étude, le rôle de la silice précipitée et de la porosité sur la résistivité des membranes a été clarifié. Il est montré que la silice précipitée permet de rendre la porosité mouillable à l'électrolyte sans toutefois modifier la porosité totale de la membrane qui est principalement contrôlée par la quantité d'huile. En effet, pour que les pores soient mouillables par l'électrolyte, il est nécessaire que de la silice soit présente en surface des pores. Cette influence sur la mouillabilité de la porosité conduit à un contrôle indirect de la résistivité des membranes par la quantité et la qualité de dispersion de la silice. Un paramètre empirique α , qui correspond au ratio entre la porosité mouillable et la porosité totale de la membrane, a été introduit. Ce paramètre α est particulièrement pertinent pour comparer l'influence du procédé ou du grade de silice précipitée sur la résistivité de membrane avec la même composition. Par exemple, dans le cas de notre étude, l'efficacité des trois grades de silice utilisés peut être différenciée. Le grade T43 conduit à des résistivités plus basses que le grade Z1165 qui est lui-même plus efficace que le grade Z175. En perspective, il est également important de noter que l'utilisation du paramètre α pour discriminer l'efficacité des grades de silice est limitée. En effet, pour des membranes avec $\alpha = 1$ (la porosité mouillable à l'électrolyte est égale à la porosité totale de la membrane), le paramètre α n'est plus utile pour comparer les membranes et dans ce cas, seule une mesure de résistivité pourra permettre de comparer ces membranes totalement mouillable par l'électrolyte. Néanmoins, dans ce cas précis ($\alpha = 1$), la combinaison dispersion/distribution de la silice précipitée dans la membrane peut être considéré comme parfaitement efficace et il apparaît inutile d'essayer d'améliorer son état de dispersion dans le but de diminuer la résistivité des membranes.

6 GENERAL CONCLUSION

Most work found in the literature studying PE-separators is focused on the final properties (electrical resistance and mechanical properties) without considering the effects of the formulation and/or the process on the crystallinity and on the porosity of membranes. The main objective of this work was thus to provide a better understanding of the influence of the formulation, and more precisely of the precipitated silica, on the elaboration of PE-separators and on their porosity and electrical resistivity. As evoked in chapter 1, the aim of this thesis work was thus to answer these questions:

- How the formulation of a PE-separator influences the final properties of the porous membranes?
- How the precipitated silica participates to reduce the electrical resistivity of PE-separators?
- Is it possible to discriminate and predict the efficiency of various precipitated silica grades on the electrical resistivity of PE-separators?

In order to answer these questions, the first part of this work consisted in a bibliographic review which permitted to identify several ways to study the influence of the formulation on the questions defined above.

Therefore, this thesis began with the understanding of the influence of the formulation and temperature conditions on the crystallization of the blends of UHMW-PE/oil/precipitated silica. First, the influence of the formulation on the crystallization was discussed and several key parameters were identified. This work reports, for the first time, that the precipitated silica helps to avoid exudation of oil in the blend during and after the TIPS process. For a weight ratio oil/PE = 7.5, a ratio of Si/PE = 1 (≈ 5 vol % of precipitated silica) is sufficient to keep almost all of the oil in the blend during the cooling step. Moreover, the precipitated silica exhibits no nucleating effect on the crystallization of the UHMW-PE and can be considered as an inert phase in the blends. The polyethylene crystallization is only controlled by the amount of naphthenic oil in the blend. For the three types of used polyethylenes, the melting and crystallization temperatures of these polyethylenes are linearly dependent on the volume fraction of naphthenic oil in the considered binary system. In accordance with the literature, the crystallization and melting temperatures both decrease with increasing the volume fraction of oil. Moreover, with the help of the Flory-Huggins theory applied to the melting temperature of blends with various, it has been determined that the interaction parameter for naphthenic oil / polyethylene systems is really close to 0 which indicates a good miscibility between

the used naphthenic oil (EDELEX 946) and the used polyethylenes. However, the influence of the amount of oil on the polyethylene crystallinity is not the same for the three kinds of polyethylene used. For the HDPE and the L-LDPE there is no influence of the amount of oil on their crystallinity after non-isothermal crystallization at 10 °C/min. For the UHMW-PE, there is a strong dependency between the amount of oil and the crystallinity of the UHMW-PE after non-isothermal crystallization. This work reports that the increase of the amount of oil makes it possible to achieve higher crystallinity for UHMW-PE. To our knowledge this was not previously shown in the literature. With the increase of the oil content from 0 vol% to 90 vol% there is an increase of UHMW-PE crystallinity from 40 % to 65 %. This phenomenon is attributed to the ability of the solvent to provide necessary mobility the polymer chains leading to a more perfect crystallization. Moreover, this improvement of mobility of the chains of UHMW-PE has been confirmed by isothermal protocol crystallization. To sum up, the exudation of oil at ambient temperature is avoided in presence of the precipitated silica and this excess of oil advantageously permits a more complete crystallization by providing even more mobility to the UHMW-PE macromolecules. Hence, it is possible to reach again the initial crystallinity, of the UHMW-PE powder but by a process other than sintering.

This work was also dedicated to the study of the porosity and resistivity of PE-separators with various formulations. It was shown that the ratio oil/PE controls the amount of porosity in PE-separators. Moreover, the amount of porosity in the membranes is not influenced by the amount of precipitated silica. However, this work has revealed that the amount of precipitated silica in the membranes is responsible of the wettable part of the porosity. Indeed, the porosity may be not fully wettable by the electrolyte. Thus, this wettable part of the porosity increases with increasing the amount of the precipitated silica in the membranes. Furthermore, it has been shown that the precipitated silica participates to reduce the electrical resistivity of PE-separators by coating the surface of the pores. Therefore, an empirical parameter α has been proposed to quantify the efficiency of the coating of the precipitated silica. The parameter α is defined by the ratio between the wettable part of the porosity on the total amount of the porosity. This parameter is equal to 1 for a complete coating of pores by the precipitated silica and below 1 for partial coating of the pores. It has been shown that the parameter α was more relevant than the only wettable porosity to comprise the porosity and the tortuosity effect on the electrical resistivity. Moreover, with this parameter α and for a same given amount of each component in the membranes, it is possible to compare the efficiency of a precipitated silica grade or of an elaboration process to enhance the coating of the porosity. Hence, for the elaboration process used in this thesis work, it appears that the precipitated silica grade T43 is more efficient to coat the porosity than the grade Z1165 which is itself more efficient than the grade Z175.

This thesis work first intended to provide a better understanding of the effect of the precipitated silica and discriminate the efficiency of various grade on the resistivity of PE-separator. The obtained results permit to understand also the role of each component of the membrane on the crystallization of the UHMW-PE. Moreover, the comprehension of the role of precipitated silica on the electrical resistivity of the membranes makes it also possible to discriminate the efficiency of the silica grades used during this study. As a perspective, the challenge is to elaborate PE-separators which are fully wettable by the electrolyte and then try to find the key parameters which control the morphology of the porous structure in order to reduce the electrical resistivity by decreasing the tortuosity. Moreover, in order to predict the efficiency of a precipitated silica grade for the battery separator application, it will be great to highlight a relationship between a structure parameter of the precipitated silica and the final efficiency of the dispersion/distribution of the silica in the PE-separators.

This work was focused on PE-separators, but the obtained results here can also be helpful for other type of porous structure or blends using UHMW-PE. Moreover, this study presents an empirical parameter to quantify the repartition of porous hydrophilic filler in the porous structures of hydrophobic polymers. This could also be helpful to compare the efficiency of various grades of components or different kinds of process for the elaboration of PE-separator.

CONCLUSION GENERALE

La plupart des travaux de recherche trouvés dans la littérature sur les séparateurs en polyéthylène se concentrent sur les propriétés finales des séparateurs (résistance électrique et propriétés mécaniques) sans tenir compte des effets de la formulation et / ou du procédé sur la cristallinité et sur la porosité des membranes. L'objectif principal de ce travail était donc de mieux comprendre l'influence de la formulation, et plus précisément de la silice précipitée, sur l'élaboration des séparateurs en polyéthylène, leur porosité et leur résistivité. Comme nous l'avons évoqué au chapitre 1, le but de ce travail de thèse était donc de répondre aux questions suivantes :

- Comment la formulation d'un séparateur en PE influence-t-elle les propriétés finales des membranes poreuses ?
- Quel est le mécanisme d'action de la silice précipitée pour réduire la résistivité des séparateurs en PE ?
- Est-il possible de discriminer et de prédire l'efficacité de plusieurs grades de silice précipités sur la résistivité des séparateurs de PE ?

Pour répondre à ces questions, la première partie de ce travail a consisté en une revue bibliographique qui a permis d'identifier plusieurs façons d'étudier l'influence de la formulation sur les questions définies ci-dessus.

Par conséquent, cette thèse a commencé par la compréhension de l'influence de la formulation et des conditions de température sur la cristallisation des mélanges d'UHMW-PE / huile / silice précipitée. Tout d'abord, l'influence de la formulation sur la cristallisation a été discutée et plusieurs paramètres clés ont été identifiés. Ce travail rapporte, pour la première fois, que la silice précipitée permet d'éviter l'exsudation d'huile dans le mélange pendant et après le procédé TIPS. Pour un rapport massique huile/PE = 7,5, un rapport Si/PE = 1 (5% en volume de silice précipitée) est suffisant pour conserver la quasi-totalité de l'huile dans le mélange pendant l'étape de refroidissement. De plus, la silice précipitée n'a pas d'effet nucléant sur la cristallisation de l'UHMW-PE et peut être considérée comme une phase inerte dans les mélanges. La cristallisation de l'UHMW-PE n'est contrôlée que par la quantité d'huile naphténique dans le mélange. Pour les trois types de polyéthylène utilisés, les températures de fusion et de cristallisation des polyéthylènes dépendent linéairement de la fraction volumique d'huile naphténique dans le système binaire considéré. En accord avec la littérature, les températures de cristallisation et de fusion diminuent avec l'augmentation de la fraction volumique

d'huile. De plus, à l'aide de la théorie de Flory-Huggins appliquée sur la température de fusion des mélanges, il a été déterminé que le paramètre d'interaction pour les systèmes huile naphtéénique / polyéthylène est proche de 0 ce qui indique une bonne miscibilité entre l'huile naphtéénique (EDELEX 946) et les polyéthylènes utilisés.

Ce travail a également été consacré à l'étude de la porosité et de la résistivité des séparateurs en polyéthylène. Il a été montré que le rapport huile / PE contrôle la quantité de porosité dans les séparateurs en polyéthylène. De plus, la quantité de porosité dans les membranes n'est pas influencée par la quantité de silice précipitée. Cependant, la quantité de silice précipitée dans les membranes est responsable de la partie mouillable de la porosité. En effet, la porosité de la membrane peut ne pas être totalement mouillable par l'électrolyte. Ainsi, cette partie mouillable de la porosité augmente en même temps avec l'accroissement de la quantité de silice précipitée dans les membranes. En outre, il a été montré que la silice précipitée participe à la réduction de la résistivité des séparateurs de PE en revêtant la surface des pores des membranes. Par conséquent, un paramètre empirique α a été proposé pour quantifier l'efficacité du revêtement de la silice précipitée. Le paramètre α est défini par le rapport entre la partie mouillable de la porosité sur la quantité totale de la porosité. Ce paramètre est égal à 1 pour un revêtement complet des pores par la silice précipitée et inférieur à 1 pour un revêtement partiel des pores. Il a été montré que le paramètre α était plus pertinent que la seule porosité mouillable pour comprendre l'effet combiné de la porosité et de la tortuosité sur la résistivité des membranes. De plus, avec ce paramètre α et pour une quantité donnée de chaque composant dans les membranes, il est possible de comparer l'efficacité de différents grades de silices précipitées ou de plusieurs procédés d'élaboration pour améliorer le revêtement de la porosité par la silice. Par conséquent, pour les procédés d'élaboration utilisés dans ce travail de thèse, il apparaît que le grade de silice précipitée T43 est plus efficace pour revêtir la porosité que le grade Z1165 qui est lui-même plus efficace que le grade Z175.

Ce travail de thèse avait pour premiers objectifs de fournir une meilleure compréhension de l'effet de la silice précipitée ainsi que de discriminer l'efficacité de divers grades de silice précipitées sur la résistivité des séparateurs en polyéthylène. Les résultats obtenus permettent de comprendre également le rôle de chaque composant de la membrane sur la cristallisation de l'UHMW-PE. De plus, la compréhension du rôle de la silice précipitée sur la résistivité des membranes permet également de discriminer l'efficacité des grades de silice utilisés au cours de cette thèse. Comme perspective de ce travail, le défi consistera à élaborer des séparateurs en polyéthylène entièrement mouillables par l'électrolyte. Puis, il faudra ensuite essayer de trouver les paramètres clés qui contrôlent la morphologie de la structure poreuse afin de réduire la résistivité en diminuant la tortuosité. De plus, pour prédire l'efficacité d'un grade de silice précipitée pour l'application du séparateur de batterie,

il sera important de mettre en évidence une relation entre un paramètre structural de la silice précipitée et l'efficacité finale de la qualité de dispersion / distribution de la silice à l'intérieur des séparateurs. Ce travail a porté sur les séparateurs de PE, mais les résultats obtenus ici peuvent également être utiles pour d'autres types de structures poreuses ou bien pour l'étude de mélanges utilisant de l'UHMW-PE. Par ailleurs, cette étude présente un paramètre empirique pour quantifier la répartition d'une charge hydrophile poreuse dans des structures poreuses hydrophobes. Cela pourrait également être utile pour comparer l'efficacité de divers grade de composants ou différents types de processus pour l'élaboration de PE-séparateur.

REFERENCES

- [1] J. Garche, On the historical development of the lead/acid battery, especially in Europe, *J. Power Sources*. 31 (1990) 401–406.
- [2] P. Ruetschi, Review on the lead—acid battery science and technology, *J. Power Sources*. 2 (1977) 3–120.
- [3] C. Pillot, Market review at the batteries congress 2014, (2014). <http://www.rechargebatteries.org/knowledge-base/market/>.
- [4] B. Cullen, Global market for industrial lead acid batteries – past, present and future, *J. Power Sources*. 116 (2003) 287.e7–287.e10. doi:10.1016/S0378-7753(02)00678-X.
- [5] Advancing Sustainable Materials Management: 2013 Fact Sheet, U. S. Environ. Prot. Agency Solid Waste Emerg. Response 5306P Wash. DC 20460. (2013) 5.
- [6] P. Krivik, P. Bac, Electrochemical Energy Storage, in: A. Zobaa (Ed.), *Energy Storage - Technol. Appl., InTech*, 2013. http://www.intechopen.com/books/energy-storage-technologies-and-applications/electrochemical_energy_storage (accessed September 30, 2016).
- [7] P. Arora, Z. (John) Zhang, Battery Separators, *Chem. Rev.* 104 (2004) 4419–4462. doi:10.1021/cr020738u.
- [8] W. Böhnstedt, A review of future directions in automotive battery separators, *J. Power Sources*. 133 (2004) 59–66. doi:10.1016/j.jpowsour.2003.11.031.
- [9] W. Böhnstedt, Aspects of optimizing polyethylene separators.pdf, *J. Power Sources* 95. (2001).
- [10] R.W. Pekala, Lead acid battery separator with improved electrical and mechanical properties, Google Patents, 2004. <http://www.google.it/patents/EP1390993A1?cl=en>.
- [11] M.J. Weighall, Battery separator design requirements and technology improvements for the modern lead/acid battery, *J. Power Sources*. 53 (1995) 273–282.
- [12] W. Böhnstedt, Automotive lead/acid battery separators: a global overview, *J. Power Sources*. 59 (1996) 45–50.
- [13] W. Böhnstedt, Challenges for automotive battery separator development, (1996).
- [14] Y. Zeng, J. Hu, W. Ye, W. Zhao, G. Zhou, Y. Guo, Investigation of lead dendrite growth in the formation of valve-regulated lead-acid batteries for electric bicycle applications, *J. Power Sources*. 286 (2015) 182–192. doi:10.1016/j.jpowsour.2015.03.139.
- [15] J.K. Whear, 4 Lead-Acid Batteries, *Lead-Acid Battery Technol. Fundam. Mater. Appl.* 8 (2015) 111.
- [16] C. Daniel, J.O. Besenhard, *Handbook of Battery Materials*, John Wiley & Sons, 2013.
- [17] Separator Resistance - How Low Can You Go?, Entek. (n.d.). <http://entek.com/news/posts/separator-resistance-low-can/> (accessed October 5, 2016).
- [18] B.G. Rowland, G.E. Monigold Jr, R.L. Brendle, F.V. Rosse, Battery separator and method of making same, Google Patents, 1993.
- [19] E.H. Miller, J.G. Yaritz, M.T. Demeuse, J.K. Whear, A microporous material and method of making same, Google Patents, 2013. <http://www.google.com/patents/EP2586609A1?cl=en>.

- [20] K. Takita, H. Funaoka, N. Kaimai, S. Kobayashi, K. Kono, Polyolefin microporous film and method for preparing the same, Google Patents, 2003. <https://www.google.com/patents/US6566012> (accessed June 2, 2015).
- [21] R.W. Pekala, M. Khavari, Freestanding microporous separator including a gel-forming polymer, Google Patents, 2003.
- [22] J. Jung, L. Zhang, J. Zhang, eds., Lead-acid battery technologies: fundamentals, materials, and applications, CRC Press, Taylor & Francis Group, Boca Raton London New York, 2016.
- [23] Lead-acid Battery Separators ENTEK, (n.d.). <http://entek.com/lead-acid/> (accessed October 14, 2016).
- [24] L.D. Wayne, K.C. Leroy, Battery separator, Google Patents, 1967.
- [25] W.M. Choi, A. Samii, Battery separator with sodium sulfate, Google Patents, 1997. <http://www.google.com/patents/US5618642>.
- [26] L.C. Wang, M.K. Harvey, J.C. Ng, U. Scheunemann, Ultra-high molecular weight polyethylene (UHMW-PE) and its application in microporous separators for lead/acid batteries, *J. Power Sources*. 73 (1998) 74–77.
- [27] R.W. Pekala, Battery separators containing reactive functional groups, Google Patents, 2007.
- [28] J.K. Whear, E.H. Miller, M.R. Roberts, Improved lead acid battery separators, batteries and related methods, Google Patents, 2013. <http://www.google.com/patents/EP2619824A1?cl=en>.
- [29] P. Ruetschi, Aging mechanisms and service life of lead–acid batteries, *J. Power Sources*. 127 (2004) 33–44. doi:10.1016/j.jpowsour.2003.09.052.
- [30] A.J. Peacock, THE CHEMISTRY OF POLYETHYLENE*, *J. Macromol. Sci. Part C Polym. Rev.* 41 (2001) 285–323.
- [31] J.M. Kelly, ULTRA-HIGH MOLECULAR WEIGHT POLYETHYLENE*, *J. Macromol. Sci. Part C Polym. Rev.* 42 (2002) 355–371. doi:10.1081/MC-120006452.
- [32] Celanese(TM), UHMWPE_Ticona_introduction, (n.d.). http://www.pipeandbuoy.com.au/pdf/UHMWPE_Ticona_Introduction.pdf (accessed January 8, 2014).
- [33] W. Böhnstedt, Separators and organics for lead–acid batteries, *J. Power Sources*. 158 (2006) 1102–1105. doi:10.1016/j.jpowsour.2006.02.003.
- [34] K.J. Whear, J.P. Perry, J.K. Chambers, L.A. Spickard, J.R. Timmons, LEAD-ACID BATTERY SEPARATORS, ELECTRODES, BATTERIES, AND METHODS OF MANUFACTURE AND USE THEREOF, US Patent 20,150,318,529, 2015.
- [35] Extruders, Entek. (n.d.). <http://entek.com/extruders/> (accessed October 16, 2016).
- [36] D.R. LLOYD, Microporous membrane formation via thermally induced phase separation. I. Solid-liquid phase separation, *J Membr Sci.* 52 (1990) 239–261. doi:0376-7388/90/\$03.50.
- [37] H. Ding, Y. Tian, L. Wang, B. Liu, Preparation of ultrahigh-molecular-weight polyethylene membranes via a thermally induced phase-separation method, *J. Appl. Polym. Sci.* 105 (2007) 3355–3362. doi:10.1002/app.26521.
- [38] S.S. Kim, D.R. Lloyd, Thermodynamics of polymer/diluent systems for thermally induced phase separation: 2. Solid-liquid phase separation systems, *Polymer*. 33 (1992) 1036–1046. doi:10.1016/0032-3861(92)90020-W.
- [39] C.-F. Zhang, Y.-X. Bai, J. Gu, Y.-P. Sun, Crystallization kinetics of ultra high-molecular weight polyethylene in liquid paraffin during solid-liquid thermally induced phase

- separation process, *J. Appl. Polym. Sci.* 122 (2011) 2442–2448. doi:10.1002/app.34429.
- [40] C. Zhang, Y. Xia, K. Zuo, Y.-P. Zeng, The effect of silica addition on the microstructure and properties of polyethylene separators prepared by thermally induced phase separation, *J. Appl. Polym. Sci.* 131 (2014) n/a-n/a. doi:10.1002/app.40724.
- [41] S. Liu, C. Zhou, W. Yu, Phase separation and structure control in ultra-high molecular weight polyethylene microporous membrane, *J. Membr. Sci.* 379 (2011) 268–278. doi:10.1016/j.memsci.2011.05.073.
- [42] D. Li, W.B. Krantz, A.R. Greenberg, R.L. Sani, Membrane formation via thermally induced phase separation (TIPS): Model development and validation, *J. Membr. Sci.* 279 (2006) 50–60. doi:10.1016/j.memsci.2005.11.036.
- [43] C. Zhang, B. Zhu, G. Ji, Y. Xu, Studies on nonisothermal crystallization of ultra-high molecular weight polyethylene in liquid paraffin, *J. Appl. Polym. Sci.* 99 (2006) 2782–2788. doi:10.1002/app.22645.
- [44] P.J. Flory, *Principles of Polymer Chemistry*, Cornell University Press, 1953.
- [45] B. Wunderlich, *Thermal analysis of polymeric materials*, Springer, Berlin, 2005.
- [46] F. Chen, M.P. Wolcott, Miscibility studies of paraffin/polyethylene blends as form-stable phase change materials, *Eur. Polym. J.* 52 (2014) 44–52. doi:10.1016/j.eurpolymj.2013.09.027.
- [47] A. Akbari, R. Yegani, Study on the impact of polymer concentration and coagulation bath temperature on the porosity of polyethylene membranes fabricated via TIPS method, *J. Membr. Sep. Technol.* 1 (2012) 100.
- [48] Daramic, blue technical header - Oil in Polyethylene Separators1 small.pdf, n.d. http://www.daramic.com/uploads/data_sheets/Oil%20in%20Polyethylene%20Separators1%20small.pdf (accessed October 12, 2016).
- [49] H. Matsuyama, H. Okafuji, T. Maki, M. Teramoto, N. Kubota, Preparation of polyethylene hollow fiber membrane via thermally induced phase separation, *J. Membr. Sci.* 223 (2003) 119–126. doi:10.1016/S0376-7388(03)00314-4.
- [50] L. Aerts, M. Kunz, H. Berghmans, R. Koningsveld, Relation between phase behaviour and morphology in polyethylene/diphenyl ether systems, *Makromol. Chem.* 194 (1993) 2697–2712.
- [51] Z. Tadmor, C.G. Gogos, *Principles of Polymer Processing*, John Wiley & Sons, 2006.
- [52] N. Li, C.F. Xiao, Preparation and properties of UHMWPE/SiO₂ hybrid hollow fiber membranes via thermally induced phase separation—stretching method, *Ira Polym J.* 18 (2009) 479–489.
- [53] H. Sun, K.B. Rhee, T. Kitano, S.I. Mah, High-density polyethylene (HDPE) hollow fiber membrane via thermally induced phase separation. I. Phase separation behaviors of HDPE–liquid paraffin (LP) blends and its influence on the morphology of the membrane, *J. Appl. Polym. Sci.* 73 (1999) 2135–2142.
- [54] C.W. Bunn, The crystal structure of long-chain normal paraffin hydrocarbons. The “shape” of the CH_2 group, *Trans Faraday Soc.* 35 (1939) 482–491. doi:10.1039/TF9393500482.
- [55] C. Vasile, ed., *Handbook of polyolefins*, 2nd ed., and expanded, Marcel Dekker, New York, 2000.
- [56] E.A. Cole, D.R. Holmes, Crystal lattice parameters and the thermal expansion of linear paraffin hydrocarbons, including polyethylenes, *J. Polym. Sci.* 46 (1960) 245–256.
- [57] E.R. Walter, F.P. Reding, Variations in unit cell dimensions in polyethylene, *J. Polym. Sci.* 21 (1956) 561–562. doi:10.1002/pol.1956.120219925.

- [58] P.W. Teare, D.R. Holmes, Extra reflections in the x-ray diffraction pattern of polyethylenes and polymethylenes, *J. Polym. Sci.* 24 (1957) 496–499. doi:10.1002/pol.1957.1202410724.
- [59] T. Seto, T. Hara, K. Tanaka, Phase transformation and deformation processes in oriented polyethylene, *Jpn. J. Appl. Phys.* 7 (1968) 31.
- [60] A. Turner-Jones, The triclinic crystal form of polymethylenes and polyethylenes, *J. Polym. Sci.* 62 (1962).
- [61] D.C. Bassett, S. Block, G.J. Piermarini, A high-pressure phase of polyethylene and chain-extended growth, *J. Appl. Phys.* 45 (1974) 4146–4150.
- [62] M. Yasuniwa, R. Enoshita, T. Takemura, X-ray studies of polyethylene under high pressure, *Jpn. J. Appl. Phys.* 15 (1976) 1421.
- [63] A.J. Peacock, *Handbook of polyethylene: structures, properties, and applications*, Marcel Dekker, New York, 2000.
- [64] H. Zhou, G.L. Wilkes, Comparison of lamellar thickness and its distribution determined from d.s.c., SAXS, TEM and AFM for high-density polyethylene films having a stacked lamellar morphology, *Polymer*. 38 (1997) 5735–5747. doi:10.1016/S0032-3861(97)00145-6.
- [65] T. Kawai, A. Keller, On the effect of the crystallization temperature on the habit and fold length of polyethylene single crystals, *Philos. Mag.* 11 (1965) 1165–1177. doi:10.1080/14786436508224926.
- [66] H.D. Keith, F.J. Fadden, Deformation mechanisms in crystalline polymers, *J. Polym. Sci.* 41 (1959) 525–528.
- [67] A. Keller, A note on single crystals in polymers: Evidence for a folded chain configuration, *Philos. Mag.* 2 (1957) 1171–1175. doi:10.1080/14786435708242746.
- [68] C.M. Guttman, E.A. DiMarzio, J.D. Hoffman, Calculation of SANS intensity for polyethylene: effect of varying fold planes and fold plane roughening, *Polymer*. 22 (1981) 597–608. doi:10.1016/0032-3861(81)90347-5.
- [69] W. Kevin, Innovations in Enhanced Flooded Lead-Acid Batteries, (21:57:00 UTC). <http://fr.slideshare.net/PeteSmith14/innovations-in-enhanced-flooded-leadacid-batteries> (accessed October 18, 2016).
- [70] G. Lopatin, L.Y. Yen, Microporous membranes of ultrahigh molecular weight polyethylene, Google Patents, 1988. <https://www.google.com/patents/US4778601>.
- [71] S.H. Tabatabaei, P. Carreau, A. Ajji, Cast films, microporous membranes, and method of preparation thereof, Google Patents, 2010. <https://www.google.fr/patents/WO2010148492A1?cl=en>.
- [72] A.J. Pennings, Bundle-like nucleation and longitudinal growth of fibrillar polymer crystals from flowing solutions, in: *J. Polym. Sci. Polym. Symp.*, Wiley Online Library, 1977: pp. 55–86. <http://onlinelibrary.wiley.com/doi/10.1002/polc.5070590106/abstract> (accessed October 19, 2016).
- [73] A. Keller, M.J. Machin, Oriented crystallization in polymers, *J. Macromol. Sci. Part B Phys.* 1 (1967) 41–91.
- [74] A. Keller, M.R. Mackley, Chain orientation and crystallization, *Pure Appl. Chem.* 39 (1974) 195–224.
- [75] L. Lin, A.S. Argon, Structure and plastic deformation of polyethylene, *J. Mater. Sci.* 29 (1994) 294–323.
- [76] F.L. Tye, Tortuosity, *J. Power Sources*. 9 (1983) 89–100.

- [77] A.A. Garrouch, L. Ali, F. Qasem, Using Diffusion and Electrical Measurements to Assess Tortuosity of Porous Media, *Ind. Eng. Chem. Res.* 40 (2001) 4363–4369. doi:10.1021/ie010070u.
- [78] K.M. Abraham, Directions in secondary lithium battery research and development, *Electrochimica Acta*. 38 (1993) 1233–1248. doi:10.1016/0013-4686(93)80054-4.
- [79] K.M. Abraham, M. Alamgir, D.K. Hoffman, Polymer electrolytes reinforced by Celgard® membranes, *J. Electrochem. Soc.* 142 (1995) 683–687.
- [80] J. Cannarella, C.B. Arnold, Ion transport restriction in mechanically strained separator membranes, *J. Power Sources*. 226 (2013) 149–155. doi:10.1016/j.jpowsour.2012.10.093.
- [81] K. Peters, Influence of separator structure on the performance of valve-regulated batteries, *Proc. Third Eur. Lead Battery Conf.* 42 (1993) 155–164. doi:10.1016/0378-7753(93)80144-E.
- [82] K.K. Patel, J.M. Paulsen, J. Desilvestro, Numerical simulation of porous networks in relation to battery electrodes and separators, *J. Power Sources*. 122 (2003) 144–152. doi:10.1016/S0378-7753(03)00399-9.
- [83] I.V. Thorat, D.E. Stephenson, N.A. Zacharias, K. Zaghib, J.N. Harb, D.R. Wheeler, Quantifying tortuosity in porous Li-ion battery materials, *J. Power Sources*. 188 (2009) 592–600. doi:10.1016/j.jpowsour.2008.12.032.
- [84] R.B. MacMullin, G.A. Muccini, Characteristics of porous beds and structures, *AIChE J.* 2 (1956) 393–403.
- [85] D. Djian, F. Alloin, S. Martinet, H. Lignier, J.Y. Sanchez, Lithium-ion batteries with high charge rate capacity: Influence of the porous separator, *J. Power Sources*. 172 (2007) 416–421. doi:10.1016/j.jpowsour.2007.07.018.
- [86] S. Padmanabhan, K.R. Sarma, S. Sharma, Synthesis of Ultrahigh Molecular Weight Polyethylene Using Traditional Heterogeneous Ziegler–Natta Catalyst Systems, *Ind. Eng. Chem. Res.* 48 (2009) 4866–4871. doi:10.1021/ie802000n.
- [87] T. Deplancke, O. Lame, F. Rousset, R. Seguela, G. Vigier, Mechanisms of Chain Reentanglement during the Sintering of UHMWPE Nascent Powder: Effect of Molecular Weight, *Macromolecules*. 48 (2015) 5328–5338. doi:10.1021/acs.macromol.5b00618.
- [88] H.D. Chanzy, E. Bonjour, R.H. Marchessault, Nascent structures during the polymerization of ethylene, *Colloid Polym. Sci.* 252 (1974) 8–14.
- [89] J. Loos, M. Arndt-Rosenau, U. Weingarten, W. Kaminsky, P.J. Lemstra, Melting behavior of nascent polyolefins synthesized at various polymerization conditions, *Polym. Bull.* 48 (2002) 191–198.
- [90] S.M. Kurtz, *UHMWPE Biomaterials Handbook: Ultra High Molecular Weight Polyethylene in Total Joint Replacement and Medical Devices*, Academic Press, 2009.
- [91] E. Rudnik, Z. Dobkowski, Thermal degradation of UHMWPE, *J. Therm. Anal. Calorim.* 49 (1997) 471–475.
- [92] Specification for Ultra-High-Molecular-Weight Polyethylene Molding and Extrusion Materials, ASTM International, n.d. <http://dx.doi.org/10.1520/d4020-11>.
- [93] Power Sonic, Battery specification, (n.d.). http://www.power-sonic.com/images/powersonic/technical/1277751263_20100627-TechManual-Lo.pdf (accessed September 28, 2016).
- [94] A.Y. Coran, C.E. Anagnostopoulos, Polymer–diluent interactions. III. Polyethylene–diluent interactions, *J. Polym. Sci.* 57 (1962) 13–23.

- [95] W.J. Wood, R.G. Maguire, W.H. Zhong, Improved wear and mechanical properties of UHMWPE–carbon nanofiber composites through an optimized paraffin-assisted melt-mixing process, *Compos. Part B Eng.* 42 (2011) 584–591. doi:10.1016/j.compositesb.2010.09.006.
- [96] C. Perrier, Study of oils and mixtures based on mineral oil for power transformers – Research of the best mixture, Theses, Ecole Centrale de Lyon, 2005. <https://tel.archives-ouvertes.fr/tel-00141418>.
- [97] Technical data sheet shell edelex oil 946, n.d. http://www.epc.shell.com/Docs/GPCDOC_GTDS_Shell_Edelex_946_%28en%29_TDS_v1.pdf (accessed January 28, 2014).
- [98] M. Ricaud, Le point des connaissances sur les silices amorphes, Institut national de recherche et de sécurité, 2007.
- [99] What is silica ?, (n.d.). <http://www.asasp.eu/sas.html> (accessed December 13, 2016).
- [100] R.K. Iler, The chemistry of silica: solubility, polymerization, colloid and surface properties, and biochemistry, Wiley, New York, 1979.
- [101] G. Schramm, A practical approach to rheology and rheometry, Haake Karlsruhe, 1994.
- [102] T. Dumas, Renforcement des pneumatiques par la silice. Caracterisation physio-chimique et dispersion des granules de silice., Ecole Nationale Supérieure des Mines de Saint-Etienne, 2012. <https://tel.archives-ouvertes.fr/tel-00740183/> (accessed October 4, 2016).
- [103] C. Fayolle, Influence de la dispersion de la silice sur les propriétés viscoélastiques et mécaniques des élastomères renforcés, 2015. <http://www.theses.fr/2015LYO10059/document>.
- [104] H. Winkler, Microstructure of PE-separators, *J. Power Sources.* 113 (2003) 396–399.
- [105] W.B. Jensen, The origin of the Soxhlet extractor, *J Chem Educ.* 84 (2007) 1913.
- [106] M.D. Luque de Castro, F. Priego-Capote, Soxhlet extraction: Past and present panacea, *J. Chromatogr. A.* 1217 (2010) 2383–2389. doi:10.1016/j.chroma.2009.11.027.
- [107] BCI Battery technical Manual (section 03B), BCI Battery Tech. Man. (2002) 22–(section 03B).
- [108] G.C. Claver, R. Buchdahl, R.L. Miller, Spherulitic fine structure in polyethylene, *J. Polym. Sci.* 20 (1956) 202–205.
- [109] E.W. Washburn, The dynamics of capillary flow, *Phys. Rev.* 17 (1921) 273.
- [110] M.J. Moura, P.J. Ferreira, M.M. Figueiredo, Mercury intrusion porosimetry in pulp and paper technology, *Powder Technol.* 160 (2005) 61–66. doi:10.1016/j.powtec.2005.08.033.
- [111] E.W. Washburn, Note on a Method of Determining the Distribution of Pore Sizes in a Porous Material, *Proc. Natl. Acad. Sci. U. S. A.* 7 (1921) 115–116.
- [112] M.-T.I.I. all rights reserved, Density Determination, (n.d.). http://www.mt.com/us/en/home/products/Laboratory_Weighing_Solutions/Accessories/Density.html (accessed October 12, 2016).
- [113] J. Landesfeind, J. Hattendorff, A. Ehrl, W.A. Wall, H.A. Gasteiger, Tortuosity Determination of Battery Electrodes and Separators by Impedance Spectroscopy, *J. Electrochem. Soc.* 163 (2016) A1373–A1387.
- [114] F. Toquet, L. Guy, B. Schlegel, P. Cassagnau, R. Fulchiron, Effect of the naphthenic oil and precipitated silica on the crystallization of ultrahigh-molecular-weight polyethylene, *Polymer.* 97 (2016) 63–68. doi:10.1016/j.polymer.2016.05.021.

- [115] J.. Fatou, C. Marco, L. Mandelkern, The crystallization kinetics of low-molecular-weight polyethylene fractions, *Polymer*. 31 (1990) 890–898. doi:10.1016/0032-3861(90)90052-Z.
- [116] F. Bustos, P. Cassagnau, R. Fulchiron, Effect of molecular architecture on quiescent and shear-induced crystallization of polyethylene, *J. Polym. Sci. Part B Polym. Phys.* 44 (2006) 1597–1607. doi:10.1002/polb.20820.
- [117] C.M. Cormier, B. Wunderlich, Equilibrium dissolution temperatures of polyethylene and the surface free energy of folded-chain single crystals, *J. Polym. Sci. Part -2 Polym. Phys.* 4 (1966) 666–667.
- [118] U. Gedde, *Polymer Physics*, Chapman & Hall London, 1995.
- [119] X. Zhang, Z. Wang, R. Zhang, C.C. Han, Effect of Liquid–Liquid Phase Separation on the Lamellar Crystal Morphology in PEH/PEB Blend, *Macromolecules*. 39 (2006) 9285–9290. doi:10.1021/ma061801a.
- [120] A. Shakoor, N.L. Thomas, Talc as a nucleating agent and reinforcing filler in poly(lactic acid) composites, *Polym. Eng. Sci.* 54 (2014) 64–70. doi:10.1002/pen.23543.
- [121] D. Jauffrès, O. Lame, G. Vigier, F. Doré, Microstructural origin of physical and mechanical properties of ultra high molecular weight polyethylene processed by high velocity compaction, *Polymer*. 48 (2007) 6374–6383. doi:10.1016/j.polymer.2007.07.058.
- [122] P. Gao, Man Ken Cheung, T.Y. Leung, Effects of compaction pressure on cohesive strength and chain mobility of low-temperature compacted nascent UHMWPE, *Polymer*. 37 (1996) 3265–3272. doi:10.1016/0032-3861(96)88472-2.
- [123] B.P. Rotzinger, H.D. Chanzy, P. Smith, High strength/high modulus polyethylene: synthesis and processing of ultra-high molecular weight virgin powders, *Polymer*. 30 (1989) 1814–1819. doi:10.1016/0032-3861(89)90350-9.
- [124] Y.L. Joo, O.H. Han, H.-K. Lee, J.K. Song, Characterization of ultra high molecular weight polyethylene nascent reactor powders by X-ray diffraction and solid state NMR, *Polymer*. 41 (2000) 1355–1368.
- [125] D. Xiang, E. Harkin-Jones, D. Linton, Effect of cooling rate on the properties of high density polyethylene/multi-walled carbon nanotube composites, in: 2015: p. 070005. doi:10.1063/1.4918440.
- [126] S. Liu, W. Yu, C. Zhou, Molecular Self-Assembly Assisted Liquid–Liquid Phase Separation in Ultrahigh Molecular Weight Polyethylene/Liquid Paraffin/Dibenzylidene Sorbitol Ternary Blends, *Macromolecules*. 46 (2013) 6309–6318. doi:10.1021/ma400915g.
- [127] L. Minkova, M. Mihailov, Kinetics of nonisothermal crystallization and melting of normal high density and ultra-high molecular weight polyethylene blends, *Colloid Polym. Sci.* 267 (1989) 577–582.
- [128] F. Bustos, *Cristallisation sous cisaillement du polyéthylène : effets de l'architecture moléculaire*, 2004.
- [129] T. Ohta, F. Okada, M. Hayashi, M. Mihoichi, High-performance materials from gel-like spherulites of ultra-high-molecular-weight polyethylene, *Polymer*. 30 (1989) 2170–2173. doi:10.1016/0032-3861(89)90244-9.
- [130] N. Li, C. Xiao, Z. Zhang, Effect of polyethylene glycol on the performance of ultrahigh-molecular-weight polyethylene membranes, *J. Appl. Polym. Sci.* 117 (2010) 720–728. doi:10.1002/app.30500.
- [131] M.J. Park, S.C. Noh, C.K. Kim, Effects of the Phase Behavior of the Diluent Mixture on the Microstructure of Polyethylene Membranes Formed by Thermally Induced Phase

- Separation Process, Ind. Eng. Chem. Res. 52 (2013) 10690–10698. doi:10.1021/ie4010282.
- [132] H.-H. Chang, K.G. Beltsios, H.-F. Yu, Y.-H. Wu, L.-P. Cheng, Novel phase inversion process for symmetric membrane formation through thermal quenching of polymer solution in same solvent, J. Appl. Polym. Sci. 132 (2015) 42282. doi:10.1002/app.42282.
- [133] J.I. Calvo, A. Hernandez, P. Pradanos, L. Martinez, W.R. Bowen, Pore size distributions in microporous membranes II. Bulk characterization of track-etched filters by air porometry and mercury porosimetry, J. Colloid Interface Sci. 176 (1995) 467–478.
- [134] C.S. Kong, D.-Y. Kim, H.-K. Lee, Y.-G. Shul, T.-H. Lee, Influence of pore-size distribution of diffusion layer on mass-transport problems of proton exchange membrane fuel cells, J. Power Sources. 108 (2002) 185–191.
- [135] A. L. Ferreira, Battery additives: any influence on separator behavior?, J. Power Sources 95. (2001). http://ac.els-cdn.com/S0378775300006224/1-s2.0-S0378775300006224-main.pdf?_tid=675540fe-7d0b-11e3-a93a-00000aabb0f26&acdnat=1389697548_ecc3379be743e5e853fe6ba42781d0b9 (accessed January 14, 2014).
- [136] C. Zhang, Y. Xia, K. Zuo, Y.-P. Zeng, The effect of silica addition on the microstructure and properties of polyethylene separators prepared by thermally induced phase separation, J. Appl. Polym. Sci. (2014) n/a-n/a. doi:10.1002/app.40724.
- [137] K. Meyer, P. Klobes, Comparison between different presentations of pore size distribution in porous materials, Fresenius J. Anal. Chem. 363 (1999) 174–178.
- [138] D. Ihm, J. Noh, J. Kim, Effect of polymer blending and drawing conditions on properties of polyethylene separator prepared for Li-ion secondary battery, J. Power Sources. 109 (2002) 388–393.

APPENDICES

The figures 56 to 68 are linked to the section 5.1 of this thesis work. This section of the thesis work presents the effect of the amount of precipitated silica on the porosity of the PE-separators. As evoked before, the same conclusions have been obtained for the membranes elaborated with the grades of precipitated silica T43, Z175 and Z1165. Thus only the results related to the membranes with the grade T43 have been discussed before. Therefore the results related to the membranes with the grades Z175 and Z1165 are presented here in addition.

From Figure 58, it can be seen that ϵ_{IPA} and ϵ_{hg} are always equal. Furthermore, an increase of the precipitated silica amount does not mean an increase of the total membrane porosity but only an increase of the part of porosity wettable by water for the both grades of silica (Z175 and Z1165). Moreover, as it can be seen for both grades of silica, the more there is precipitated silica inside the blend, the more ϵ_{ww} increases.

As it can be seen in Figure 59, for the three precipitated silica grades used, the parameter α increases with the increasing of the precipitated silica volume fraction. Moreover, there is no obvious difference between the values of α of the three grades of precipitated silica for a same amount of silica.

From the figure 58 to 65, the pore distributions of membranes elaborated in the internal mixer are presented. As it has been observed before for membranes with the silica grade T43, there are three kinds of pores: the “bubbles” around 100 μ m, the pores seen in SEM analysis between 4 μ m and 50 nm and the pores attributed to the porous structure of the silica around 20 nm. The variation of these three kinds of peaks as a function of the amount of silica grade Z175 or Z1165 is similar as the variations reported in the section 5.1.2 for membranes with T43.

The Figure 68 presented in this section is very similar to the Figure 48 of the chapter 5. For the three silica grades, the porosity attributed to the peak of the precipitated silica increases with the increasing of the silica amount as well as ϵ_{ww} . Moreover, for a same amount of precipitated silica, there is almost no difference in the value of ϵ_{ww} as a function of the silica grade used.

The Figure 69 and Figure 70 present respectively the electrical resistivity and the tortuosity of membranes elaborated in the internal mixer for all these grades of precipitated silica. For the three silica grades, between 5 vol% and 10 vol% of precipitated silica in the formulation, there is a big drop of the resistivity and the tortuosity. Then, the decrease of the electrical resistivity with the increase of the

volume fraction of silica is smoother between 10 and 18 vol% of precipitated silica. However, the membranes with Z175 have a resistivity and a tortuosity a little higher than the membranes with Z1165 or T43. This difference can be explained by a silica dispersion a little less efficient for membranes with the grade Z175 than for the membranes with the grade T43 or the grade Z1165.

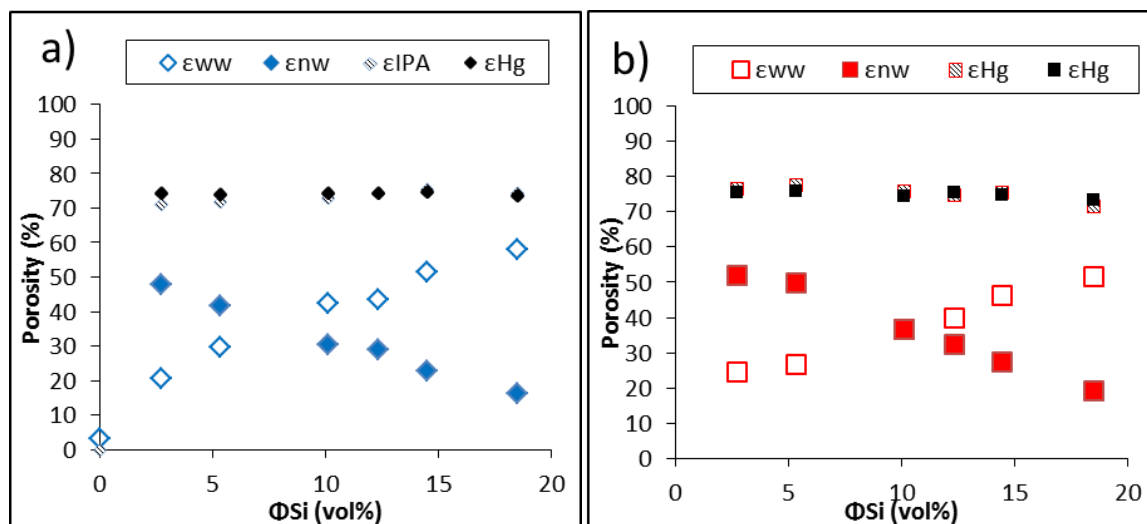


Figure 58: Comparison of water porosities, IPA porosity and mercury intrusion porosimetry porosities for samples processed using the internal mixer with the grade Z1165 (a) and the grade Z175 (b) of precipitated silica as a function of the volume fraction of silica in the formulation of the membranes.

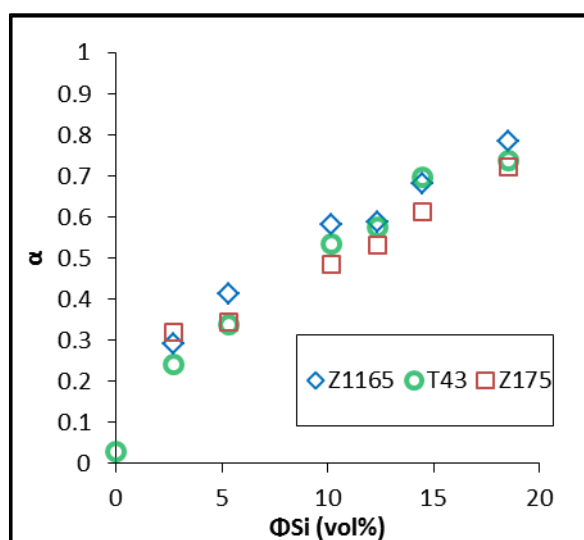


Figure 59: The parameter α as a function of the precipitated silica volume fraction in the formulation of the membranes before process for samples processed by internal mixer with the grades of precipitated silica T43, Z1165, Z175 and T43.

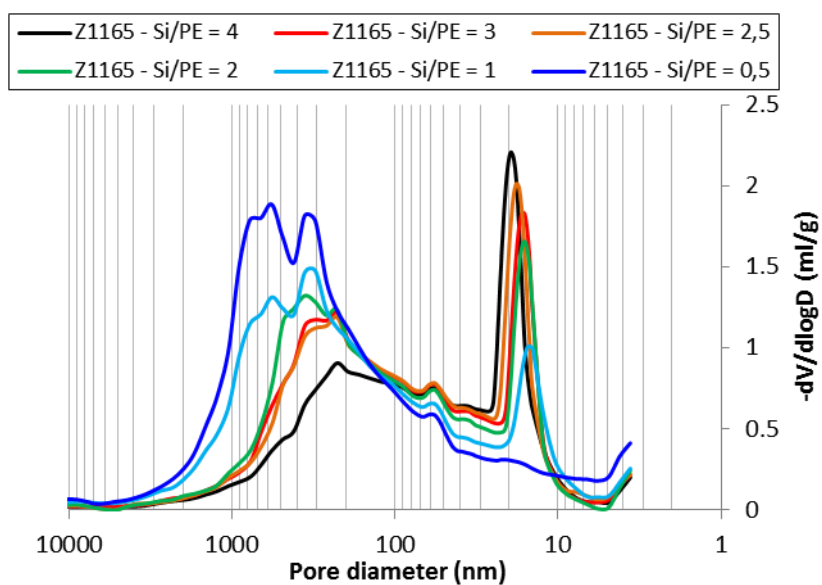


Figure 60: Differential pore size distribution for samples elaborated in the internal mixer with the grade Z1165 of precipitated silica.

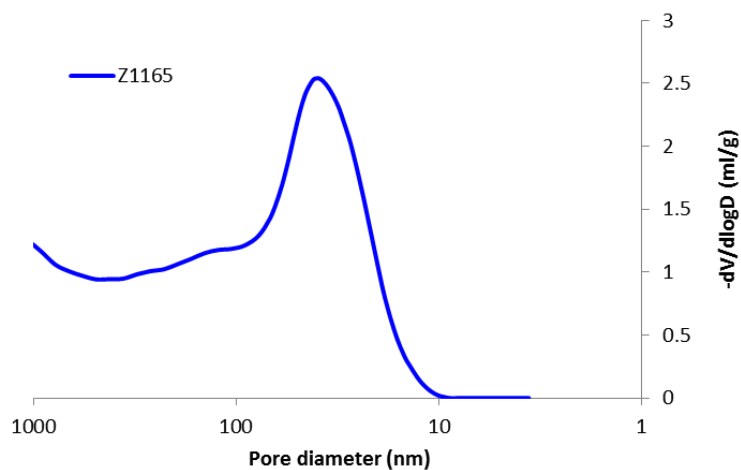


Figure 61: Differential pore size distribution for grade of precipitated silica Z1165 obtained by porosimetry by mercury intrusion

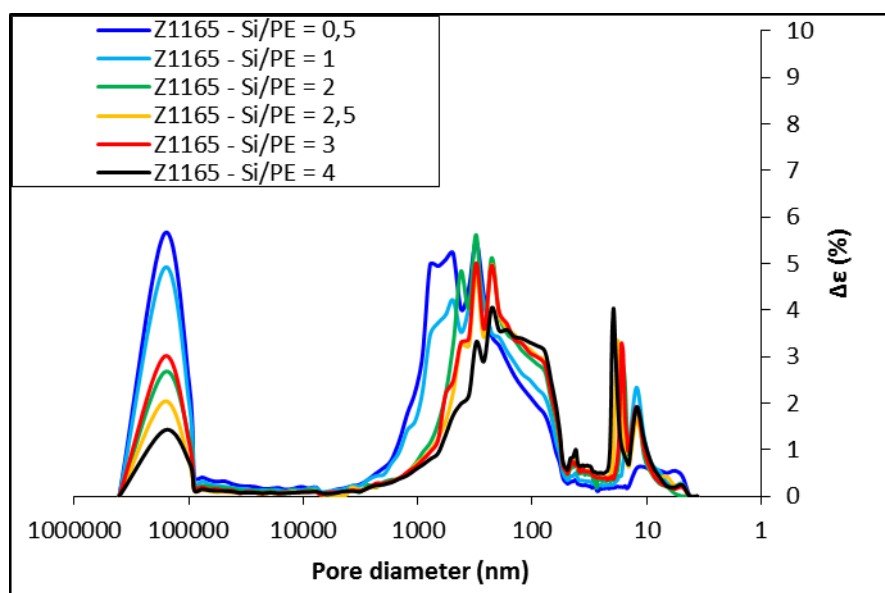


Figure 62: Incremental porosity in percentage as function of the diameter of the pores for membranes with H/PE=7.5 using the grade Z1165 of precipitated silica for different Si/PE ratios.

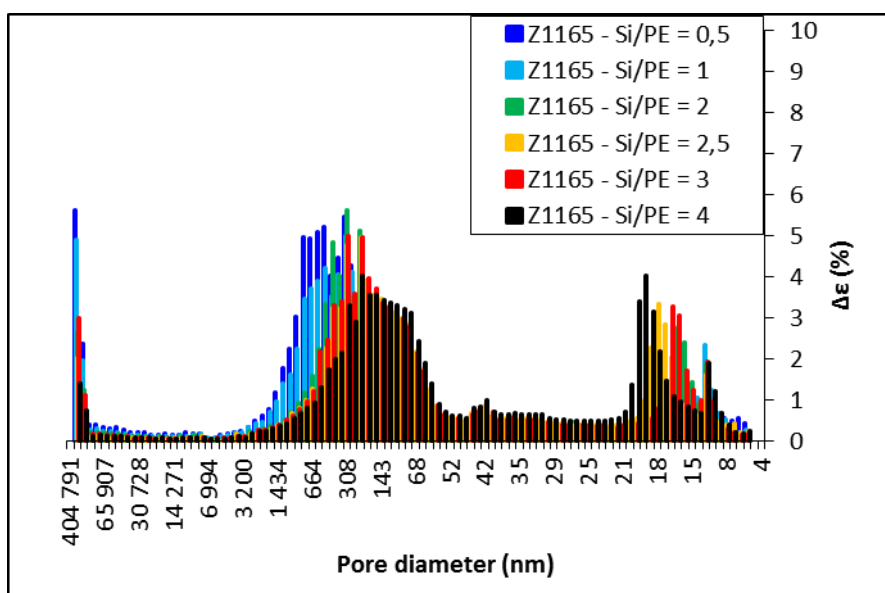


Figure 63: Incremental porosity as function of diameter of the pores with a non-linear axis obtained in porosimetry by mercury intrusion. Membranes with H/PE=7.5 using the grade Z1165 of precipitated silica for different Si/PE ratios.

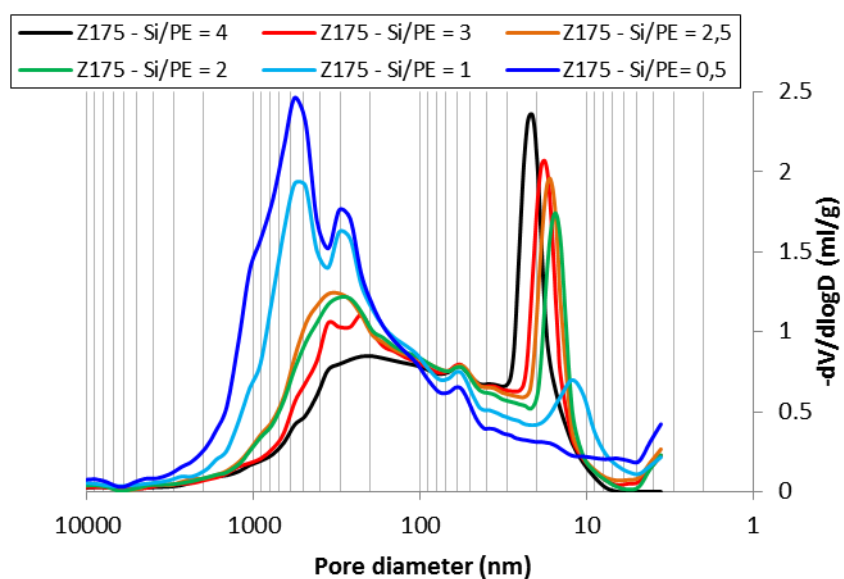


Figure 64: Differential pore size distribution for samples elaborated in the internal mixer with the grade Z175 of precipitated silica.

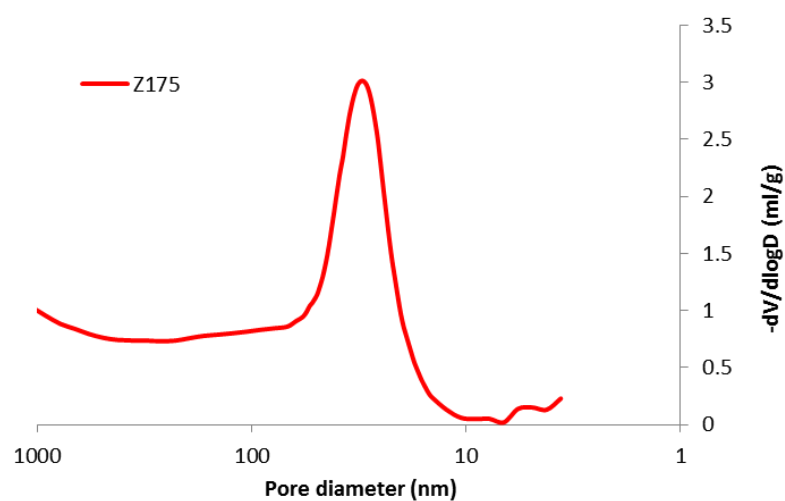


Figure 65: Differential pore size distribution for grade of precipitated silica Z175 obtained by porosimetry by mercury intrusion

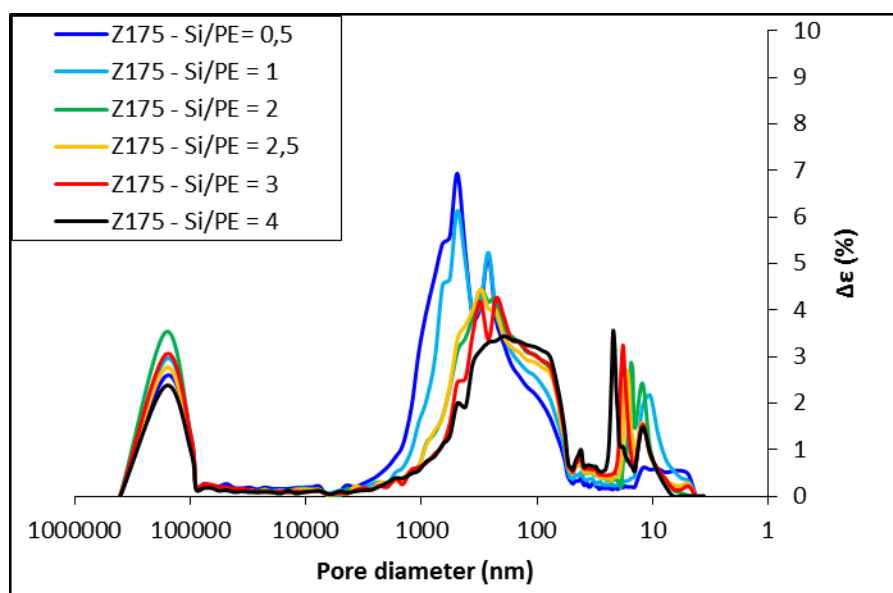


Figure 66: Incremental porosity in percentage as function of the diameter of the pores and Membranes with H/PE=7.5 using the grade Z175 of precipitated silica for different Si/PE ratios.

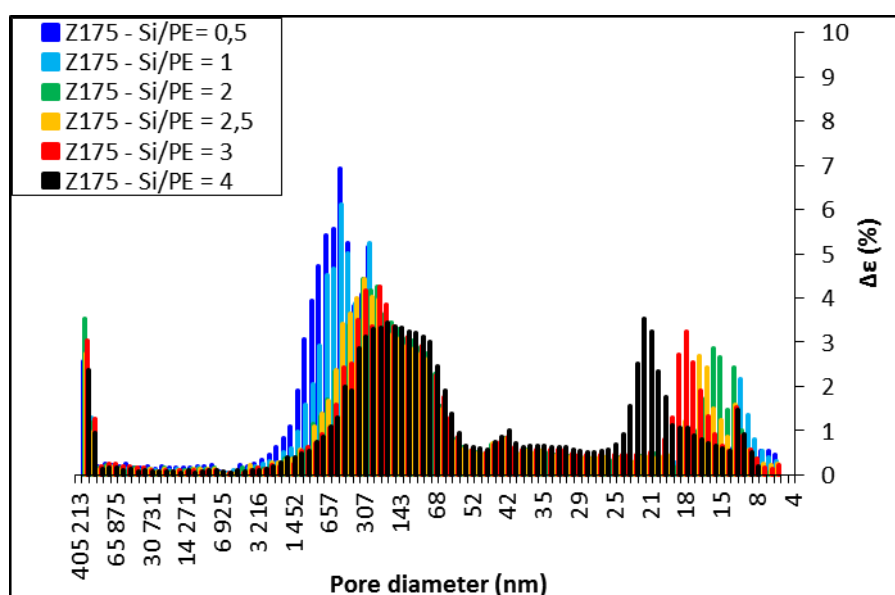


Figure 67: Incremental porosity as function of diameter of the pores with a non-linear axis obtained in porosimetry by mercury intrusion. Membranes with H/PE=7.5 using the grade Z175 of precipitated silica for different Si/PE ratios.

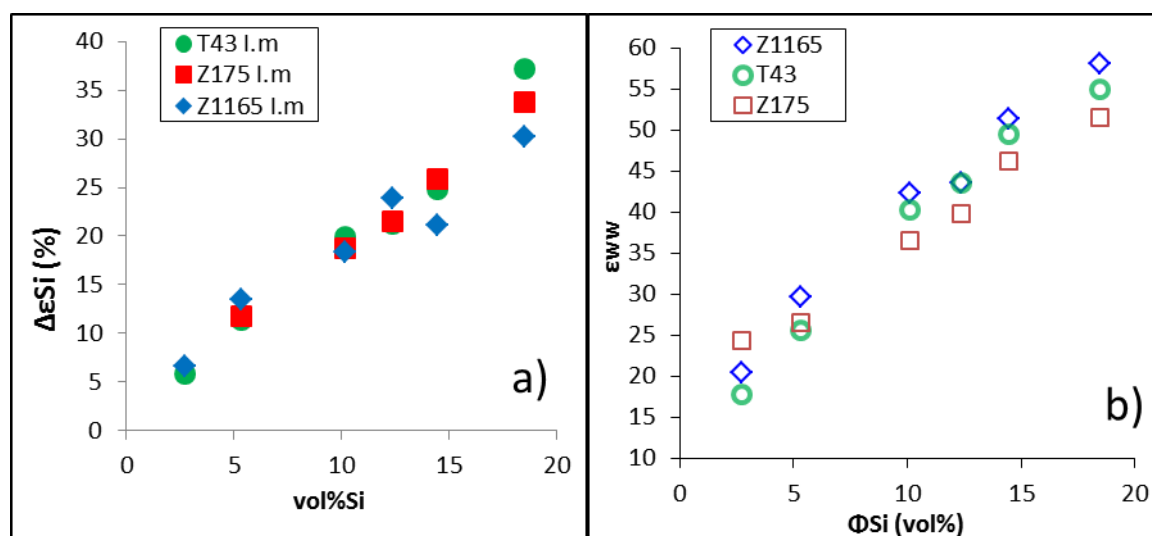


Figure 68: a) Porosity attributed to the peak of silica observed in mercury intrusion porosimetry as a function of the amount of precipitated silica in the formulation before process of membranes. b) Porosity accessible to water as a function of the porosity attributed to the peak of silica observed in mercury intrusion porosimetry.

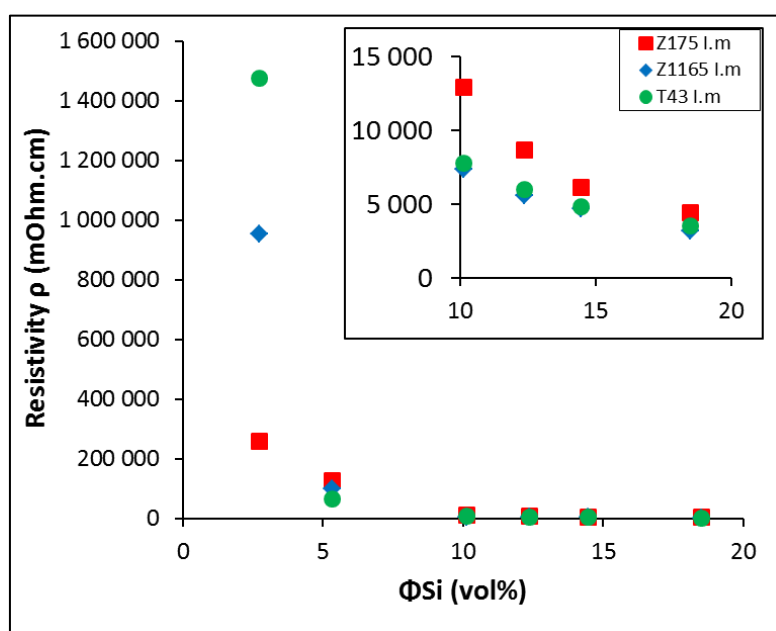


Figure 69: Resistivity of membranes with the grades of precipitated silica T43, Z1165 and Z175 as a function the amount of silica (before process). A focus on membranes with more than 10 vol% (Si/PE=2) of silica in the insert

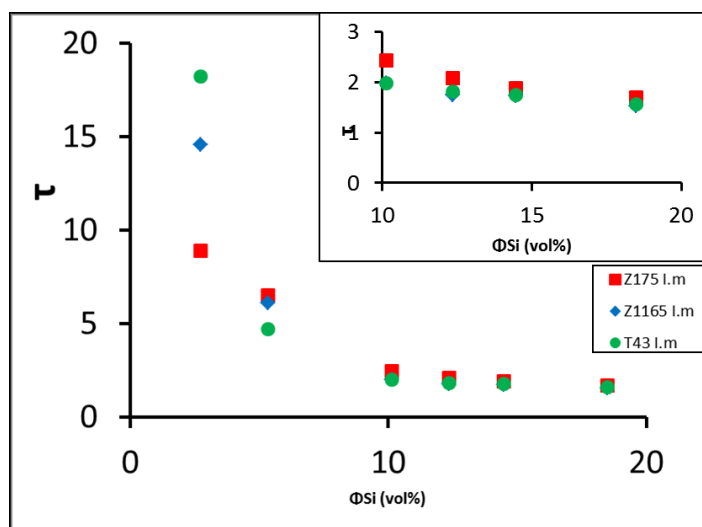


Figure 70: Tortuosity of samples processed by internal mixer with the grades T43, Z175 and Z1165 as a function of the volume fraction of precipitated silica T43 in the formulation before process.